This is to certify that the

dissertation entitled

CHEMILUMINESCENCE: A MECHANISTIC PROBE OF ELECTRON-TRANSFER REACTIONS

presented by

Robert Dorsey Mussell

has been accepted towards fulfillment
of the requirements for

Ph.D. degree in **Chemistry**

Daniel G Nocera
Major professor

Date **September 15, 1988**

CHEMILUMINESCENCE: A MECHANISTIC PROBE OF ELECTRON-TRANSFER REACTIONS

By

Robert Dorsey Mussell

A DISSERTATION

Submitted to
Michigan State University
in partial fulfillment of the requirements
for the degree of

DOCTOR OF PHILOSOPHY

Department of Chemistry

1988

ABSTRACT

CHEMILUMINESCENCE: A MECHANISTIC PROBE OF ELECTRON-TRANSFER REACTIONS

by

Robert Dorsey Mussell

The chemiluminescent reactivity of $M_6X_8Y_6^{2-}$ (M = Mo, W; X, Y = Cl, Br, I) clusters in nonaqueous solution has been used to investigate the mechanism of electron transfer reactions. The partitioning of the electrochemical excitation energy upon annihilation of electrogenerated $Mo_6Cl_{14}^{3-}$ with a series of $W_6X_8Y_6^-$ ions has been determined from overall electrogenerated chemiluminescence (ecl) quantum yields and chemiluminescence spectra. The electrochemical excitation energy is partitioned to produce $Mo_6Cl_{14}^{2-*}$ and $W_6X_8Y_6^{2-*}$ with essentially equal probability. Analysis of the equal distribution with current electron-transfer theories suggests that the electronic coupling and reorganizational energy for the conversion of $M_6X_8Y_6^- \longrightarrow M_6X_8Y_6^{2-*}$ and $M_6X_8Y_6^{3-} \longrightarrow M_6X_8Y_6^{2-*}$ by simple electron exchange are equal. The free-energy dependence of the $M_6X_8Y_6^{2-}$ ecl in acetonitrile and dichloromethane was

investigated with four series of structurally and electronically related electroactive organic compounds. The yields for the formation of electronically excited $Mo_6Cl_{14}^{2-}$ ion produced by the electron-transfer reaction of $Mo_6Cl_{14}^{3-}$ with electroactive organic acceptors and the reaction of $Mo_6Cl_{14}^{-}$ with electroactive organic donors have been measured over a wide potential range by simply varying the reduction potential of the electroactive organic reagents. The dependence of the formation yield of $Mo_6Cl_{14}^{2-*}$, ϕ_{es}, on the driving force of the annihilation reaction is similar for the four series in both solvents. ϕ_{es} is immeasurable ($<10^{-5}$) for reactions with free energies positive of a threshold value. Over a narrow free energy range just negative of threshold, ϕ_{es} rapidly increases. And with increasing exergonicity of the electron-transfer reaction, ϕ_{es} asymptotically approaches a limiting value less than unity. Analysis of these excited-state production yields using Marcus theory reveals that unit efficiencies for excited-state production are circumvented by long-distance electron transfer. The distance this electron transfer occurs can be mediated by solvent and solute interactions, and calculations establish that the electron-transfer distance is equal to the radii of the reactants plus the diameter of two solvent molecules. Ecl efficiencies of the hexanuclear cluster ions are not only perturbed by intermolecular factors but also are dramatically

effected by ligand coordination sphere. Additionally, the effects of temperature and potential step sequence on the ecl efficiencies of the hexanuclear cluster ions have also been investigated.

ACKNOWLEDGEMENTS

I thank all the Nocera group members, especially I-Jy Chang, for making each day in the lab a unique and sometimes scientifically stimulating experience. I especially thank Dan Nocera for his friendship and unbridled (non-stop) direction during my research career here at MSU. Dan's ability to always see the "big picture" definitely made my graduate journey a much smoother trip. Mark Newsham, Dan Kassel, Joe Skowyra and Randy "a fifth isn't excessive" King get a special thanks for their friendship and their efforts to make sure that all chemistry students are not viewed upon as nerds. I am indebted to Dr. Tom Pinnavaia for serving as my second reader and Dr. Bob Cukier for his many helpful discussions and also for serving on my committee. A big thanks goes to Sharon Corner for being a good friend as well as an excellent typist.

I would like to acknowledge the support of fellowships from Dow Chemical Company and the College of Natural Science during the 1987-1988 academic year.

Outside of chemistry I would like to express my thanks to all the past and present team members of the "Froggers", which will go down as one of the great intramural teams in MSU history, for the opportunity to participate in basketball and softball with so many great individuals. Also thanks go to all my friends, Tom Brege, Tommy Oosdyke,

John Childers, Richard Hahn, Tom Murphy and Bob Lane, who have stood by me and helped me keep a prospective on the true meaning of life.

I want to especially thank my parents and family for their support, understanding and love during all my school years. Without them none of this would have been possible.

And finally, my deepest gratitude to my wife Joy. Her patience, support, and love during the past five years have made this experience much more enjoyable.

TABLE OF CONTENTS

Page

LIST OF TABLES

Page

Page

LIST OF FIGURES

Page

CHAPTER I

I. INTRODUCTION

Electron transfer reactions play a fundamental role in chemical and biological processes. Many important chemical reactions involve oxidation-reduction processes especially including those in inorganic chemistry in which transition metal complexes are versatile redox reagents. Small molecule activation[1], photocatalysis[2,3], and homogeneous[4] and heterogeneous catalysis[5] are fundamental inorganic processes involving the transfer of an electron or electrons to or from a metal reaction center. In biological systems, oxidation-reduction transformations at inorganic reaction centers control several essential biological processes.[6,7] Some of these include electron transfer between the heme centers of cytochromes and reduction of O_2 by cytochrome oxidase in oxidative phosphorylation, the reduction of dinitrogen at a molybdenum center of nitrogenase, and four-electron oxidation of water to oxygen at the manganese center of the oxygen-evolving complex in photosystem II. Owing to the importance of oxidation-reduction reactions, experimental and theoretical elucidation of the factors that govern the rates of electron-transfer events, has been a central theme of mechanistic chemistry during the past two decades.[8-11]

Electron-transfer reactions can be described in classical terms by activated complex theory. As first proposed by Marcus,[12] electron transfer can be represented by potential energy curves for reactants and products such as those depicted in Figure 1. In this diagram, the

Figure 1. Potential energy curve for an electron transfer reaction accompanied by a net chemical change. ΔG° is the driving force for the electron transfer, ΔG^{*} is the activation barrier, and the splitting at the intersection is equal to $2H_{AB}$.

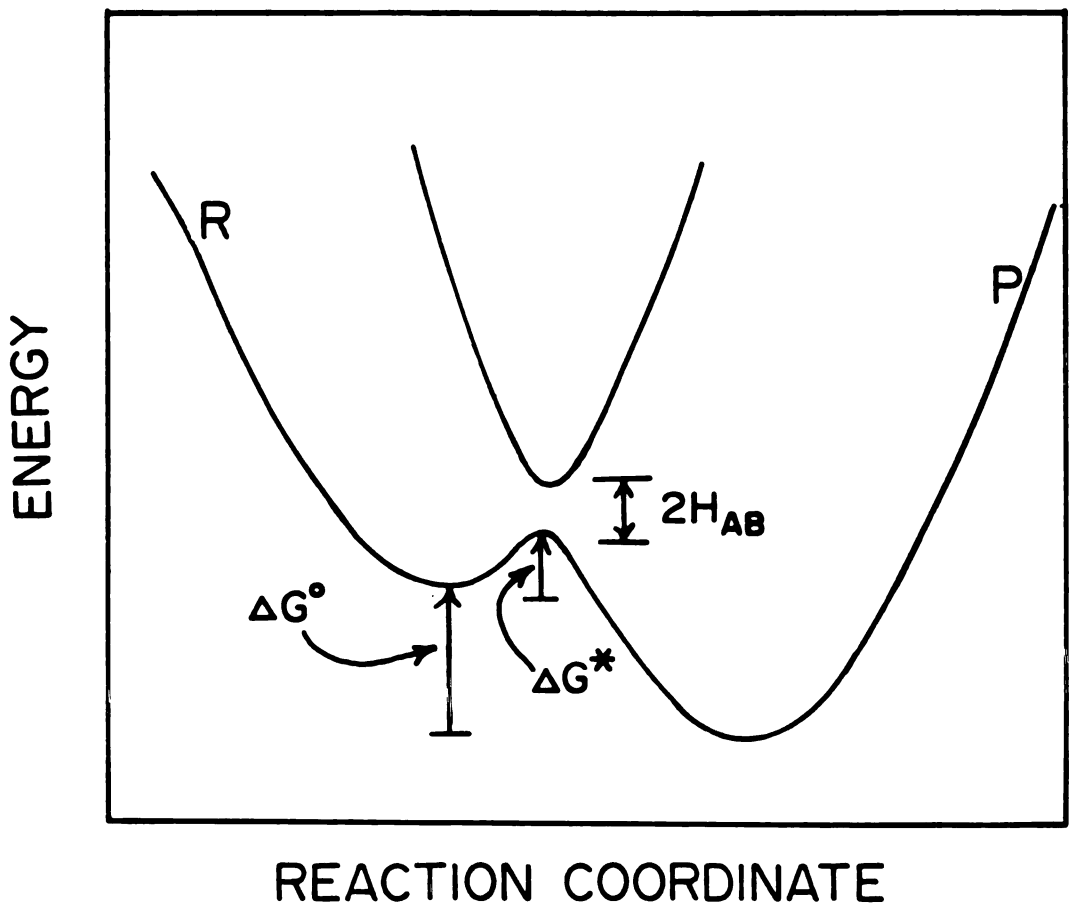

Figure 1

electron transfer reaction, which is defined in many-coordinate space, (N-1, where N defines the positions of all molecules, their orientations and their vibrational coordinates) is simplified by choosing a one dimensional generalized reaction coordinate involving a vibration which is important to the reaction along a reaction coordinate, x, which represents the positions of the reactant and product molecules and their solvent coordination spheres. The ordinate defines the relative potential energy of the system. The intersection of the reactant and product potential energy curves occurs at an intermediate configuration, called the activated complex, where the nuclei are in a position halfway between the reactants and products. The barrier height from reactants to the activated complex defines the activation energy, ΔG^*, and the rate of electron transfer can be described by the

$$k_{et} = Z \exp [\Delta G^*/k_B T] \qquad (1)$$

classical expression shown in eq 1, where Z is the collisional frequency of the uncharged reactions in solution. Marcus has defined the contributions to ΔG^* by eq 2 where ΔG^* is the driving force for the reaction, λ is the

$$\Delta G^* = w_r + (\Delta G^\circ + \lambda)^2 / 4\lambda \qquad (2)$$

reorganizational energy which contains inner-sphere, λ_i, and outer-sphere, λ_o, contributions and w_r is the work required to bring the two reactants together. Marcus has shown that in a dielectric continuum, the outer-sphere reorganizational energy is given by,

$$\lambda_o = \Delta e^2 \ (1/2a_1 + 1/2a_2 - 1/r) \ (1/D_{op} - 1/D_s) \qquad (3)$$

where a_1 and a_2 are the radii of the two reactants, r is the distance between centers of the two reactants in the activated complex (usually assumed equal to $a_1 + a_2$), and D_{op} and D_s are the optical and static dielectric constants, respectively. The inner-sphere reorganizational parameter, which depends on differences in equilibrium bond lengths and angles between reactants and products, is defined by eq 4.[13] In this equation $f_i = 2f_2f_3/(f_2 + f_3)$ is a reduced force

$$\lambda_i = 1/2 \sum_i f_i \ (d_2{}^\circ - d_3{}^\circ)_i{}^2 \qquad (4)$$

constant for the ith inner-sphere vibration and $(d_2{}^\circ - d_3{}^\circ)_i$ is the corresponding difference in equilibrium bond distances of the reactants and products. The summation is over all the intramolecular vibrations. The work term, w_r, is approximated by a Debye-Huckel formalism where z

$$w_r = \frac{z_1 z_2 \ e^2}{D_s r(1 + \beta_{DH} \ r \sqrt{u})} \qquad (5)$$

$$\beta_{DH} = \left[\frac{8000\pi Ne^2}{1000\ D_s k_B T} \right]^{1/2} \qquad (6)$$

and z_2 are the usual charges of the two reactants and μ is the ionic strength of the solution. It is noteworthy that this classical approach assumes that reaction to products occurs from the activated complex with unity. For this case the electron-transfer reaction is said to be adiabatic.

More generally, electron transfer can be mediated significantly by the electronic coupling between the reactant and product surfaces and nuclear tunneling through the barrier. To this end, a more accurate expression of the electron transfer rate is given by eq 7 where nuclear tunneling and nonadiabatic effects are accounted for by Γ_n

$$k_{et} = Z\kappa_E \Gamma_n \exp\ [\Delta G^*/k_B T] \qquad (7)$$

and κ_E, respectively.[14-17] Because nuclear tunneling will increase the reaction rate, with respect to the activated electron transfer, Γ_n takes on values ≥ 1. At room temperature tunneling does not typically contribute to the overall rate ($\Gamma_n \cong 1$), but becomes significant when (i) either the barrier height is large, (ii) the reaction is very exergonic, or (iii) the temperature of the reaction is low. These quantum mechanical aspects of nuclear tunneling have been treated by several authors in recent years.[18-20]

More important to chemical and biological electron transfer under typical reaction conditions is the mediation of the overall rate by the electronic coupling strength.[15,21,24] Quantitatively, the probability that the electron transfer will occur in the activated complex is given by eq 8 where κ_E in eq 7 is related to κ_E' by $\kappa_E = 1-\exp(-\kappa_E')$ and H_{AB}° is the electronic coupling matrix element between reactant and product surfaces,[17] calculated usually by the Landau-Zener

$$\kappa_E' = \left[\frac{2(H_{AB}^\circ)^2}{k_BT}\right]\left[\frac{\pi^3}{\lambda k_BT}\right]^{1/2} \qquad (8)$$

treatment of avoided crossings. This is represented in Figure 1 by the splitting at the intersection which is equal to 2 H_{AB}°. For adiabatic reactions, H_{AB}° is large and κ_E = 1; reactions with $\kappa_E < 1$ are said to be nonadiabatic. The semi-classical electron-transfer expression, eq 7 reduces to the classical formalism when κ_E and Γ_n are unity.

The energy dependence of the rate in both classical and semi-classical treatments of electron transfer follows directly from eq 2. Ignoring work terms for the moment, for a weakly exergonic reaction ($\Delta G^\circ > -\lambda$) the rate will increase with increasing negative free energy, maximize when the activation barrier is zero ($\Delta G^\circ = -\lambda$) and then decrease for driving forces more exergonic than $-\lambda$ (i.e. $\Delta G^\circ < -\lambda$) (Figure 2). This latter region, called the inverted region, is illustrated in Figure 2c, where the product curve, at

Figure 2. Potential energy curves for electron transfer as a function of increasing driving force: (a) $\Delta G^\circ > -\lambda$; (b) $\Delta G^\circ = -\lambda$; (c) $\Delta G^\circ < -\lambda$.

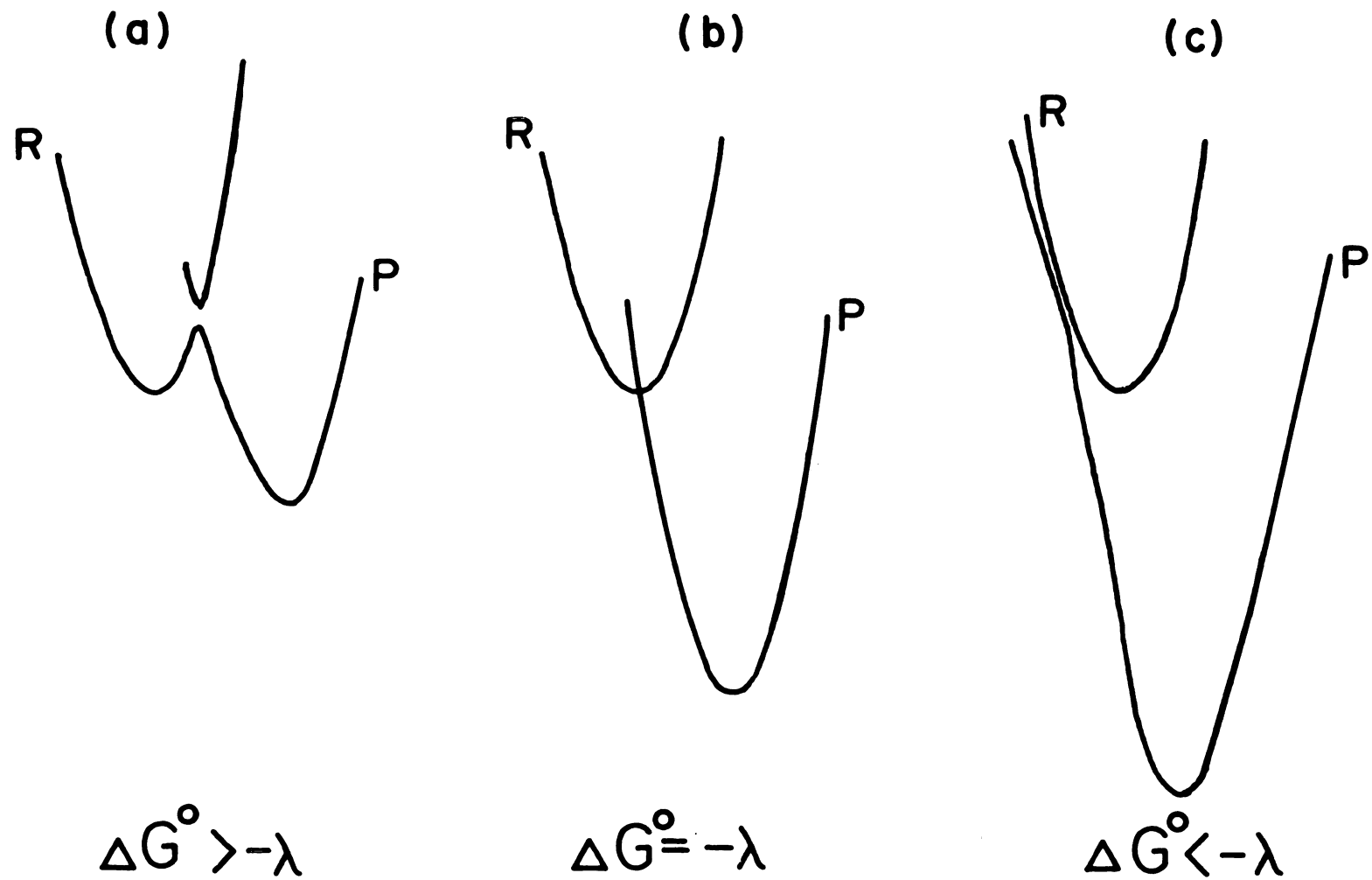
(a)
R
P
$\Delta G^{\circ} > -\lambda$
(b)
R
P
$\Delta G^{\circ} = -\lambda$
(c)
R
P
$\Delta G^{\circ} < -\lambda$

Figure 2

exergonicities greater than activationless transfer, climbs up the back side of the reactant curve thereby introducing again a positive activation energy.

Significant strides in the understanding of the contributions of electronic, nuclear, and driving force effects on the rate of electron transfer have been made in recent years with the preparation of systems in which electron donor and acceptor sites are molecularly linked over fixed distances. One such approach to the design of electron donor-acceptor systems is based on covalently binding a transition metal complex (e.g. $-Ru(NH_3)_5^{2+}$) to polypeptide residues of proteins such as cyctochrome c and myoglobin.[8,25a] In these semi-synthetic metalloproteins the electron transfer rates between transition metal complex and the heme center of the protein have been measured. A modification of this approach has been to substitute Zn for Fe in the heme center of hemoglobin, cytochromes, and myoglobin.[25-27] The Zn modified protein is structurally similar to the native protein and hence can be complexed with its biologically relevant electron-transfer counterpart (i.e. cytc-Zncytc peroxidase). In these systems the electron transfer is activated by absorption of a photon by the long-lived Zn porphyrin. The photochemically activated Zn site acts as an acceptor or donor with the heme center of the complexed protein. In many instances the return electron-transfer rate can also be measured. Results from both of these approaches have led to quantification of

biological inner-sphere reorganizational energies as well as the effect of distance on the electronic coupling between biological reaction centers.[8,25,27] Alternatively a less biological approach has relied on molecularly linking organic acceptor and donor sites via rigid spacers.[28-33] These systems have provided a direct comparison to biological electron transfer and, for the case of aromatic molecules bridged by steroid spacers, provided the first verification of the inverted region.

Not surprisingly, the initial studies of electron transfer, beginning with Rehm and Weller's studies on fluorescence quenching of aromatic molecules,[34] did not rely on the design of synthetically complicated intramolecular samples, but focussed on simple electron transfer reactions between freely diffusing reactants. Since that landmark study of Rehm and Weller, numerous experimental studies of bimolecular systems have provided ample data for electron transfer reorganizational energies, self-exchange rate constants, and free energy dependencies in which the rate increases and levels with increasing free energy (i.e., the normal electron transfer region).[35-40] However, unlike the fixed distance electron donor-acceptor systems, observation of a decrease in rate at high exergonicities (i.e., the inverted region) has proven experimentally more elusive. The inability to detect the inverted region prompted the utilization of empirical free energy relationships, first proposed by Rehm and Weller[34,42] and modified by

others,[43,44] to fit the observed data. In a more quantitative approach, several theoretical studies have involved quantum mechanical treatments to rationalize the absence of the inverted region.[17,19,45-49] Although these studies attenuate the magnitude of the inverted effect predicted by classical theories, a decrease in rate at high exergonicity is maintained. The shortcomings of classical, semi-classical and quantum mechanical rate expressions in the highly exergonic region have been attributed to several factors: (1) Truncation of the predicted rate curve by the diffusion-controlled limiting rate as shown in Figure 3 will obscure the inverted effect. Inverted behavior, which will only be observed for rates below k_d, occur at experimentally inaccessible driving forces. (2) Electron transfer does not proceed directly to ground state (in the inverted region) but to electronically excited products (in the normal region) which then decay efficiently to ground state products.[50] (3) And finally, the introduction of competitive chemical pathways, such as H-atom transfer followed by proton exchange with the solvent and exciplex formation that can circumvent a simple electron transfer pathway.[51,52]

More recently, Marcus and Siders have shown that the inverted effect is diminished at large distances.[53] This is an important result because it was generally assumed for bimolecular reactions that electron transfer takes place only at closest contact. A typical bimolecular reaction

Figure 3. Truncation of very fast electron transfer rates by diffusion. The diffusion limiting rate is represented by the dotted horizontal line. Thus, the rates are leveled until ΔG° becomes very large.

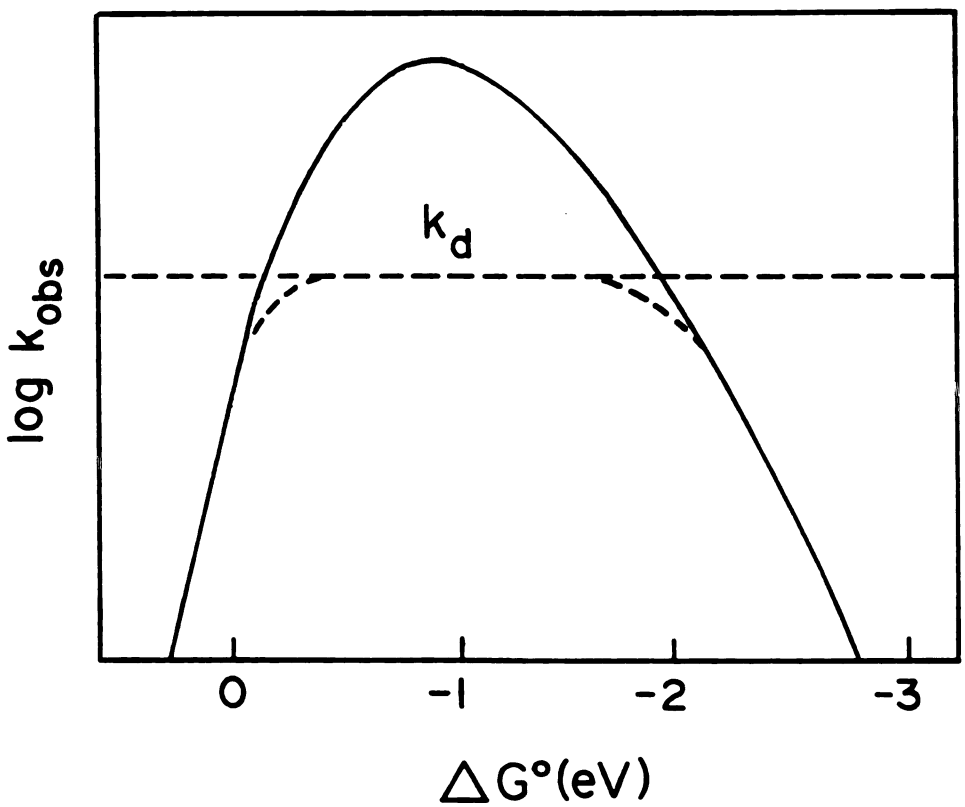

Figure 3

model for electron transfer is shown in Scheme 1. The first step is the diffusion together of the two reactants to form a precursor complex. This is followed by electron transfer within the precursor complex to form the successor complex

$$M^- + N^{3-} \underset{k_{-d}}{\overset{k_d}{\rightleftharpoons}} M^-\cdots N^{3-} \xrightarrow{k_{et}} M^{2-}\cdots N^{2-} \longrightarrow M^{2-} + N^{2-}$$

Scheme 1

and the ultimate separation of the successor complex to form products. The assumption of closest contact is valid for a reaction in which equilibrium is established (i.e., $k_{et} < k_d$). However, equilibrium is not achieved for the fastest reaction (i.e., $k_{et} \geq k_d$) and longer distance electron transfer ($r > \sigma$) is possible. Electron transfer at distances larger than closest contact may occur if the reactants are carrying a solvent shell or a counterion, both of which can inhibit the closest approach of the reactants.

The long distance effect for bimolecular reactions can be made quantitative by formulating the overall rate constant as the harmonic mean of the diffusion-limited, k_{diff}, and the activated, k_{act}, rates,

$$1/k_{obsd} = 1/k_{diff} + 1/k_{act} \qquad (9)$$

Under steady-state conditions k_{diff} and k_{act} can be approximated by eqs 10 and 11[54-56] where k(r) is the

$$k_{diff} = \frac{4\pi ND}{1000} \Big/ \int_{\sigma}^{\infty} g_e(r)\ r^{-2}\ dr \qquad (10)$$

$$k_{act} = \frac{4\pi N}{1000} \int_{\sigma}^{\infty} g_e(r)\ k(r)\ r^2\ dr \qquad (11)$$

unimolecular rate of the electron-transfer reaction between reactants at a fixed center-to-center separation r, D is the sum of the reactant's diffusion coefficient, σ is the distance of closet approach, and $g_e(r)$ is the equilibrium pair distribution function given in eq 12 where U(r) represents the intermolecular potential between the reactants.

$$g_e(r) = \exp\ [-U(r)/k_BT] \qquad (12)$$

Typically, U(r) is described by the Debye-Huckel relation given by eqs 5 and 6. For nonadiabatic electron transfer, k(r) is given by eqs 13 and 14.

$$k(r) = \left[\frac{2H_{AB}^2}{h}\right]\left[\frac{\pi^3}{\lambda k_BT}\right]^{1/2} \exp\left[-\frac{(\lambda + \Delta G^\circ)^2}{4\lambda k_BT}\right] \qquad (13)$$

$$H_{AB}^2 = (H_{AB}^\circ)^2 \exp[-\beta(r-\sigma)] \qquad (14)$$

The distance dependence of the bimolecular electron transfer rate can be assessed by substituting the previously described nonadiabatic electron transfer rate expression

into eqs 10 and 11. Eq 14 accounts for the distance dependence of H_{AB}, where β is a measure of the conductivity of the medium between the two redox centers, and follows from the straightforward treatment of tunneling through a classically impenetrable barrier.[57]

A major problem with testing the validity of bimolecular theories, such as the ones described above, lies in the difficulty with designing homogeneous systems which incorporate both the effects of normal and inverted electron transfer and the dependence of these two pathways on distance. To this end, chemiluminescence (cl) is an excellent probe of bimolecular electron transfer processes. A chemiluminescence reaction is described by the potential energy curve diagram shown in Figure 4 where driving force to produce excited state and ground state products is defined by ΔG°_{es} and ΔG°_{gs} respectively, and the activation barrier for excited state production is ΔG_{es}^{*}.[58] In this figure the reaction is so exergonic that the reactant well has become imbedded in the ground state product well. Unlike a typical thermal reaction a luminescent excited state product well is now energetically accessible and can be populated by classical barrier crossing. The excited state production efficiency, ϕ_{es}, is related to the ratio of the two competing pathways for excited state and ground state production (defined by k_{es} and k_{gs}, respectively).

$$\phi_{es} = k_{es} / (k_{es} + k_{gs}) \qquad (15)$$

Figure 4. Potential energy curve description of chemiluminescence. ΔG°_{es} and ΔG°_{gs} are reaction free energies for electron transfer to produce excited- and ground-state products, respectively, and ΔG^{*} is the activation energy for the excited-state reaction. k_{es} and k_{gs} are the electron transfer rates for production of excited- and ground-state products, respectively.

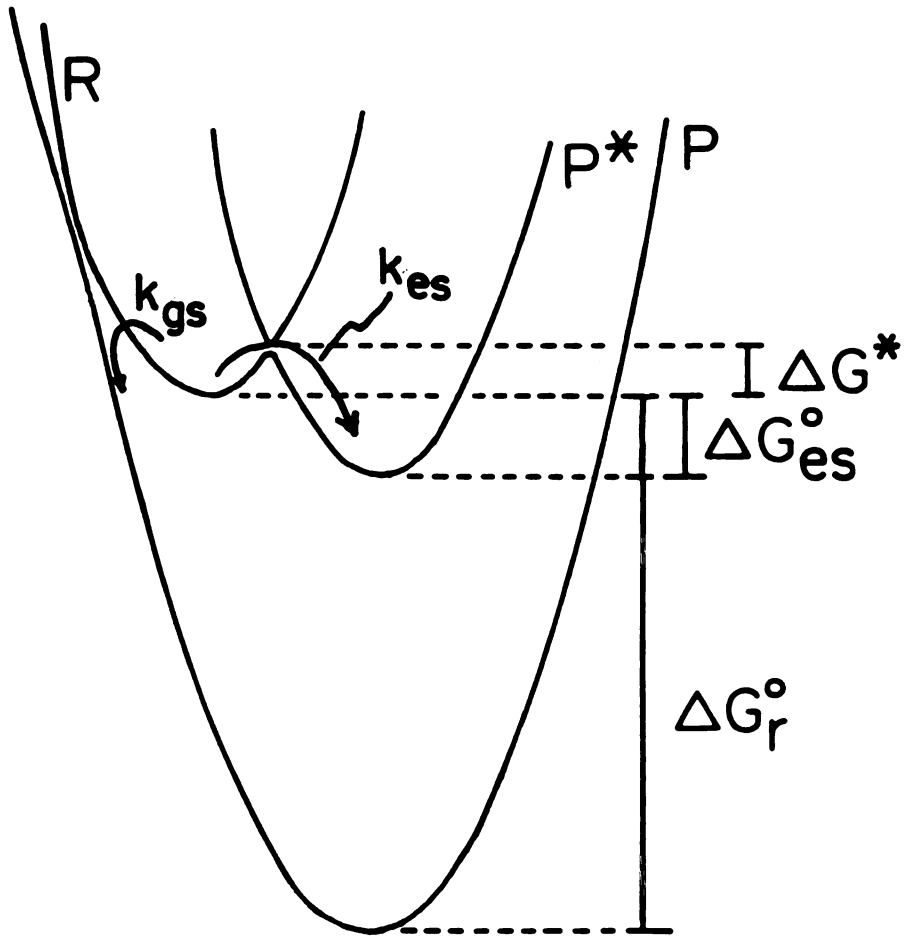

Figure 4

The overall quantum yield of chemiluminescence, ϕ_{cl}, is simply the product of ϕ_{es} and the steady-state emission quantum yield ϕ_e.

$$\phi_{cl} = \phi_e \phi_{es} \tag{16}$$

Since ϕ_e is an intrinsic property of the luminescent excited state, it is ϕ_{es} that is fundamentally descriptive of the efficiency of the chemiluminescent process. In a chemiluminescent system, electron transfer in the normal region (i.e., chemiluminescence pathway) will produce a photon, while reaction in the inverted region (i.e., ground state pathway) will be photometrically silent. Thus a measure of the photons emitted per electrons transferred allows ϕ_{cl} to be experimentally determined, and by eq 16 provides a direct probe of kinetics of electron transfer in the normal and inverted region.

The issue of chemiluminescence efficiencies is not only important for determining fundamental mechanistic features of highly exergonic electron transfer but is also important in a practical sense. Because cl represents a chemical energy to light energy conversion process, several applications of cl chemistry to the design of chemical based laser systems,[59-60] light emitting devices,[62,63] and electro-optical devices have been suggested. Of course the

practical development of such devices relies on developing systems with high overall efficiencies.

Our interest in cl has centered on the electron-transfer chemistry of the hexanuclear cluster system $M_6X_8Y_6^{2-}$ (M = Mo, W; X, Y = Cl, Br, I) whose structure consists of an octahedral core of metal atoms coordinated by eight face-bridging and six axial halides (Figure 5). These cluster systems exhibit long-lived highly emissive excited states [e.g. τ_o = 180 μsec, ϕ_e = 0.20 for $Mo_6Cl_{14}^{2-}$ in CH_3CN at 23°C] and also can be oxidized and reduced by one-electron in nonaqueous solution.[64a] The magnitude of these oxidation and reduction potentials, coupled with the low energy of the emissive excited state of these clusters permits the luminescent excited state to be populated directly upon the exchange of an electron between $M_6X_8Y_6^-$ and $M_6X_8Y_6^{3-}$. If the reactant precursors are generated electrochemically, the overall process is called electrogenerated chemiluminescence (ecl). The ecl chemistry of the $M_6X_8Y_6^{2-}$ clusters is exemplified by the molybdenum chloride cluster, whose spectroscopic and electrochemical properties are summarized in the energy diagram in Scheme 2.

Figure 5. Structure of $M_6X_8Y_6^{2-}$ ions: ● = Mo(II), W(II); X,Y = Cl, Br, I.

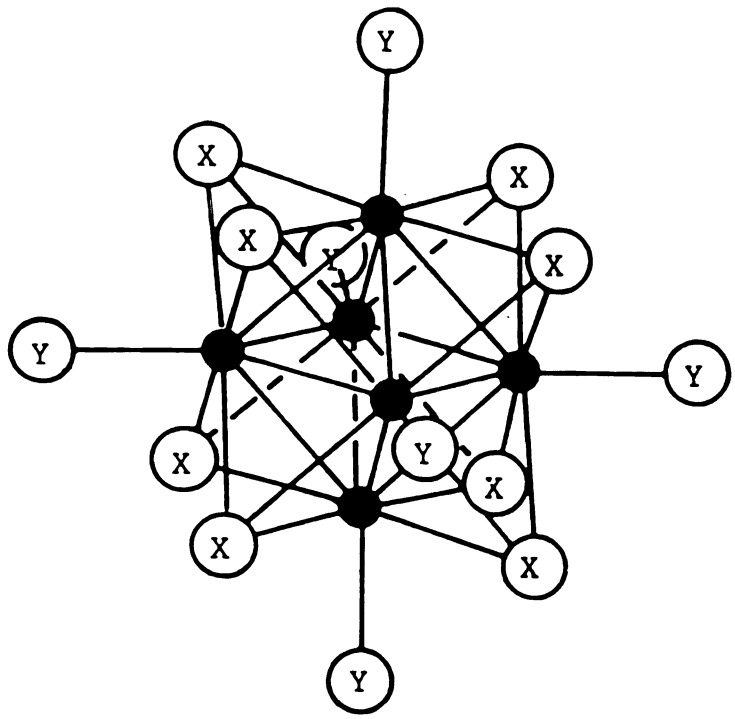

Figure 5

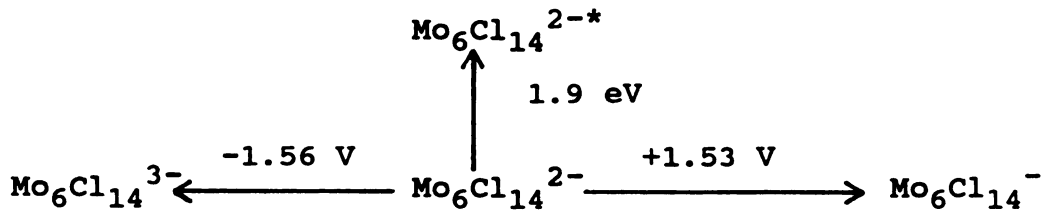

Potentials versus SCE

Scheme 2

Electrogeneration of $Mo_6Cl_{14}^{-}$ and $Mo_6Cl_{14}^{3-}$ leads to red cl attributable to the production of electronically excited $Mo_6Cl_{14}^{2-*}$ according to the following annihilation reaction,[65]

$$Mo_6Cl_{14}^{-} + Mo_6Cl_{14}^{3-} \longrightarrow Mo_6Cl_{14}^{2-*} + Mo_6Cl_{14}^{2-} \quad (17)$$

The $M_6X_8Y_6^{2-}$ clusters offer an unique opportunity to study the mechanism of bimolecular electron transfer in the normal and inverted region, and provides an ideal system to elucidate the factors governing chemiluminescence efficiencies. Described herein is our electron-transfer studies of the $M_6X_8Y_6^{2-}$ system. A fundamental issue in ecl chemistry that heretofore has not been addressed is how the electrochemical excitation energy between the electrogenerated oxidized and reduced parent molecules is distributed. As presented in Chapter III the cluster systems have allowed the issue of energy distribution to be addressed for the first time. Moreover, the cluster ions possess unique properties which allow other important ecl

and electron transfer mechanistic issues to be investigated. A problem of paramount importance that has eluded identification is the factors governing partitioning between the inverted and normal reaction pathways. The large overpotential in the $M_6X_8Y_6^{2-}$ ecl reaction, has allowed the driving force dependence of the ecl efficiencies and hence the partitioning, to be defined. These studies are discussed in Chapter IV. With the information garnered from the studies of Chapters III and IV, the effects of solvent, supporting electrolyte, temperature and ligand substitution on ecl efficiencies are described in Chapter V.

CHAPTER II

II. EXPERIMENTAL

A. Synthetic Methods

1. Preparation of Hexanuclear Molybdenum Clusters

Molybdenum dichloride, purchased from Cerac Inc., was dissolved in 6 M HCl and filtered to remove any insoluble impurities. The volume of the yellow HCl solution was reduced approximately to one quarter. As the solution cooled, long narrow yellow crystals of $(H_3O)_2Mo_6Cl_{14}$ formed in the beaker. The crystals were collected, heated to 150°C for 2 h in vacuo to remove any excess HCl and H_2O, and subsequent heating to 210 °C decomposed $(H_3O)_2Mo_6Cl_{14}$ to Mo_6Cl_{12}. The 150 °C preheating step improved the quality of the final Mo_6Cl_{12} product. The tetrabutylammonium salt was prepared by the addition of NBu_4Cl (Southwestern Analytical) to a 6 M HCl solution containing Mo_6Cl_{12}. The yellow precipitate was collected and washed several times with water and ethanol. The $(NBu_4)_2Mo_6Cl_{14}$ was multiply recrystallized by slow evaporation of CH_2Cl_2 previously dried over $MgSO_4$.

Disubstituted clusters, $Mo_6Cl_{12}X_2^{2-}$ (X = Br, I, SCN), were prepared by addition of X^- to an ethanolic solution of Mo_6Cl_{12}. For the case of $Mo_6Cl_{12}(SCN)_2^{2-}$, the complex slowly precipitated out of solution upon simple addition of NBu_4SCN (made by the metathesis of NaSCN and NBu_4Cl in ethanol) to Mo_6Cl_{12} solution. For the halide clusters, a small amount of the appropriate hydrohalic acid was initially added to the ethanolic solution of Mo_6Cl_{12}. Subsequent addition of excess NBu_4Br or NBu_4I, yielded the

tetrabutylammonium salt of the cluster. The purification of thiocyanate and halide cluster complexes was accomplished by multiple recrystallizations from methanol and dichloromethane, respectively.

The axially substituted $Mo_6Cl_8X_6^{2-}$ (X = Br, Cl, I) clusters were prepared by dissolving Mo_6Cl_{12} in ethanol and then adding enough HBr or HI to yield a 1:1 volume ratio of ethanol:hydrohalic acid.[66] The exchange of the axial chlorides with either bromide or iodide, was accomplished by boiling the solution until the volume was reduced by 50 percent. A small volume of ethanol was added to redissolve the solid that formed during the heating process. Addition of NBu_4I or NBu_4Br to hot solutions promptly afforded a yellow precipitate of $(NBu_4)_2Mo_6Cl_8Br_6$ or $(NBu_4)_2Mo_6Cl_8I_6$, respectively. The suspensions were gently heated and stirred overnight to ensure complete exchange of the axial halides. These cluster complexes were purified by using procedures analogous to that of the tetrabutylammonium salt of $Mo_6Cl_{14}^{2-}$.

The preparation of $Mo_6Cl_8Cl_{6-n}Y_n$ (n = 3,4,5; Y = Br, I, SCN) necessitates stoichiometric control of the substitution reaction at the axial ligand sites. This was accomplished by removing the axial chloride ligands of Mo_6Cl_{12} with the appropriate number of equivalents of silver ion. For example, $(NBu_4)_2Mo_6Cl_{10}(SCN)_4$ was obtained with the addition of two equivalents of silver p-toluenesulfonate (Aldrich) to a methanol solution of Mo_6Cl_{12}. The AgCl precipitate was

removed from solution by filtration and the tetrathiocyanate cluster was obtained by addition of an excess of NBu_4SCN to the filtrate. The precipitate was collected, washed with ethanol, and recrystallized from methanol. The chloro-bromo and chloro-iodo clusters were synthesized by similar procedures; however, recrystallization of these compounds was performed in CH_2Cl_2.

The preparation of $NBu_4Mo_6Cl_{13}$ was accomplished by the addition of slightly more than one equivalent of silver p-toluenesulfonate to an acetonitrile solution of $(NBu_4)_2Mo_6Cl_{14}$. The reaction was performed under dilute conditions (< 5 mmolar) and stirred overnight to (i) ensure the removal of only one chloride ligand and (ii) inhibit the precipitation of $Ag_2Mo_6Cl_{14}$. The AgCl precipitate was removed by filtration and the filtrate was evaporated to dryness in vacuo to yield $NBu_4Mo_6Cl_{13}$. The crude product was dissolved in CH_2Cl_2 and filtered to remove any insoluble Mo_6Cl_{12} that had formed during reaction. The filtered solution was dried over $MgSO_4$, and the CH_2Cl_2 was evaporated to yield crystalline product.

Monosubstituted bromide, iodide, pyridine and thiocyanate clusters were made by adding slightly more than one equivalent of the corresponding ligand (tetra-butylammonium salts of the anion donor ligand) to an acetonitrile solution of $Mo_6Cl_{13}^-$. The solvent was then removed under vacuum and the resulting solid was washed with

methanol to remove any excess ligand. All the monosubstituted clusters were recrystallized from CH_2Cl_2.

The preparation of Mo_6 bromide clusters was facilitated by the fact that molybdenum dibromide could be purchased from Cerac Inc. The commercial $MoBr_2$ was purified by dissolving it into ethanol followed by filtration to remove any insoluble impurities. The ethanol was removed by evaporation leaving a yellow-orange residue of Mo_6Br_{12}-$(HOCH_2CH_3)_2$. Mo_6Br_{12} could be isolated by heating the ethanol complex under vacuum for several hours.

The tetrabutylammonium salt of $Mo_6Br_{14}^{2-}$ was prepared by addition of NBu_4Br to a ethanolic/HBr solution of Mo_6Br_{12}. The dark yellow precipitate was washed with water and ethanol, and recrystallized several times from CH_2Cl_2 which had been dried over $MgSO_4$. The tetrabutylammonium salts of the substituted molybdenum bromide clusters $Mo_6Br_8Br_{6-n}Y_n$ (n = Cl, I) were prepared and purified by the analogous procedure described for that of the corresponding substituted $Mo_6Cl_8Cl_{6-n}Y_n$ clusters.[67]

2. <u>Preparation of Hexanuclear Tungsten Clusters</u>

The method of Dorman and McCarley[68] was used with slight modification to prepare tungsten dichloride. In a typical reaction 15 g of WCl_6, 1.35 g of Al metal, 6.75 g of NaCl, and 10.00 g of $AlCl_3$ were added in a dry box to a quartz reaction tube. The tube was capped with a rubber septum, removed from the drybox and connected to a high

vacuum manifold, evacuated for 1 h, and then flame sealed under dynamic vacuum. The contents were thoroughly mixed and the reaction vessel was placed into a high temperature furnace. The furnace was heated to a temperature of 210 °C to initiate the reaction which was allowed to equilibrate at this temperature for 6 h. The temperature was then raised to 450 °C over a 3 h period, held at 450 °C for 9 h, and finally raised to 550 °C where it was held for 24 h. The tube was allowed to cool to room temperature. The contents were collected by wrapping the tube in several sheets of paper, and carefully cracking it open with a blunt object (**Caution:** violent explosions sometimes resulted). The black fused solid was dissolved in 6 M HCl/ethanol solution and was filtered to remove any insoluble reaction products. The light yellow filtrate was reduced in volume and, upon cooling, greenish-yellow crystals of $(H_3O)_2W_6Cl_{14}$ formed. The crystals were collected and heated in a furnace at 350 °C for 2 h under a dynamic vacuum to form W_6Cl_{12}. The tetrabutylammonium salt of $W_6Cl_{14}^{2-}$ was prepared by addition of NBu_4Cl to an ethanolic/HCl solution of W_6Cl_{12}. The precipitate was collected, washed with water and ethanol, and recrystallized several times from CH_2Cl_2.

Tungsten dibromide was prepared in a similar manner as tungsten dichloride. To the quartz reaction tube 15 g of WBr_5, 0.72 g of Al metal, 7.50 g of NaBr, and 13.0 g of $AlBr_3$ were added in the drybox. The reaction conditions were identical to those used for the preparation of W_6Cl_{12}.

The black solid product was dissolved into a solution of 6 M HBr and ethanol, the solution was filtered, and evaporated over gentle heating to near dryness. The residue was collected, dissolved in ethanol, and the insoluble alkali salts were removed by filtration. The ethanol was allowed to evaporate to afford greenish crystals of $W_6Br_{12}(HOCH_2CH_3)_2$. The tetrabutylammonium salt of $W_6Br_{14}^{2-}$ was prepared by addition of NBu_4Br to an ethanol:HBr solution of $W_6Br_{12}(HOCH_2CH_3)_2$. $(NBu_4)_2W_6Br_{14}$ was recrystallized several times from acetonitrile solutions.

Tungsten diiodide was prepared by the method of Hogue and McCarley[69] with slight modifications. To a quartz reaction tube 1.00 g of $K_2W_6Cl_{14}$, 9.97 g of KI and 3.60 g of LiI were added in the dry box. The reaction tube was removed from the drybox, placed under vacuo, and after 1 h it was flame sealed under dynamic vacuum. The reaction tube was placed into a furnace and the temperature was raised over a 1 1/2 h period to 550 °C. After 1 h at 550 °C the tube was allowed to cool to room temperature and was opened carefully (**Caution**: violent explosions sometimes resulted). The black solid was washed with water to remove alkali salts and iodine. The remaining yellow-brown solid was extracted with ethanol to give a deep golden brown solution of W_6I_{12} which was isolated by evaporation of ethanol and subsequent heating of the solid under vacuum. The tetrabutylammonium salt of $W_6I_{14}^{2-}$ is obtained by addition of NBu_4I to an ethanol solution of W_6I_{12}. The dark yellow powder was

collected, washed several times with ethanol, and recrystallized several times from dry CH_3CN to yield pure $(NBu_4)_2W_6I_{14}$.

Mixed tungsten halide clusters, $W_6X_8Y_6^{2-}$ (X, Y = Cl, Br, I) were prepared by dissolving $(W_6X_8)X_4$ in ethanol and 6 M hydrohalic acid HY where $X \neq Y$. The solubility of the cluster in HY decreases along the series HCl > HBr > HI and thus a larger amount of ethanol must be added. To ensure complete exchange of axial halides the resultant solution was evaporated to near dryness with moderate heating. When preparing $W_6I_8Y_6$ (Y = Cl, Br), gentle heating under a vacuum aspirator was required. An insoluble precipitate formed when the solution was heated too rigorously. The residue, collected from solvent evaporation was redissolved in ethanol: 6 M HY solutions. The tetrabutylammonium salt was obtained by addition of excess NBu_4Y to the ethanol/HY solution. The mixed halide tungsten clusters $(NBu_4)_2W_6X_8Y_6$ were recrystallized several times from either dry CH_3CN or CH_2Cl_2.

3. <u>Organic Donors and Acceptors</u>

Nitroaromatics and aromatic amines, with the exception of tris(p-tolyl)amine which was synthesized following published procedures[70], were obtained from commercial sources (Aldrich Chemical Company, Alfa Products, and Pfaltz and Bauer). Solids were purified by recrystallization followed by vacuum sublimation and liquids

were purified by fractional distillation. The pyridinium salts were synthesized by addition of either methyl iodide or benzyl chloride to a 1:1 acetone/ethanol solution of the appropriately substituted pyridine. Isonicotinamide (Sigma), 4-cyanopyridine (Aldrich) and isonitotinic acid ethyl ester (Sigma) were used without subsequent purification. The bipyridinium salts were synthesized by dissolving the appropriate bipyridine (4,4'-dimethyl-2,2'-bipyridine, 4,4'-bipyridine, 2,4-bipyridine, 2,2'-bipyridine and 1,2-bis(2-pyridyl)ethylene were purchased from Aldrich and used as received) in a neat solution of methyl iodide, 1,2-dibromoethane (Aldrich), 1,3-dibromopropane (Matheson, Coleman & Bell) or 1,4-dibromobutane (Aldrich), and by gently heating these solutions overnight. The resulting precipitate was collected and washed with ethanol and acetonitrile to remove any starting compound or monosubstituted products. The filtrate could be heated further to generate additional disubstituted product. Pyridinium and bipyridinium hexafluorophosphate salts were obtained by the addition of ammonium hexafluorophosphate to aqueous solutions of the bromo, chloro or iodo salt, and were twice recrystallized from acetone/water solutions.

4. Supporting Electrolytes

Tetrabutylammonium hexafluorophosphate and perchlorate (Southwestern Analytical Chemicals) and tetrabutylammonium tetrafluoroborate (Aldrich) were

dissolved in ethyl acetate, dried over $MgSO_4$, and recrystallized from pentane/ethyl acetate solutions. The salts were dried in vacuo for 12 h at 60 °C to ensure that the ethyl acetate was completely removed. Tetramethylammonium and tetraethylammonium hexafluorophosphate (Fluka) were dissolved in acetonitrile and recrystallized from a water/acetonitrile solution and dried in vacuo for 12 h at 100 °C. Potassium hexafluoroarsenate (Ozark-Mahoning) and trifluoromethane sulfonic acid were converted into their corresponding tetrabutylammonium salts by dissolving them in water and adding excess NBu_4Br. The resulting precipitate was collected and dried in vacuo at 60°C for 12 h. Lithium and sodium perchlorate (Fischer Scientific) were recrystallized from acetonitrile solution and dried under vacuo at 100°C for 6 h.

5. Solvents

Dichloromethane, acetonitrile, acetone, dimethylformamide, and 1,2-dichloroethane purchased from Burdick & Jackson Laboratories (distilled in glass grade), were subjected to seven freeze-pump-thaw (fpt) cycles and vacuum distilled onto 4-Å molecular sieves (except acetonitrile where 3-Å molecular sieves were used) contained in a 1-liter round-bottom flask equipped with a high-vacuum Teflon value. Because acetone undergoes a condensation reaction in acidic media to produce mesityl oxide, it was vacuum distilled from the sieves after 24 h. Butyronitrile and benzonitrile were

purchased from Aldrich (Gold Label) and were used as received. Propionitrile, purchased from Aldrich was treated with dilute HCl to remove isonitrile and after the extraction, was sequentially dried over $MgSO_4$ and CaH_2, and finally fractionally distilled from P_2O_5. Butyronitrile, benzonitrile, and propionitrile were subjected to seven fpt cycles and vacuum distilled onto 4-Å molecular sieves.

B. Experimental Methods

1. Characterization of Molybdenum and Tungsten Clusters

A thorough characterization of all the molybdenum and tungsten cluster systems was performed by negative ion Fast Atom Bombardment Mass Spectrometry (FABMS). The technique utilizes a 10 keV Xenon beam which bombards a sample placed in a high viscosity, low vapor pressure matrix. The energy from the beam is transferred to the matrix which causes desorption of matrix sample ions into the gas phase. The negative ions generated during the absorption process, were isolated and recorded to give fingerprint spectra of each cluster. FABMS is a superior analytical method for the synthesized clusters because substituted halide clusters are easily detected. The detailed experimental results and a general discussion of the usefullness of this technique is presented elsewhere.[71]

2. Electrochemical Measurements

Formal reduction potentials of acceptors and donors were determined by cyclic voltammetry using a Princeton Applied Research (PAR) Model 173 potentiostat, Model 175 programmer, and a Model 179 digital coulometer. The output of the digital coulometer was fed directly into a Houston Instrument Model 2000 X-Y recorder. A three-electrode system was used with a standard H-cell configuration. The working electrode was a Pt button, the auxiliary electrode was a Pt gauze and an Ag wire served as an adequate reference potential by using ferrocene as an internal standard.[72] Potentials were related to the SCE reference scale by using a ferrocenium-ferrocene couple of 0.31 V *vs.* SCE. The molybdenum and tungsten cluster potentials were measured under high vacuum conditions in a single compartment cell (vida infra) to obtain accurate $E_{1/2}$ potentials.

3. Quenching Measurements

Electron-transfer quenching rate constants for the reaction of $Mo_6Cl_{14}^{2-*}$ with nitroaromatics, aromatic amines, and pyridinium compounds in CH_3CN and CH_2Cl_2 ($[(NBu_4)_2Mo_6Cl_{14}]$ = 3 mM, μ = 0.1 M NBu_4ClO_4) were determined from Stern-Volmer plots of the $Mo_6Cl_{14}^{2-*}$ luminescence intensity. The quenching rate constants of $Mo_6Cl_{14}^{2-*}$ by 4,4′-dimethoxydiphenylamine and 3,5-dichloro-*p*-benzoquinone in CH_3CN, acetone and propionitrile

[$(NBu_4)_2Mo_6Cl_{14}$ = 1 mM] were determined from Stern-Volmer plots of $Mo_6Cl_{14}^{2-*}$ lifetimes. Additionally, the Stern-Volmer lifetime method was used to study the energy-transfer quenching of $Mo_6Cl_{14}^{2-*}$ and $W_6X_8Y_6^{2-*}$ by $W_6X_8Y_6^{2-}$ or $Mo_6Cl_{14}^{2-}$, respectively, in CH_2Cl_2. Stern-Volmer experiments were performed over a quencher concentration range of 5 x 10^{-4} to 1 x 10^{-1} M and Stern-Volmer constants were calculated by using $\tau_o(Mo_6Cl_{14}^{2-*})$ = 180 μ sec in CH_3CN, = 160 μ sec in CH_2Cl_2, = 170 μ sec in acetone, = 148 μ sec in propionitrile, $\tau_o(W_6I_{14}^{2-*})$ = 19 μ sec in CH_2Cl_2 and $\tau_o(W_6I_8Br_6^{2-*})$ = 16 μ sec in CH_2Cl_2 at 23 °C.

Quenching experiments were performed in a specially constructed high-vacuum cell, consisting of a 1-cm cuvette attached to a sidearm terminating with a 10-ml round-bottom flask. Solvents were vacuum distilled into the quenching cell and freeze-pump-thawed three times. All quencher additions were performed under high vacuum conditions. Luminescence intensities (λ_{exc} = 436 nm) were measured on a high resolution emission spectrometer and emission lifetimes (λ_{exc} = 355 nm) were acquired with a pulsed laser system (Nd:YAG, FWHM = 8ns). Both instruments were constructed at Michigan State University and are described elsewhere.[73]

4. <u>Electrogenerated Chemiluminescence</u>

(i) <u>Quantum Yields</u>

A triple step square wave potential sequence generated by the PAR 175 programmer was used to establish

ecl reactions. The potential limits of the program sequence were chosen to ensure production of electrogenerated intermediates in the mass-controlled region. The electrochemical cell employed in ecl measurements was a cylindrical, single-compartment high-vacuum cell. A sidearm permitted solvents to be transferred into the cell by vacuum distillation and two sample chargers allowed cluster and electroactive acceptor or donor to be added independently to the working electrode compartment while maintaining the isolated environment of the electrochemical cell. Two tungsten wires sealed in uranium glass served as electrical leads to the Pt mesh auxiliary electrode and an Ag wire quasi-reference electrode. The auxiliary and reference electrodes were positioned parallel to a Pt disk working electrode (A = 0.0314 cm^2) which was positioned centrosymmetrically along the cylindrical axis of the working compartment. The Pt disk was spectroscopically viewed through a fused silica window which constituted the bottom surface of the electrochemical cell. After each experiment the Pt disk electrode was polished with 1 μm diamond paste and 0.05 μm alumina purchased from Bioanalytical Systems.

Ecl spectra and quantum yield experiments were performed in solutions containing 0.1 M supporting electrolyte and equimolar concentrations of $Mo_6Cl_{14}^{2-}$ and electroactive acceptor or donor. Samples for all ecl experiments were prepared by transferring the appropriate

amount of solvent under a high-vacuum manifold (1×10^{6} to 5×10^{-6} torr) into the cell sidearm which contained supporting electrolyte previously heated at 100 °C for 1 h. After 3 fpt cycles, the solution was thoroughly mixed and poured into the working chamber by slowly rotating the cell by 90°. The current response of the solution containing only supporting electrolyte was recorded before undertaking ecl measurements. Background current densities of 48 $\mu A/cm^2$ in CH_3CN and 35 $\mu A/cm^2$ in CH_2Cl_2 were measured at potential limits of -2.0 V and +2.0 V.

The quantum yield for ecl is defined by the following expression where I is the total ecl intensity (einsteins/sec)

$$\phi_{ecl} = \int_0^t I dt/Q \qquad (18)$$

over a finite period of time t and Q is the total cathodic or anodic charge. The ecl yield is equivalent to the number of photons produced per electron transferred and consequently ϕ_{ecl} can be determined by measuring the number of photons emanating from the electrode surface and the number of equivalents of electrogenerated species. The latter quantity can be measured coulometrically by monitoring the anodic, Q_A, or cathodic, Q_C, charge passed into solution during an ecl experiment. Q_A and Q_C were determined by pulsing from the foot of one wave to the

diffusion controlled region of the other. In regard to the former quantity, absolute ecl intensity measurements were performed by using an EG & G Electro-Optics 550-19 integrating sphere and an EG & G Model 550-1 photometer/radiometer equipped with an EG & G Model 550-2 multiprobe detector. A flat response between 450 and 1100 nm was achieved by fitting the multiprobe with a radiometric filter attachment provided by EG & G. Appropriate corrections were made for the radiometric filter attachment which allowed only 14 percent of the light to be transmitted. Integration of the ecl intensity was accomplished by using a Model 550-3 pulse integrator. Calibration of the integrating sphere was performed by EG & G Electro-Optics Division by using photometric sources certified by the National Bureau of Standards. This calibration led to a correction factor of 3774 at the wavelength of $Mo_6Cl_{14}^{2-}$ emission.

Ecl yields were calculated with appropriate corrections for reflectivity of the electrode and non-faradaic contributions to the integrated current according to the methods described by Bard.[74] The reflectance of the polished Pt disk electrode was taken to be 0.67 at the wavelength of $Mo_6Cl_{14}^{2-}$ emission. The double layer charging components q_A and q_C were measured by pulsing the electrode between an anodic limiting potential set at the foot of the oxidation wave and a cathodic limiting potential set at the foot of the reduction wave. From these potential limits,

q_A's and q_C's were measured in 200 mV increments by setting the anodic and cathodic limiting potential 200 mV negative and positive, respectively. Plots of q_A and q_C vs. $\Delta E^{3/2}$ were linear and the background current passed at potentials used in ecl experiments were obtained by extrapolation of this plot.

Measurements of the ecl efficiency of $Ru(bpy)_3^{2+}$, which has been determined in several previous studies, was undertaken in an effort to allow us to check our experimental apparatus and procedure. An acetonitrile solution containing $Ru(bpy)_3^{2+}$ (μ = 0.1 M NBu_4ClO_4, $[Ru(bpy)_3^{2+}]$ = 3 mM) was prepared in the high-vacuum electrochemical cell and ecl measurements were performed with the integrating sphere contained in a light-tight box. An ecl yield for a single run was determined from twenty measurements of the intensity generated from a single triple-step potential sequence. The system was allowed to equilibrate 30 seconds between each pulse sequence. The overall yield calculated from five separate experiments was $\phi_{ecl}[Ru(bpy)_3^{2+}] = 0.046 \pm 0.004$. This value is in good agreement with the previously reported efficiency of 0.05 in CH_3CN at 23°C.[75]

Quantum yield measurements of all ecl systems followed procedures similar to those described above. For $Mo_6Cl_{14}^{2-}$/acceptor and donor systems the cluster ion and electroactive reagent were contained in separate sample chargers. Prior to the addition of a given acceptor or

calculated directly from the following expression, where ϕ°_{ecl} is the ecl efficiency of

$$\phi_{ecl} = \phi^{\circ}_{ecl} \cdot \frac{Q^{\circ}}{Q} \cdot \frac{I}{I_o} \qquad (19)$$

$Mo_6Cl_{14}^{2-}$ (μ = 0.1 M NBu_4ClO_4 in CH_3CN or CH_2Cl_2 at 23°C), Q° and Q are the charges passed into solution, and I° and I are the measured integrated photon intensities of solution containing cluster and solution containing cluster and donor or acceptor, respectively. Ecl yields were calculated from averaging three experimental runs of ten measurements; error limits of ϕ_{ecl}, measured by this method, were ± 15% in CH_3CN and ± 10% in CH_2Cl_2.

Ecl quantum yields for the $Mo_6Cl_{14}^{2-}/W_6X_8Y_6^{2-}$ systems and all systems described in Chapter V were calculated relative to ϕ_{ecl} of $Mo_6Cl_{14}^{2-}$ for the former and to ϕ_{ecl} of $Ru(bpy)_3^{2+}$ for the latter.

(ii) Spectra

Ecl spectra of $Mo_6Cl_{14}^{2-}$/acceptor and donor systems were recorded between 350 and 1100 nm, and between 550 nm and 1050 nm for $Mo_6Cl_{14}^{2-}/W_6X_8Y_6^{2-}$ ecl spectra. Spectra were obtained interfacing the specially designed electrochemical cell directly to the detection side of the emission spectrometer. The lock-in amplifier was referenced to the ecl signal with the cycle synchronous output of the

donor to the working electrode compartment, the ecl yield of a solution containing only $Mo_6Cl_{14}^{2-}$ was determined from the average of a minimum of ten pulses. Donor or acceptor was then introduced to the solution and ϕ_{ecl} was measured by using a pulse sequence with potential limits appropriate to the system under investigation. This procedure permitted us to identify anomalous ecl measurements by monitoring the $Mo_6Cl_{14}^{2-}$ ecl efficiency. Error limits for $Mo_6Cl_{14}^{2-}$/donor and acceptor ϕ_{ecl} values, determined from three experimental runs composed of ten ecl intensity measurements, were ± 12% in CH_3CN and ± 10% in CH_2Cl_2.

Accurate determination of ϕ_{ecl} for acceptor and donor systems exhibiting the weakest ecl intensities were hampered by the low throughput of the integrating sphere. For these systems, the electrochemical cell was positioned directly on the face of the multiprobe detector. The ecl efficiencies of $Mo_6Cl_{14}^{2-}$/acceptor and donor systems were estimated using $Mo_6Cl_{14}^{2-}$ as a relative standard. In an experimental run, $Mo_6Cl_{14}^{2-}$, was initially added to the solution and the ecl yield was determined from a minimum of twenty intensity measurements. The electroactive organic reagent was then added to the solution and the ecl yield for the $Mo_6Cl_{14}^{2-}$ /acceptor or donor system was recorded. In this manner, errors due to geometric positioning of the cell on the detector were minimized. Because the spectral distributions of the two experiments are identical, the ecl quantum yield of $Mo_6Cl_{14}^{2-}$/acceptor and donor system, ϕ_{ecl}, can be

PAR 175 programmer. The single compartment cell is very similar to the one previously described except the optical window is on the side of the cell. The working electrode is a platinum disk (area = 0.0707 cm^2) sealed in glass but whose face is now perpendicular to the bottom of the cell. The Pt disk electrode was positioned at the focal point of the collection lens on the detection side of the emission spectrometer. The ecl was generated by using a cyclic square wave (10 to 20 Hz) with potential limits appropriate for the system under investigation.

Ecl spectra were recorded on a Zenith microcomputer. The deconvolution of $Mo_6Cl_{14}^{2-}/W_6X_8Y_6^{2-}$ ecl spectra was performed by a band shape analysis in which varying ratios of the steady state emission spectra of the discrete cluster systems were added until their sum identically matched that of the measured ecl spectrum. Energy partitioning values were obtained by normalizing the calculated ratio with the emission quantum yields of the two cluster systems. Errors in the partitioning ratio were determined by three measurements of the $Mo_6Cl_{14}^{2-}/W_6X_8Y_6^{2-}$ ecl spectrum and multiple deconvolutions of each spectrum.

CHAPTER III

III. ELECTROCHEMICAL EXCITATION ENERGY PARTITIONING IN MIXED CLUSTER ELECTRON TRANSFER REACTIONS

A. Background

A fundamental issue of chemiluminescence reactivity, which heretofore has not been resolved, involves the parentage of the luminescent excited molecule produced in the electron transfer reaction between electrogenerated oxidized and reduced reactants. For instance, in the $M_6X_8Y_6^{2-}$ system, the energy released in the annihilation reaction is sufficient to leave only one cluster anion in its excited state. The important question here is whether the electronically excited ion is generated from $M_6X_8Y_6^-$ ion or the $M_6X_8Y_6^{3-}$ ion. The energy partitioning between these two parentages is ultimately related to differences in the activation barrier heights and electronic variations of the two discrete electron transfer pathways shown below.

$$M_6X_8Y_6^- + M_6X_8Y_6^{3-} \longrightarrow M_6X_8Y_6^{2-*} + M_6X_8Y_6^{2-} \quad (20a)$$

$$M_6X_8Y_6^- + M_6X_8Y_6^{3-} \longrightarrow M_6X_8Y_6^{2-} + M_6X_8Y_6^{2-*} \quad (20b)$$

Thus, partitioning of the electrochemical excitation energy between reactants in ecl reactions has important electron transfer implications and will shed light on factors that limit the overall efficiency of ecl reactions.

For all ecl systems to date, the partitioning issue has not been successfully addressed because there has been no simple way of labelling the oxidized or reduced reactant and therefore identifying the parent of the excited state. One

approach is to employ structurally similar reactants which possess energetically distinct luminescent excited states, thereby allowing the parentage of the excited state species to be identified spectroscopically. An attempt to identify the precursor of the excited state in an ecl system was undertaken in a recent study of ruthenium polypyridine complexes where the electrochemical properties of ruthenium reactants and spectroscopic properties of the ecl products could be tuned with the polypyridyl ligation coordination sphere.[76] Relevant photophysical and electrochemical properties of these systems are shown in Table 1. The investigated reactions are shown in eq 21 and 22 where the distinct emission energies give rise to different ecl

$$Ru(DTB\text{-}bpy)_3^{3+} + Ru(bpy)_2biq^{+} \rightarrow Ru(DTB\text{-}bpy)_3^{2+*} + Ru(bpy)_2biq^{2+} \quad (21a)$$

$$Ru(DTB\text{-}bpy)_3^{3+} + Ru(bpy)_2biq^{+} \rightarrow Ru(DTB\text{-}bpy)_3^{2+} + Ru(bpy)_2biq^{2+*} \quad (21b)$$

$$Ru(bpy)_3^{3+} + Ru(bpy)_2DMCH^{+} \rightarrow Ru(bpy)_3^{2+*} + Ru(bpy)_2DMCH^{2+} \quad (22a)$$

$$Ru(bpy)_3^{3+} + Ru(bpy)_2DMCH^{+} \rightarrow Ru(bpy)_3^{2+} + Ru(bpy)_2DMCH^{2+*} \quad (22b)$$

spectra for the two pathways. However, several problems were encountered with those ruthenium polypyridyl systems. These problems included: (1) the free energy of reaction 21 is not large enough to produce the excited state of Ru(DTB-

Table 1

Excited State Energies and Electrochemical Properties of Ru-Polypyridyl Complexes in Acetonitrile

		E_{0-0}/eV[d]	$E_{1/2}(2+/+)$[e] vs. SCE/V	$E_{1/2}(3+/2+)$[f]
1.	$Ru(DTB\text{-}bpy)_3^{2+}$ [a]	2.16	-1.44	+1.11
2.	$Ru(bpy)_2(biq)^{2+}$ [b]	1.70	-0.91	+1.33
3.	$Ru(bpy)_3^{2+}$	2.13	-1.35	+1.26
4.	$Ru(bpy)_2(DMCH)^{2+}$ [c]	1.72	-1.00	+1.25

[a] DTB-bpy = ditertbutylbipyridine
[b] bpy = bipyridine and biq = 2,2'-biquinoline
[c] DMCH = 6,7-dihydro-5,8-dimethylbenzo[b,j][1,10]phenanthroline
[d] O-O energy of the ruthenium complexes emitting excited state
[e] As reduction potentials for the $Ru^{2+/+}$ couple vs. SCE
[f] As reduction potentials for the $Ru^{3+/2+}$ couple vs. SCE

bpy)$_3^{2+}$ and thus reaction pathway 21a is energetically unfavorable; (2) the oxidation potentials of Ru(bpy)$_3^{2+}$ and Ru(bpy)$_2$DMCH^{2+} are similar and hence do not permit selective production of Ru(bpy)$_3^{3+}$ and therefore the annihilation cannot cleanly be established; and finally (3) favorable energy-transfer reactions between the ruthenium products permitted the excited state energy to be redistributed between both products thereby vitiating meaningful energy partitioning ratios to be determined from measured ecl intensities. For these reasons, the authors correctly concluded that reactions 21 and 22 were not useful in gathering quantitative energy partitioning data.

Many of the problems inherent to the ruthenium polypyridyl complexes are circumvented by the $M_6X_8Y_6^{2-}$ ions. Similar to the ruthenium complexes, the luminescent excited state and electrochemical properties of $M_6X_8Y_6^{2-}$ ions can also be varied with the ligating coordination sphere; and therefore, the approach established by reactions 20a and 20b can be pursued with mixed cluster systems (e.g. $M_6X_8Y_6^{-}$ + $M_6X_8Y_6^{3-} \longrightarrow M_6X_8Y_6^{2-*}$ or $M_6X_8Y_6^{2-*}$). However, unlike the complicating problem of the system described by reaction 21, the relatively large oxidizing and reducing potentials of $M_6X_8Y_6^{2-}$ ions compared with the relatively low excited state energies allows for the possibility of either product to be left in its electronic excited state in the annihilation reaction. Furthermore, the problem associated with reaction 22 is avoided owing to significantly different redox couples

of substituted M_6 cores. Of equal significance, the poor overlap between the absorption and emitting states of substituted M_6 cores means that energy transfer is inefficient. Thus, the measured ecl emission of $M_6X_8Y_6^{2-}$ and $M_6X_8Y_6^{2-}$ should accurately reflect the original partitioning of the electrochemical excitation energy in the annihilation reaction. The results presented in this chapter successfully address for the first time, the effect of energy partitioning in an ecl annihilation event as well as shed light on important electron transfer properties of $M_6X_8Y_6^{2-}$ ions.

B. Results and Discussion

Electrochemical and photophysical properties of the molybdenum and tungsten halide cluster systems in CH_2Cl_2 at room temperature are shown in Tables 2 and 3. Most of the cluster systems exhibit reversible one-electron oxidation processes. The criteria used to establish reversibility were i_a/i_c ratios varying between 0.95 to 1.05 and linear plots of anodic and cathodic peak currents vs. (scan rate)$^{1/2}$. Anodic to cathodic peak separations of the reversible cluster systems were comparable to that measured for ferrocene (125 mV), thereby establishing that deviations of ΔE_p from the theoretical value of 59 mV are due primarily to uncompensated cell resistance. The remaining M_6 clusters either possess an irreversible oxidation couple or multiple oxidation waves with the first being chemically

Table 2

Emission Maxima and Electrochemical Properties for Mo_6 Clusters in CH_2Cl_2

Mo_6 Clusters	λ_{max}/nm[a]	$E_{1/2}(-/2-)$[b] vs. SCE/V	$E_{1/2}(2-/3-)$[b]
$Mo_6Cl_{14}^{2-}$	766	+1.36	-1.70
$Mo_6Cl_{12}Br_2^{2-}$	778	+1.37	-1.66
$Mo_6Cl_8Br_6^{2-}$	790	+1.34	-1.67
$Mo_6Cl_{12}I_2^{2-}$	799	+1.43[c], 1.52[d], 1.72[d]	-1.60
$Mo_6Cl_8I_6^{2-}$	823	+1.42[c]	-1.55
$Mo_6Cl_{12}(SCN)_2^{2-}$	767	+1.61[c], 1.64[d], 1.80[d]	-
$Mo_6Cl_{10}(SCN)_4^{2-}$	761	2.10[c], 2.16[d]	-
$Mo_6Cl_{12}(PBu_3)_2$	750	+0.71	-1.79
$Mo_6Br_{14}^{2-}$	789	+1.14	-1.81[c]
$Mo_6Br_{12}Cl_2^{2-}$	779	+1.07	-1.92[c]
$Mo_6Br_8Cl_6^{2-}$	750	+1.11	-1.89[c]
$Mo_6Br_8I_6^{2-}$	822	+1.00	-1.85[c]

[a] Emission maxima measured in CH_2Cl_2 corrected for emission spectrometer response.
[b] As reduction potentials for the $Mo_6^{-/2-}$ and $Mo_6^{2-/3-}$ couple vs. SCE.
[c] Reduction couple is irreversible, values reported are peak potentials.
[d] Multiple oxidation couples.

Table 3

Emission Maxima and Electrochemical Properties for W_6 Clusters in CH_2Cl_2

W_6 Clusters	λ_{max}/nm[a]	$E_{1/2}(-/2-)$[b] vs. SCE/V	$E_{1/2}(2-/3-)$ vs. SCE/V
$W_6Cl_{14}^{2-}$	833	+0.93	-[c]
$W_6Cl_8Br_6^{2-}$	814	+0.99	-[c]
$W_6Cl_8I_6^{2-}$	800	+0.96	-[c]
$W_6Br_{14}^{2-}$	751	+0.80	-[c]
$W_6Br_8Cl_6^{2-}$	761	+0.77	-[c]
$W_6Br_8I_6^{2-}$	746	+0.74	-[c]
$W_6I_{14}^{2-}$	698	+0.57	-[c]
$W_6I_8Br_6^{2-}$	700	+0.56	-[c]
$W_6I_8Cl_6^{2-}$	700	+0.58	-[c]

[a] Emission maximums measured in CH_2Cl_2 corrected for emission spectrometer response.
[b] As reduction potentials for the $W_6^{-/2-}$ couple vs. SCE.
[c] The $W_6^{2-/3-}$ couple is in the background of CH_2Cl_2.

irreversible. In general, clusters exhibiting multiple oxidation waves contain ligands that are weakly bonded (e.g. I^- or SCN^-) in the axial positions. For example, the cyclic voltammograms of $Mo_6Cl_{12}L_2^{2-}$ (L = SCN, I) and Mo_6Cl_{12} are shown in Figure 6. In panel a, scanning a Pt electrode immersed in a CH_3CN solution containing Mo_6Cl_{12}, anodically produces two quasireversible waves at +1.73 V and +1.92 V potentials. These two waves are preserved in the cyclic voltammograms of $Mo_6Cl_{12}(SCN)_2^{2-}$ and $Mo_6Cl_{12}I_2^{2-}$ (Figure 6b and 6c). The preceding irreversible wave at +1.43 and +1.61 in the cyclic voltammograms of $Mo_6Cl_{12}I_2^{2-}$ and $Mo_6Cl_{12}(SCN)_2^{2-}$ respectively, is due to oxidation of dissociated I^- and SCN^-. That the potentials for this oxidation do not correspond to those of free ligand suggests dissociation subsequent to cluster oxidation. Of course the absence of L in Mo_6Cl_{12} precludes the appearance of this preceding irreversible oxidation wave. The similarity of the oxidation profiles of Mo_6Cl_{12} and $Mo_6Cl_{12}L_2^{2-}$ suggest facile dissociation of the heterodonor ligand from the cluster core to give Mo_6Cl_{12}.

Whereas oxidation of the clusters is generally reversible, the reduction of the clusters are for the most part irreversible processes. This is not the case, however, for $[Mo_6Cl_8]X_6^{2-}$ and $[Mo_6Cl_8]X_5L^-$ (X = halide, L = donor ligand) ions, which possess reversible or more typically quasi-reversible one-electron reduction couples. All other Mo_6 clusters possess irreversible reduction waves. For the

Figure 6. Cyclic voltammograms of (0.1 NBu_4PF_6 at 23°C) (a) Mo_6Cl_{12} (3 mM in CH_3CN); (b) $Mo_6Cl_{12}I_2^{3-}$ (3 mM in CH_2Cl_2); (c) $Mo_6Cl_{12}(SCN)_2^{2-}$ (3 mM in CH_2Cl_2).

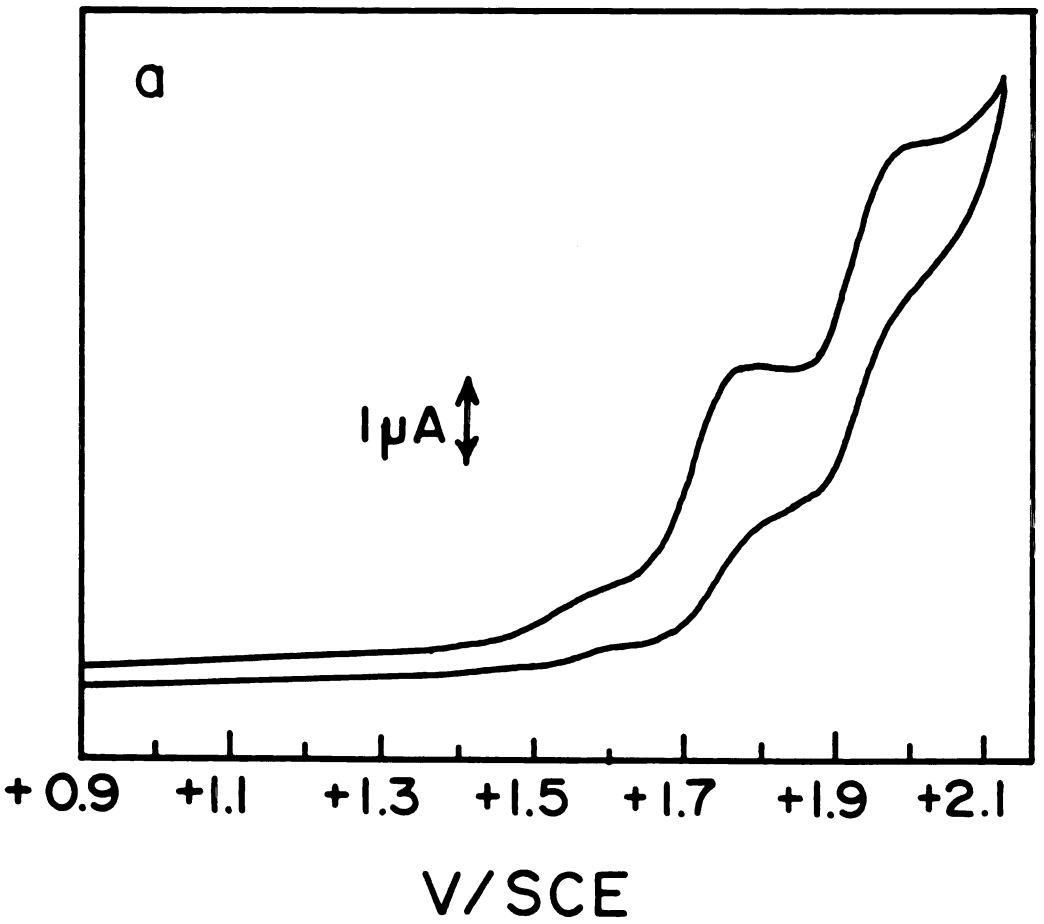

Figure 6

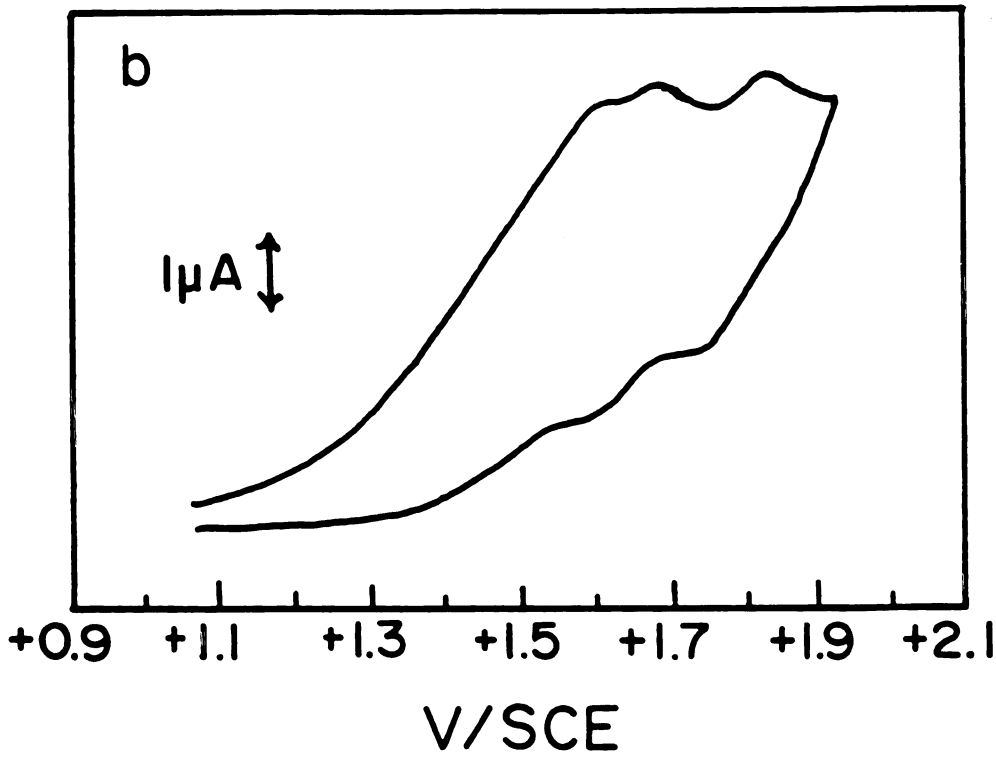

Figure 6

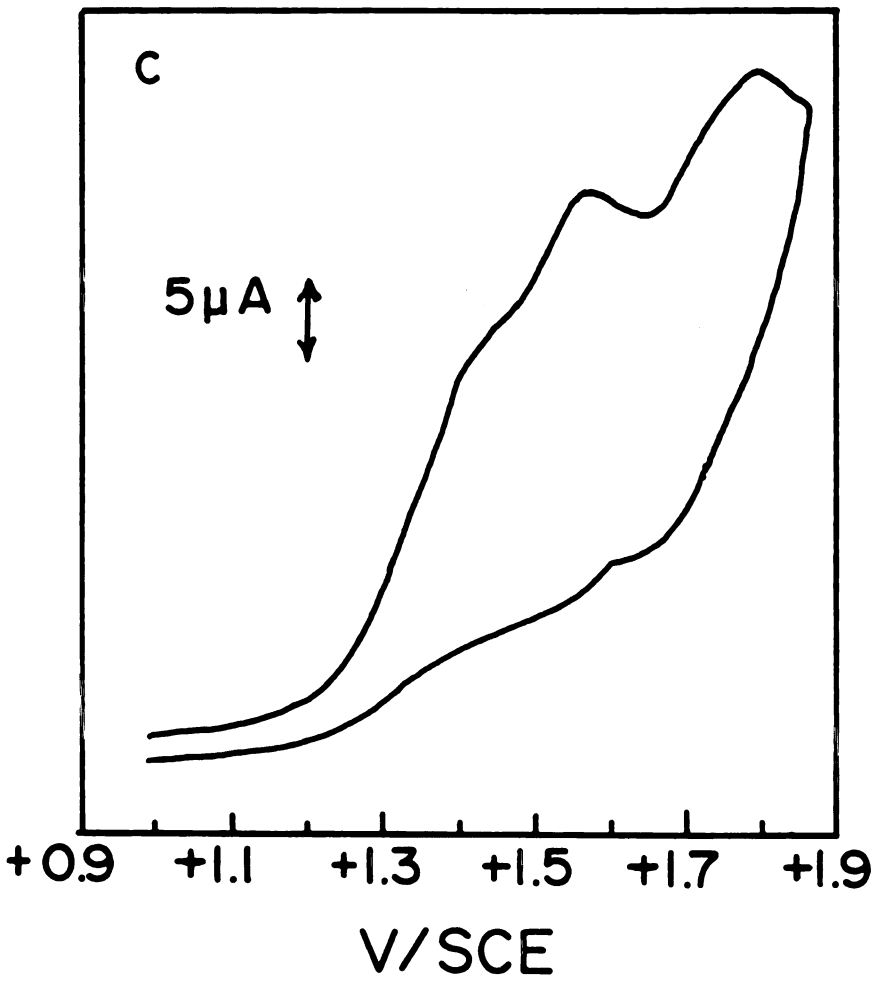

Figure 6

case of the tungsten clusters, the reduction waves are in the background of CH_2Cl_2 thereby implying reduction at potentials < -2.2 V.

Except for the thiocyanate and phosphine clusters, ecl is observed for the Mo_6 clusters shown in Table 2 at a platinum electrode according to the simple annihilation reaction shown in eq 17 (the properties of these ecl reactions will be discussed in Chapter V). Conversely, the tungsten halide clusters of Table 3 produce weak or no ecl at a platinum electrode surface ($\phi_{ecl} \leq 10^{-5}$) in THF presumably due to the fact that the reduced cluster anion $W_6X_8Y_6^{3-}$ cannot cleanly be electrogenerated. However, the issue of interest here is not ecl reactions of reactants electrogenerated from the same parent molecule, but ecl systems which permit the partitioning of the electrochemical energy to be distinguished (i.e. reaction 20). The choice of the appropriate cluster systems for such studies relies on $M_6X_8Y_6^{2-}$ and $M_6X_8Y_6^{2-}$ possessing sufficiently different emission energies such that the electrochemically produced excited state can be spectroscopically distinguished. Experimentally a difference of 50 nm in the emission spectra of $M_6X_8Y_6^{2-}$ and $M_6X_8Y_6^{2-}$ can easily be resolved. Moreover, appropriate reduction potentials are critical to the selective production of only one oxidized and one reduced reactant in the annihilation reaction. The $M_6X_8Y_6^{-/2-}$ potential must be at least 100 mV negative of the $M_6X_8Y_6^{-/2-}$ potential and the $M_6X_8Y_6^{2-/3-}$ potential must be 100 mV

positive of the $M_6X_8Y_6^{2-/3-}$ potential for reaction 20 to be established.

The choice of mixed cluster systems for ecl annihilation studies can now be made with facility upon inspection of the data in Table 2 and 3. Because the tungsten halide clusters possess reversible oxidation couples, but irreversible reduction couples, the W_6 clusters can only be used as monoanions in the annihilation reaction of mixed cluster ecl systems. The choice for a trianion in the mixed cluster ecl systems is limited to clusters with the formula of $Mo_6Cl_8Cl_nX_{6-n}^{2-}$ (n = 0-6) (X = Br, I) because only these clusters possess reversible reduction potentials. Owing to mechanistic problems (which will be discussed in Chapter V) with the ecl reaction of clusters with Br or I occupying axial coordination positions, the only reasonable choice for the trianion in the mixed cluster ecl reaction is $Mo_6Cl_{14}^{3-}$.

Because the $W_6X_8Y_6^{-/2-}$ redox couples are negative of the $Mo_6Cl_{14}^{-/2-}$ redox couple and the $W_6X_8Y_6^{2-/3-}$ redox couples are more negative than the reduction of $Mo_6Cl_{14}^{2-}$, the following electron-transfer reaction can cleanly be

$$Mo_6Cl_{14}^{3-} + W_6X_8Y_6^{-} \rightarrow Mo_6Cl_{14}^{2-*} + W_6X_8Y_6^{2-} \quad (23a)$$

$$Mo_6Cl_{14}^{3-} + W_6X_8Y_6^{-} \rightarrow Mo_6Cl_{14}^{2-} + W_6X_8Y_6^{2-*} \quad (23b)$$

$$Mo_6Cl_{14}^{3-} + W_6X_8Y_6^{-} \rightarrow Mo_6Cl_{14}^{2-} + W_6X_8Y_6^{2-} \quad (23c)$$

established by standard electrochemical techniques. Inspection of Tables 2 and 3 reveals that the $W_6X_8Y_6^{2-}$ excited state energies are significantly different than that of $Mo_6Cl_{14}^{2-}$. These features permit the calculation of partitioning ratios directly from ecl spectra of the $Mo_6Cl_{14}^{2-}/W_6X_8Y_6^{2-}$ systems if one assumes that subsequent energy transfer between the products in reactions 23a and 23b is unimportant. In order to determine whether this assumption is valid, energy transfer studies were undertaken where the quenching of $W_6X_8Y_6^{2-*}$ and $Mo_6Cl_{14}^{2-*}$ by $Mo_6Cl_{14}^{2-}$ and $W_6X_8Y_6^{2-}$, respectively, was measured. Quenching rate constants in CH_2Cl_2 for the following reactions,

$$Mo_6Cl_{14}^{2-*} + W_6X_8Y_6^{2-} \longrightarrow Mo_6Cl_{14}^{2-} + W_6X_8Y_6^{2-*} \qquad (24a)$$

$$Mo_6Cl_{14}^{2-} + W_6X_8Y_6^{2-*} \longrightarrow Mo_6Cl_{14}^{2-*} + W_6X_8Y_6^{2-} \qquad (24b)$$

were deduced from classical Stern-Volmer analysis of the cluster lifetimes and the results of these studies are displayed in Table 4. Because both cluster ions emit, the individual lifetimes were determined from a multiexponential fit of the luminescence decay with the equation $y = ae^{-t/\tau_1} + be^{-t/\tau_2}$ by using the general nonlinear curve-fitting program Kinfit[77a] where a and b represent the fractions of total emission decay described by the excited-state lifetimes τ_1 and τ_2, respectively. Convergence of the fit, monitored by the sum of the squares of the residuals, yields

Table 4

Energy Transfer Quenching of $M_6X_8Y_6^{2-}$ Clusters in CH_2Cl_2

Lumophore	Quencher	$\Delta G°/eV$[a]	$k_q/M^{-1}s^{-1}$[b]
$W_6I_8Br_6^{2-}$	$Mo_6Cl_{14}^{2-}$	-0.15	9×10^7
$W_6I_{14}^{2-}$	$Mo_6Cl_{14}^{2-}$	-0.15	2×10^7
$W_6Br_{14}^{2-}$	$Mo_6Cl_{14}^{2-}$	0.0	-
$Mo_6Cl_{14}^{2-}$	$W_6Br_8Cl_6^{2-}$	0.0	4.2×10^6
$Mo_6Cl_{14}^{2-}$	$W_6Cl_{14}^{2-}$	>-0.1	5×10^4
$Mo_6Cl_{14}^{2-}$	$W_6Cl_8Br_6^{2-}$	>-0.1	$< 10^4$

[a] Driving force for energy transfer from the lumophore to quencher; $\Delta G° = (E_{0-0}^{Q} - E_{0-0}^{L})$.

[b] Quenching rate constants determined from multiexponential fits of lifetime data.

values for a, b, τ_1 and τ_2. For an individual reaction pair, obviously only one energy transfer reaction, 24a and 24b, will be energetically downhill. Because endergonic energy transfer is a relatively inefficient process,[77b] only the exothermic energy transfer reaction will result in an attenuation of cluster's lifetime. For instance for the case of the $Mo_6Cl_{14}^{2-}/W_6I_{14}^{2-}$ system reaction 24a is endergonic and therefore the $Mo_6Cl_{14}^{2-}$ lifetime does not change. On the other hand, the exergonicity of reaction 24b (-0.15 eV) results in a quenching of the $W_6I_{14}^{2-}$ lifetime with increasing concentration of $Mo_6Cl_{14}^{2-}$. The experimental manifestation of these energetics is that the $Mo_6Cl_{14}^{2-}$ is the quencher and its lifetime is constant while $W_6I_{14}^{2-}$ is the lumophore and its lifetime follows a classical Stern-Volmer dependence. The largest quenching rates are only 10^7 despite significant driving forces for some reactions. In the context of a Forster energy transfer mechanism, the poor spectral overlap of the absorbing and emitting states precludes efficient energy-transfer quenching.[77b] In a Dexter energy transfer treatment, the good orbital overlap of reactants required for efficient energy transfer is precluded by the fact that the metal localized emissive excited state of $M_6X_8Y_6^{2-}$ ions is sterically shielded by the halide coordination sphere.[77b] Thus, because the observed energy transfer rates are well below the diffusion controlled limit of $\sim 10^9$, energy transfer is unimportant in energy partitioning studies and

measured excited state production yields should accurately reflect the partitioning of the electrochemical excitation energy.

In Table 5 are shown the photophysical properties and overall ecl quantum yields of the mixed cluster ecl systems employed for partitioning studies. Chemiluminescence from CH_2Cl_2 solutions containing $Mo_6Cl_{14}^{2-}$ and $W_6X_8Y_6^{2-}$ is observed when the applied potential of a Pt electrode is stepped into the oxidation wave of $W_6X_8Y_6^{2-}$ and the reduction wave of $Mo_6Cl_{14}^{2-}$. Overall ecl quantum yields were determined by dividing the number of einsteins emanating from the electrode surface by the number of equivalents of $Mo_6Cl_{14}^{3-}$ or $W_6X_8Y_6^{-}$ produced.

The partitioning ratios for reactions 23a and 23b for the $Mo_6Cl_{14}^{2-}/W_6I_{14}^{2-}$, $W_6I_8Br_6^{2-}$, and $W_6Cl_8Br_6^{2-}$ systems can be directly determined from ecl spectra. An exemplary mixed cluster ecl spectrum of the $Mo_6Cl_{14}^{2-}/W_6I_{14}^{2-}$ system is illustrated in Figure 7. The broad featureless band is characteristic of $M_6X_8Y_6^{2-}$ cluster emission. The larger signal-to-noise ratio of the ecl spectra, as compared to the steady-state luminescence spectra, is due to mechanical agitation of the solution over the duration of the relatively long pulse sequence typically needed for ecl experiments. The driving force to produce either $Mo_6Cl_{14}^{2-*}$ or $W_6I_{14}^{2-*}$, calculated by summing the 0-0 energy of the emitting excited state with the ground state reaction free energy ($\Delta G_{es} = \Delta G_{gs} + E_{0-0}$) as determined from standard

Table 5

Photophysical Properties and Overall Ecl Quantum Yields of $M_6X_8Y_6^{2-}$ Clusters Used in Mixed Cluster Ecl Reactions

Mixed Cluster System	ϕMo_6[a]	ϕW_6[b]	ϕecl[c]
$Mo_6Cl_{14}^{2-}/W_6I_{14}^{2-}$	0.18	0.30	0.004
$Mo_6Cl_{14}^{2-}/W_6I_8Br_6^{2-}$	0.18	0.18	0.005
$Mo_6Cl_{14}^{2-}/W_6Br_8Cl_6^{2-}$	0.18	0.09	0.040
$Mo_6Cl_{14}^{2-}/W_6Br_{14}^{2-}$	0.18	0.13	0.095
$Mo_6Cl_{14}^{2-}/W_6Cl_{14}^{2-}$	0.18	0.015	0.050
$Mo_6Cl_{14}^{2-}/W_6Cl_8Br_6^{2-}$	0.18	0.03	0.060

a Steady-state emission quantum yield measured in CH_2Cl_2 at 23°C.

b Steady-state emission quantum yields estimated from the measured lifetime in CH_2Cl_2 and measured emission quantum yields in acetonitrile (ref. 64b).

c Overall ecl quantum yields for mixed cluster ecl systems in CH_2Cl_2, μ = 0.1 M NBu_4PF_6 at 23°C.

Figure 7. Electrogenerated chemiluminescence spectrum of $Mo_6Cl_{14}^{3-}/W_6I_{14}^{-}$ in CH_3CN (μ = 0.1 M NBu_4PF_6 at 23°C).

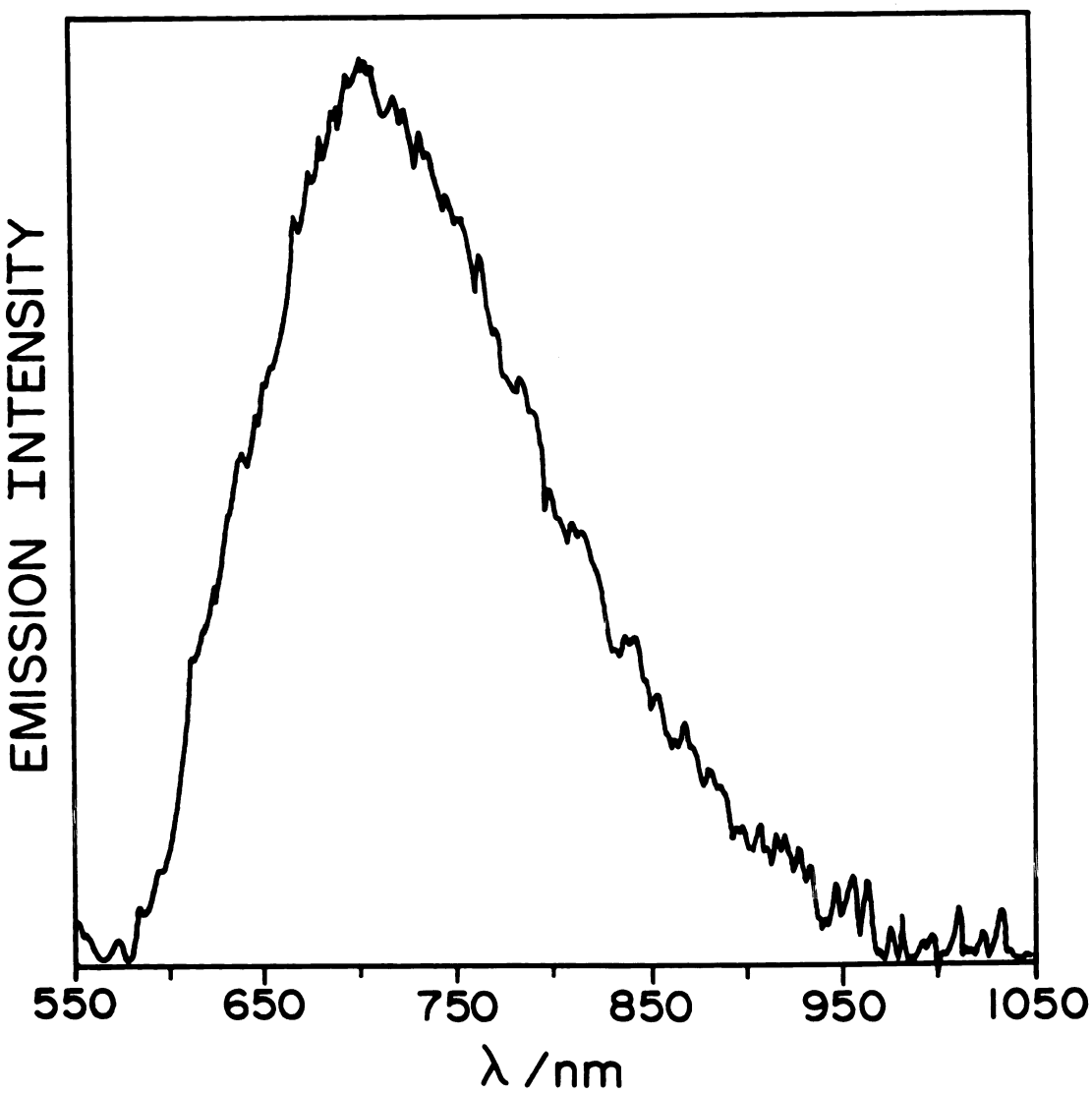

Figure 7

reduction potentials, is energetically downhill for both reaction pathways. Figure 8a shows the ecl spectrum of $Mo_6Cl_{14}^{2-}/W_6I_{14}^{2-}$ superimposed on the steady-state emission spectra of the individual cluster ions. It is clearly evident from Figure 8a, that the ecl spectrum is composed of the emission spectra of $Mo_6Cl_{14}^{2-}$ and $W_6I_{14}^{2-}$. The partitioning between reactions 23a and 23b is obtained, as shown in Figure 8b, by adding together varying amounts of the steady-state emission spectra of $Mo_6Cl_{14}^{2-}$ and $W_6I_{14}^{2-}$ until the sum is identical to the measured ecl spectrum. The partitioning value, P_R for reactions 23a and 23b is obtained by normalizing the ratio of the measured contribution of the individual (θ_{Mo_6} and θ_{W_6}) to the overall ecl spectrum with the cluster emission quantum yields (ϕ_{Mo_6} and ϕ_{W_6}), where Mo_6 and W_6 represent the $Mo_6Cl_{14}^{2-}$ and $W_6X_8Y_6^{2-}$ cluster ions, respectively.

$$P_R = \frac{\theta_{Mo_6}}{\theta_{W_6}} \times \frac{\phi_{W_6}}{\phi_{Mo_6}} \qquad (25)$$

For the $Mo_6Cl_{14}^{2-}/W_6I_{14}^{2-}$, $W_6I_8Br_6^{2-}$ and $W_6Cl_8Br_6^{2-}$ ecl systems the above analysis provides partitioning ratios, and these ratios are shown in Table 6. In each case, both excited states are produced with essentially equal probability (to within a factor of three) upon annihilation of electrogenerated $Mo_6Cl_{14}^{3-}$ and $W_6X_8Y_6^{-}$.

Figure 8. Steady-state emission and ecl spectrum in CH_3CN for (a) $W_6I_{14}^{2-}$, ——; $Mo_6Cl_{14}^{2-}$ ·····; $Mo_6Cl_{14}^{2-}/W_6I_{14}^{2-}$ ecl, ----; (b) $Mo_6Cl_{14}^{2-}/W_6I_{14}^{2-}$ ecl, ———; fit from the sum of a ratio of $Mo_6Cl_{14}^{2-}$ and $W_6I_{14}^{2-}$ emission spectra, ·····. Peak maxima are normalized to an arbritrary value.

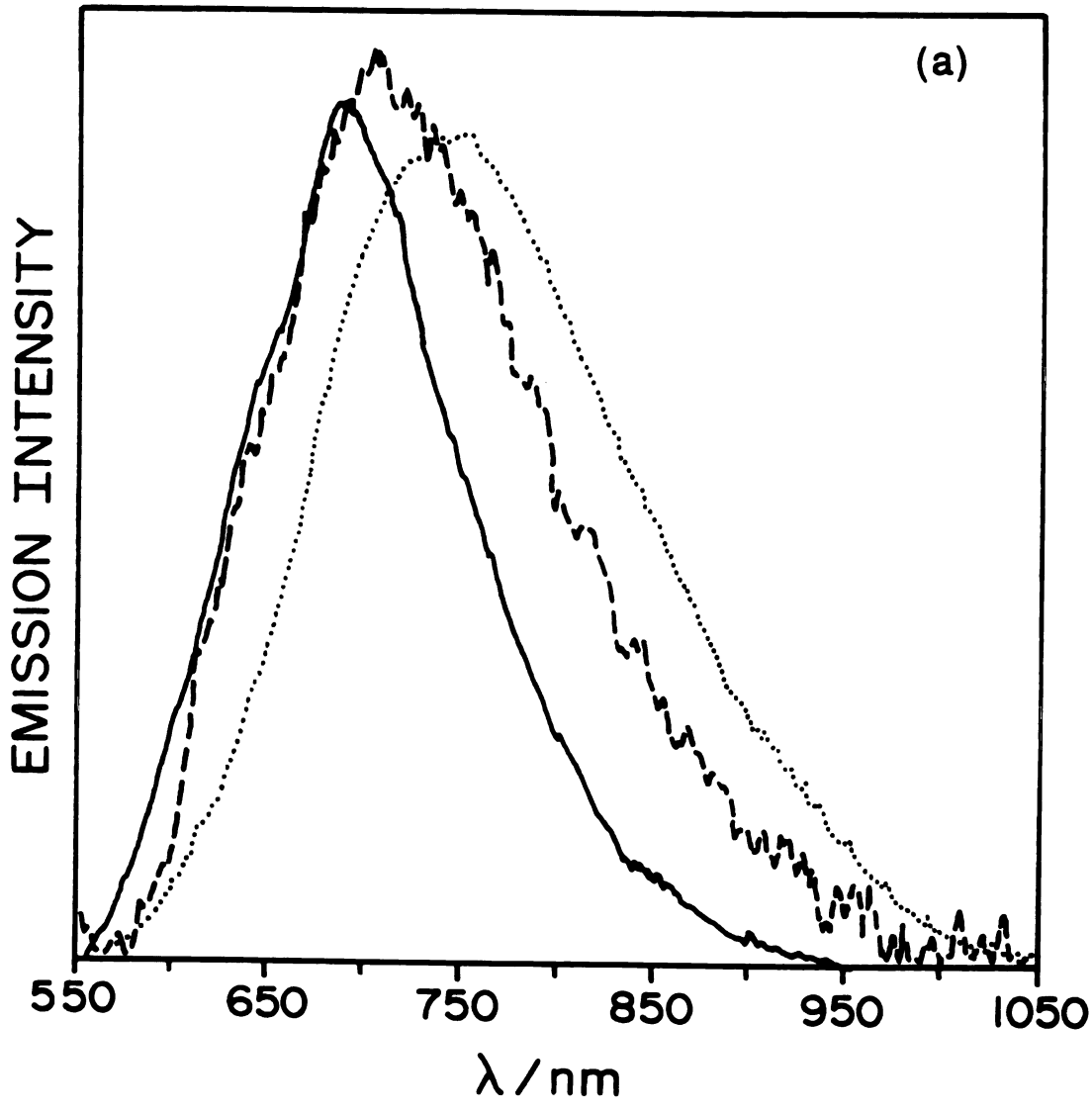

Figure 8

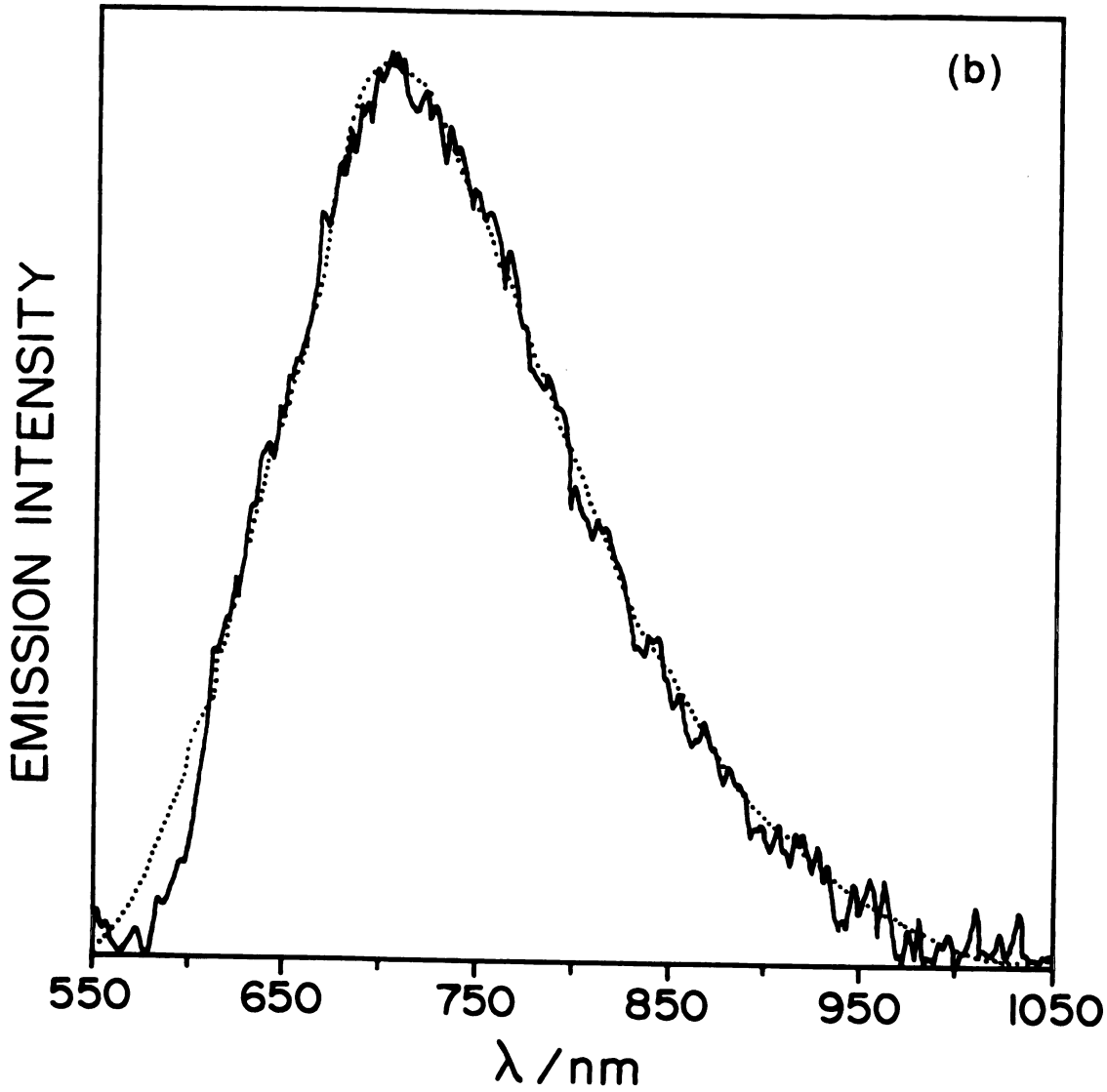
(b)
EMISSION INTENSITY
550
650
750
850
950
1050
λ /nm

Table 6

Driving Forces, Energy Partitioning Ratios and $Mo_6Cl_{14}^{2-}$ Excited State Yields in Mixed Cluster Ecl Reactions

	$Mo_6Cl_{14}^{2-}/W_6X_8Y_6^{2-}$ X,Y[a]	$\Delta G_{es_1}/eV$[b]	$\Delta G_{es_2}/eV$[c]	P_R[d] Mo_6^* : W_6^*	$\phi_{es_2Mo_6}$[e]
1.	I,I	-0.22	-0.07	0.60 : 0.40	0.0018
2.	I,Br	-0.23	-0.08	0.70 : 0.30	0.0028
3.	Br,Br	-0.50	-0.50	0.75 : 0.25	0.075
4.	Cl,Cl	-0.63	-0.53	0:50 : 0.50	0.050
5.	Cl,Br	-0.69	-0.59	0.50 : 0.50	0.050

[a] Mixed cluster ecl system where X and Y represent the face-bridging and axial halides, respectively.
[b] The excited state driving force for reactions 23a.
[c] The excited state driving force for reaction 23b.
[d] Partitioning ratio between reaction 23a and 23b.
[e] Excited state yields for the production of $Mo_6Cl_{14}^{2-*}$ in reaction 23a.

Other mixed cluster systems support this observation (such as those shown in Table 5) but their partitioning ratios can only indirectly be determined from the following equation,

$$\Phi_{ecl} = \phi_{es_1}\ \phi_{Mo_6} + \phi_{es_2}\ \phi_{W_6} \qquad (26)$$

where Φ_{ecl} is the overall ecl quantum yield of the mixed cluster ecl reaction and ϕ_{es_1} and ϕ_{es_2} are the excited state production efficiencies for $Mo_6Cl_{14}^{2-*}$ and $W_6X_8Y_6^{2-*}$, respectively, in the mixed ecl reaction. For example, the small steady-state emission quantum yield of $W_6Cl_{14}^{2-}$ (ϕ_e ($W_6Cl_{14}^{2-}$) = 0.015 vs. ϕ_e ($Mo_6Cl_{14}^{2-}$) = 0.18) requires that $W_6Cl_{14}^{2-*}$ would have to be produced at least two times more often than $Mo_6Cl_{14}^{2-*}$ to be reflected in the mixed-cluster ecl spectrum. The ecl spectrum of $Mo_6Cl_{14}^{2-}/W_6Cl_{14}^{2-}$ identically matches the steady-state emission spectrum of $Mo_6Cl_{14}^{2-}$ and Φ_{ecl} = 0.05. One explanation is that the $W_6Cl_{14}^{2-}$ is not populated upon annihilation. In this case $W_6Cl_{14}^{2-}$is simply acting as an electron acceptor. However this is unlikely because $Mo_6Cl_{14}^{3-}/A^+$ (A^+ = organic electron acceptor) annihilation (discussed in Chapter IV) reactions of similar potentials to that of the $Mo_6Cl_{14}^{2-}/W_6Cl_{14}^{2-}$ system exhibit Φ_{ecl} = 0.10 (CH_2Cl_2, μ = 0.1 M NBu_4PF_6 at 23°). Alternatively, the ϕ_{ecl}'s of the $Mo_6Cl_{14}^{3-}/A^+$ (ϕ_{ecl} = 0.10) and $Mo_6Cl_{14}^{3-}/W_6Cl_{14}^{-}$ (ϕ_{ecl} = 0.05) suggest that half of the electrochemical energy is being distributed to the

$W_6Cl_{14}^{2-}$ excited state. For this case, eq 26 reduces to $\Phi_{ecl} = \phi_{es_1}\ \phi_{Mo_6}$ because $\phi_{es_2}\ \phi_{W_6}$ (= 4 x 10^{-3}) is small compared to $\phi_{es_1}\ \phi_{Mo_6}$ (= 5 x 10^{-2}), and hence the calculated yield from eq 26 is consistent with the experimentally measured ecl yield of 0.05. Our assumption of a 0.50:0.50 partitioning ratio for the $Mo_6Cl_{14}^{2-}/W_6Cl_{14}^{2-}$ system is experimentally supported by the results of the $Mo_6Cl_{14}^{2-}/W_6Cl_8Br_6^{2-}$ system. As discussed above, the partitioning ratio directly calculated from the ecl spectrum of this system is 0.50:0.50. Owing to the similarity of $W_6Cl_{14}^{2-}$ and $W_6Cl_8Br_6^{2-}$ our assumption of a 0.50:0.50 partitioning ratio for $Mo_6Cl_{14}^{2-}/W_6Cl_{14}^{2-}$ ecl system seems reasonable. For the case of the $Mo_6Cl_{14}^{2-}/W_6Br_{14}^{2-}$ system, the emission bands are too close in energy [ΔE_B ($Mo_6Cl_{14}^{2-}$, $W_6Br_{14}^{2-}$) = 15 nm] to be discerned in ecl spectra. Analysis of this system's ecl quantum yields with eq 26 is also consistent with equal partitioning of the electrochemical excitation energy.

There is one very satisfying aspect of the results of partitioning experiments, the free energy dependence of the $Mo_6Cl_{14}^{2-}$ excited state production is independent of the type of electron transfer acceptor. Chapter IV describes the free energy dependence of the ecl quantum yield of the $Mo_6Cl_{14}^{3-}$ with aromatic amines. In these systems the $W_6X_8Y_6^{-}$ has been replaced by an acceptor in which the excited state is energetically inaccessible. A plot of the experimentally determined ecl quantum yields (calculated by

dividing the integrated $Mo_6Cl_{14}^{2-}$ ecl intensity by the number of equivalents of electrons transferred) of $Mo_6Cl_{14}^{2-*}$ for the $Mo_6Cl_{14}^{3-}/W_6X_8Y_6^-$ and $Mo_6Cl_{14}^{3-}/A^+$ (aromatic amine radical cations) systems vs. free energy is shown in Figure 9. The free energy dependence for $Mo_6Cl_{14}^{2-*}$ production in mixed ecl experiments is nearly identical to that observed for the ecl reaction of $Mo_6Cl_{14}^{3-}$ with aromatic amine acceptors. These results demonstrate that the ecl pathway is independent of whether the electrochemical excitation energy is distributed to one or between two excited states in the annihilation reaction.

Thus, the ecl studies on the $W_6X_8Y_6^{2-}$ systems clearly establishes that the electrochemical excitation energy is essentially equally distributed to both cluster reactants. This equal partitioning can be rationalized by using current electron-transfer theories. Annihilation of $Mo_6Cl_{14}^{3-}$ and $W_6X_8Y_6^-$ is described in Scheme 3 where k_d is the diffusional rate constant, k_{es_1} and k_{es_2} are the rate constants to produce the excited state of $Mo_6Cl_{14}^{2-}$ and $W_6X_8Y_6^{2-}$

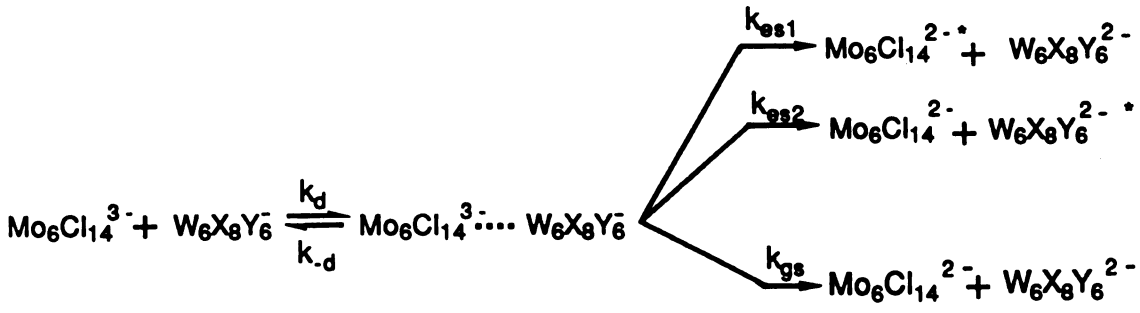

Scheme 3

respectively, and k_{gs} is the rate to produce both ground state molecules. Calculation of electron transfer rate to

Figure 9. Plot of log ϕ_{es} of $Mo_6Cl_{14}^{2-}$ in the mixed cluster ecl reaction (●) and in the reaction of $Mo_6Cl_{14}^{3-}/A^+$ (O) vs. ΔG_{es} in CH_2Cl_2 at 23°C (μ = 0.1 M NBu_4PF_6).

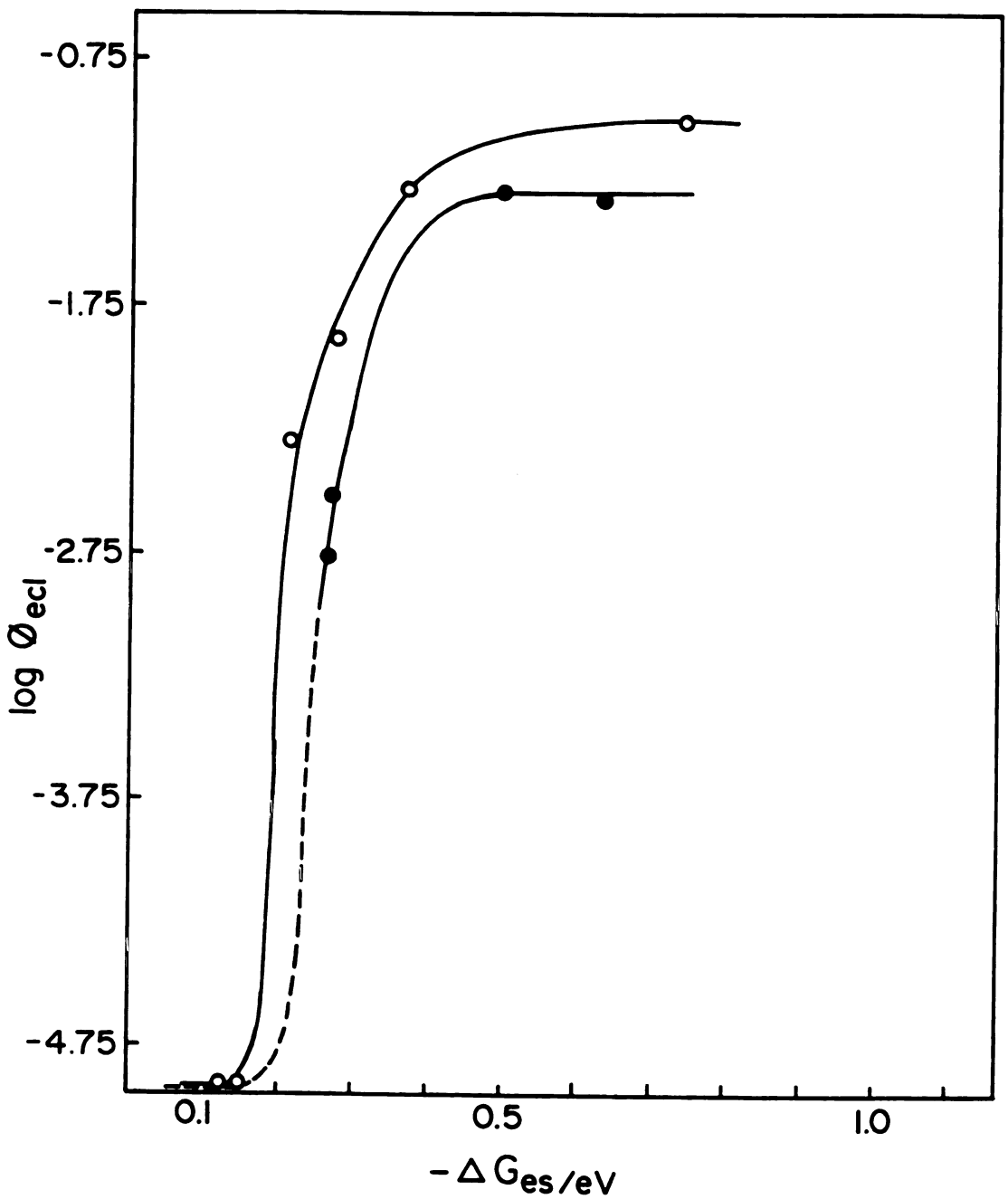

Figure 9

ground state and excited state products, as discussed in detail in Chapter IV, show that k_{gs} is slow compared to k_{es_1} and k_{es_2}. Therefore, the ground state electron-transfer pathway does not mediate the partitioning ratios. Furthermore, a kinetic analysis of the rate of appearance of $Mo_6Cl_{14}^{2-*}$ and $W_6X_8Y_6^{2-*}$ shows the production of $[Mo_6Cl_{14}^{2-*}]$ relative to $[W_6X_8Y_6^{2-*}]$ is just k_{es_1}/k_{es_2}, and is not controlled by the rate of diffusion. Thus an understanding of partitioning ratios follows directly from electron-transfer analysis of k_{es_1} and k_{es_2}.

The excited state product rates k_{es_1} and k_{es_2} are given by eq 27 where the variables have previously been described

$$k_{es_i} = \left[\frac{2(H_{AB})^2}{h}\right]\left[\frac{\pi^3}{\lambda k_B T}\right]^{1/2} \exp - \left[\frac{(\lambda + \Delta G^\circ)^2}{4\lambda k_B T}\right] \qquad (27)$$

(Chapter 1). The almost equal production of $Mo_6Cl_{14}^{2-*}$ and $W_6X_8Y_6^{2-*}$ in the mixed cluster ecl reaction implies that $k_{es_1} \cong k_{es_2}$. The values of k_{es_i}, and hence partitioning of the excited state energy, depends on the electronic coupling element, H_{AB}, the reorganizational energy, λ, and the driving force, ΔG°, of reaction 23a and 23b. From Table 6, we see that if pathways 23a and 23b are sufficiently energetic, then both excited states are produced with probabilities independent of ΔG° ($\Delta G^\circ < -0.05$). Moreover, the tungsten and molybdenum cluster compounds are almost identical in size (11 to 12.5 Å) and structure, and

therefore from eq 3, λ_o is relatively constant for all mixed cluster ecl reactions (changes in λ_o are $\leq$ 0.05 eV in the cluster series). More importantly, in a given mixed cluster ecl reaction, λ_o is independent of which reactant, $Mo_6Cl_{14}^{3-}$ or $W_6X_8Y_6^-$, is converted to the excited state. Therefore the ratio of k_{es_1} and k_{es_2} is independent of ΔG° and λ_o and energy partitioning depends solely on the H_{AB} and λ_i.

The contributions of λ_i and H_{AB} to partitioning in the ecl chemistry of the $M_6X_8Y_6^{2-}$ clusters can be understood in terms of the hexanuclear cluster's frontier molecular orbitals. Figure 10 summarizes the results of theoretical studies in recent years aimed at describing the electronic structure of the $M_6X_8Y_6^{2-}$ ions. Extended Huckel[78] and SCF-Xα-SW[79] calculations predict the HOMO and LUMO to be primarily metal in character and to possess molecular symmetries e_g and a_{2g}, respectively. These results are consistent with spectroscopic studies, which suggest that the luminescence of the $M_6X_8Y_6^{2-}$ ions originates from an excited state localized on the metal core.[80] Additionally, magnetic measurements establish a diamagnetic ground state for $M_6X_8Y_6^{2-}$ ion and the oxidized $M_6X_8Y_6^{2-}$ cluster ions display an axial EPR signal, which can be attributed to tetragonally distorted metal core resulting from the single-electron occupancy of the e_g level.[64] On the basis of these spectroscopic and theoretical results the ecl chemistry of the $Mo_6Cl_{14}^{2-}/W_6X_8Y_6^{2-}$ is described by the molecular orbital representation depicted in Figure 11. The two excited state

Figure 10. Molecular orbital diagram for $M_6X_8Y_6^{2-}$ ions.

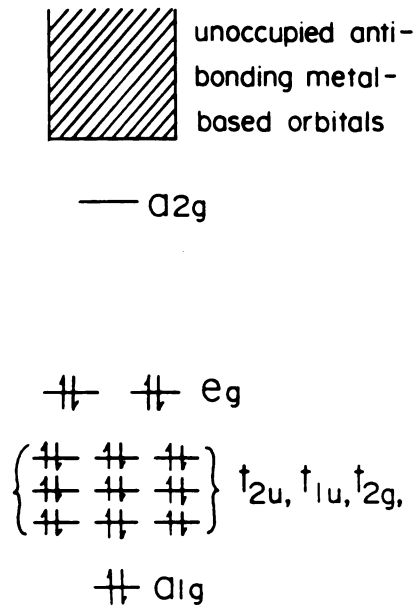
unoccupied anti-
bonding metal-
based orbitals
a2g
eg
t2u, t1u, t2g,
a1g

Figure 10

Figure 11. Molecular orbital description for electron transfer between $W_6X_8Y_6^-$ and $Mo_6Cl_{14}^{3-}$ with the excited state being produced from (a) the $W_6X_8Y_6^-$ ion and (b) the $Mo_6Cl_{14}^{3-}$ ion.

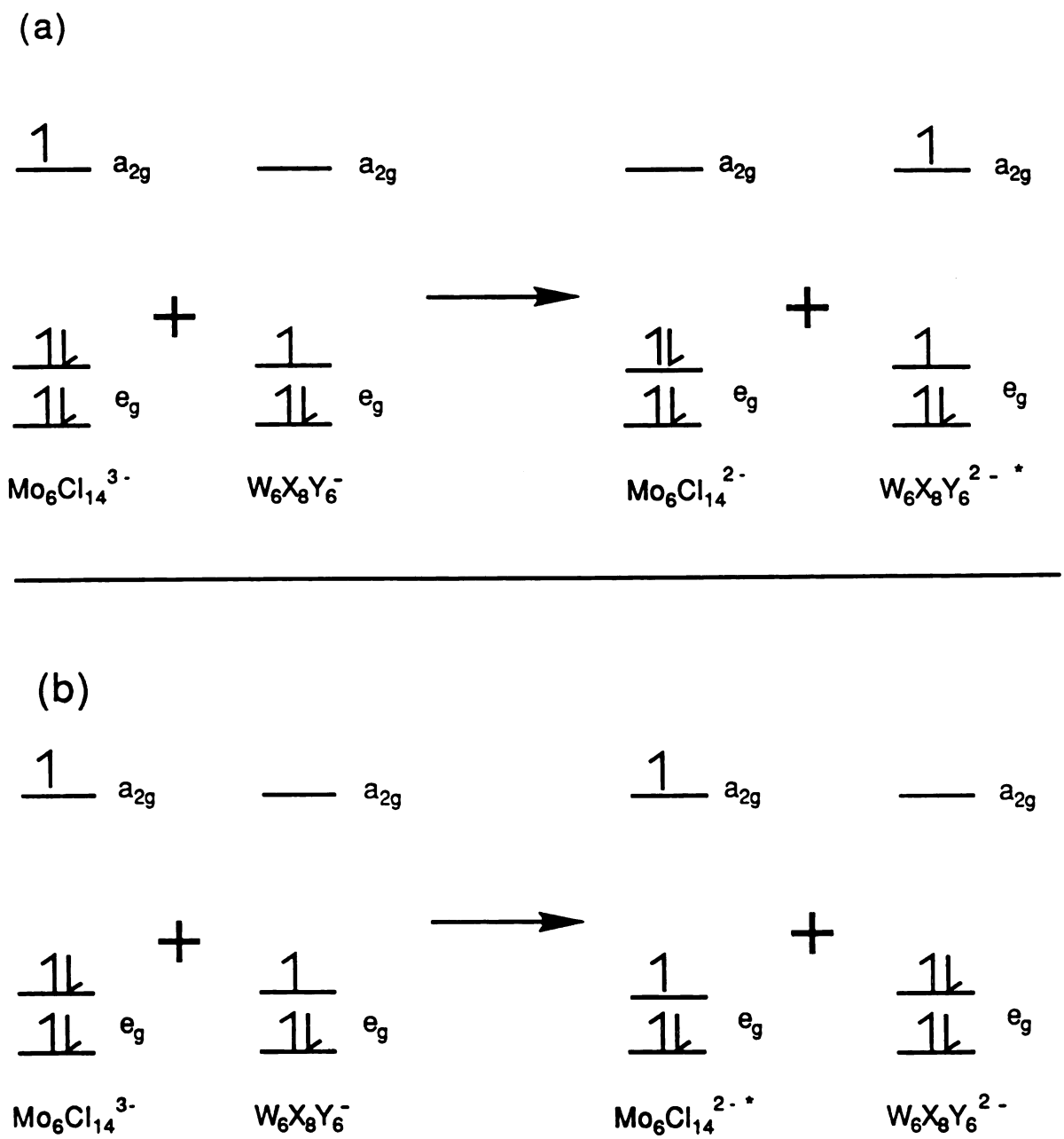
(a)
a2g
a2g
a2g
a2g
+
+
eg
eg
eg
eg
Mo6Cl14 3-
W6X8Y6-
Mo6Cl14 2-
W6X8Y6 2- *
(b)
a2g
a2g
a2g
a2g
+
+
eg
eg
eg
eg
Mo6Cl14 3-
W6X8Y6-
Mo6Cl14 2- *
W6X8Y6 2-

Figure 11

pathways of $M_6X_8Y_6^{2-}$ ecl are electronically distinct: (i) production of electronically excited $Mo_6Cl_{14}^{2-*}$ from $Mo_6Cl_{14}^{3-}$ involves the transfer of an electron from an e_g orbital of $Mo_6Cl_{14}^{3-}$ to the e_g orbital on the $W_6X_8Y_6^-$ ion; and conversely (ii) transfer of an electron from the a_{2g} orbital of $Mo_6Cl_{14}^{3-}$ to the a_{2g} orbital on the $W_6X_8Y_6^-$ ion produces electronically excited $W_6X_8Y_6^{2-*}$. Because k_{es_1} depends only on H_{AB} and λ_i and if, as observed, $k_{es_1} = k_{es_2}$ then λ_i and H_{AB} must be either equal or fortuitously counter balance each other for the reaction pathways described by 23a and 23b.

Obviously, H_{AB} will be different for the two excited state reaction pathways (i.e. $M_6X_8Y_6^- \longrightarrow M_6X_8Y_6^{2-*}$ vs. $M_6X_8Y_6^{3-} \longrightarrow M_6X_8Y_6^{2-*}$) if the respective orbital overlap of the a_{2g} orbitals is different then that of the e_g orbitals. This does not appear to be the case for the mixed cluster ecl system. The e_g (HOMO) and a_{2g} (LUMO) molecular orbitals are constructed from linear combinations of d_{xy} orbitals of adjacent metal atoms; these molecular orbitals are shown in Figure 12. Owing to the similar radical distributions of these metal-based orbitals, the electronic factors of the conversion of $Mo_6Cl_{14}^{3-}$ or $W_6X_8Y_6^-$ to the excited state should be closely related.[81]

The assumption of comparable H_{AB}'s for the two ecl reaction pathways implies that λ_i should be similar for reaction 23a and 23b. More specifically, this implies similar nuclear reorganizational energies for electron

Figure 12. Depiction of the e_g and a_{2g} metal based cluster orbitals.

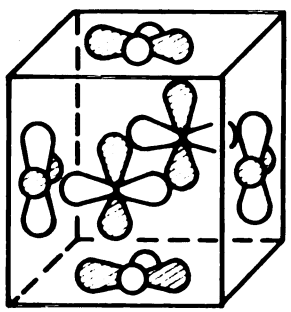

a_{2g}

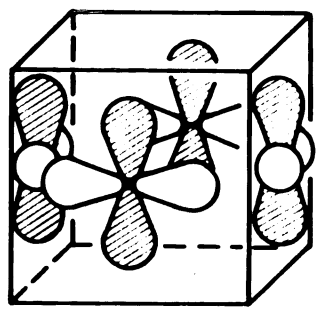

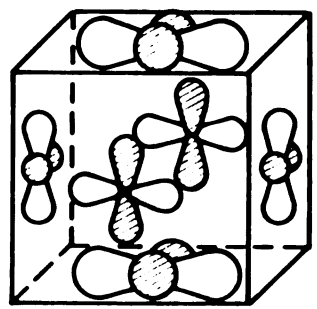

e_g

Figure 12

exchange involving either the a_{2g} or the e_g orbitals. The λ_i energies associated with electron exchange reactions involving the a_{2g} and e_g orbitals can independently be measured by electron-transfer quenching studies of the $M_6X_8Y_6^{2-*}$ with a series of organic electron donors and acceptors. The quenching studies are schematically represented below. In this reaction scheme electronically excited $M_6X_8Y_6^{2-}$

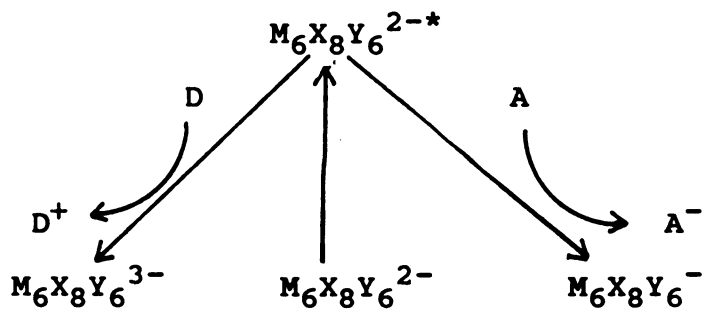

Scheme 4

donates an electron from a_{2g} orbital to acceptor molecule A to produce the reduced radical A^- and the oxidized cluster $M_6X_8Y_6^-$. Alternatively, in the presence of donor molecules D, an electron is transferred to the cluster's e_g orbital to produce oxidized D^+ and reduced cluster $M_6X_8Y_6^{3-}$. The λ_i value measured for the conversion of $M_6X_8Y_6^{2-*}$ to $M_6X_8Y_6^{3-}$ in electron transfer studies is related directly to the conversion of $M_6X_8Y_6^{3-}$ to $M_6X_8Y_6^{2-*}$ in the mixed cluster ecl reaction. Conversely, the cluster's contribution to the measured inner sphere reorganizational energy of $M_6X_8Y_6^{2-*}$/A

electron transfer is equivalent to λ_i for the conversion of $M_6X_8Y_6^-$ to $M_6X_8Y_6^{2-*}$ in the mixed cluster ecl reaction. The quenching rate constants for the reaction of $M_6X_8Y_6^{2-*}$ ions with benzoquinone (BQ) and nitroaromatic (NA) acceptors (reaction 28a), and aromatic amine (AA) donors (reaction 28b) in CH_3CN at 23°C

$$M_6X_8Y_6^{2-*} + A \longrightarrow M_6X_8Y_6^- + A^- \qquad (28a)$$

$$A = BQ,\ NA$$

$$M_6X_8Y_6^{2-*} + D \longrightarrow M_6X_8Y_6^{3-} + D^+ \qquad (28b)$$

$$D = AA$$

are shown in Tables 7 and 8, respectively. Rates were determined from Stern-Volmer analysis of the lifetime of $M_6X_8Y_6^{2-*}$ by the procedure described previously. From these data, λ_i can be evaluated with eq 29

$$k_BT \ln k_q = -1/2\Delta G^\circ + \left[-\lambda/4 + k_BT \ln \left(\frac{2H_{AB}^2}{h}\right)\left(\frac{\pi^3}{\lambda k_BT}\right)^{1/2}\right] \qquad (29)$$

which is obtained by rearranging the electron transfer rate expression of eq 27. The quadratic term of eq 27 has not been included in this rearranged rate expression owing to its small contribution to the overall observed quenching rate at low driving forces. Consequently, eq 29 predicts a

Table 7

Rate Constants for Quenching of $M_6X_8Y_6^{2-}$ Clusters by Nitroaromatics and Substituted Benzoquinones in CH_3CN at 23°C

	Lumophore	Quencher	$\Delta G°/eV^a$	$k_q/M^{-}s^{-1b}$
1.	$Mo_6Br_{14}^{2-}$	3,5-dichloro-p-benzoquinone	-0.25	9.6×10^9
2.	$W_6Br_{14}^{2-}$	p-dinitrobenzene	-0.14	3.0×10^9
3.	$Mo_6Cl_{14}^{2-}$	3,5-dichloro-p-benzoquinone	-0.04	9.0×10^8
4.	$W_6Cl_{14}^{2-}$	p-dinitrobenzene	+0.11	3.0×10^7
5.	$Mo_6Cl_{14}^{2-}$	p-benzoquinone	+0.17	2.3×10^6

[a] Driving force for the electron-transfer quenching reduction calculated from $\Delta G° = [E_{1/2}(Mo_6Cl_{14}^{-/2-}) - E_{0-0}] - E_{1/2}(A^{0/-})$.

[b] Quenching rate constants determined from steady-state lifetime measurements.

Table 8

Rate Constants for Quenching of $M_6X_8Y_6^{2-}$ Clusters by Aromatic Amines in CH_3CN at 23°C

	Lumophore	Quencher	$\Delta G°/eV$[a]	$k_q/M^{-1}s^{-1}$[b]
1.	$Mo_6Cl_{14}^{2-}$	dimethoxydiphenylamine	+0.03	2.8×10^8
2.	$Mo_6Cl_{14}^{2-}$	phenothiazine	+0.04	1.9×10^8
3.	$Mo_6Cl_{14}^{2-}$	10-methylphenothiazine	+0.15	2.3×10^7
4.	$Mo_6Cl_{14}^{2-}$	N,N'-dimethyl-p-toluidine	+0.17	2.0×10^7
5.	$Mo_6Cl_{14}^{2-}$	tris(p-tolyl)amine	+0.21	8.0×10^6

[a] Driving force for the electron-transfer quenching reaction calculated from $\Delta G° = [E_{1/2}(Mo_6Cl_{14}^{2-/3-} + E_{O-O}] + E_{1/2}(D^{+/0})$.

[b] Quenching rate constants determined from steady-state emission measurements.

linear plot of k_BTlnk_q vs. $\Delta G°$ with slope of -0.5 and an intercept equal to the bracketed term.[38,82]

Plots for the rates of acceptor and donor quenching pathways are shown in Figures 13a and 13b. The linear dependence of the rate constant on $\Delta G°$ and slopes of -0.49 and -0.51 for $M_6X_8Y_6^{2-*}/A$ and $M_6X_8Y_6^{2-*}/D$ systems, respectively, agree well with theory. By assuming adiabatic electron transfer (H_{AB} = .022 eV), overall reorganizational energies $\lambda(=\lambda_o + \lambda_i)$ of 1.11 eV and 1.01 eV are calculated from the intercepts of Figures 13a and 13b, respectively. By accounting for λ_o = 0.86 eV (eq 3), λ_i values of 0.25 eV and 0.15 eV are obtained for quenching reactions 28a and 28b, respectively. The relevant parameters for these electron transfer calculations are summarized in Table 9.

The inner sphere reorganizational energy for the $M_6X_8Y_6^{2-}/A$ system is composed of the nuclear reorganization associated with $M_6X_8Y_6^{2-*}$ / $M_6X_8Y_6^{-}$ and A / A^- conversions. Similarly, the $M_6X_8Y_6^{2-*}$ / $M_6X_8Y_6^{3-}$ and D / D^+ conversions compose the λ_i for reaction 28a. Calculations by using self-exchange rate constants measured by EPR line broadening techniques have shown that λ_i's associated with the electron transfer reactions of aromatic amines and nitroaromatics are < 0.05 eV. Therefore the calculated values of λ_i directly reflect the inner-sphere reorganizational energy of $M_6X_8Y_6^{2-*}/M_6X_8Y_6^{-}$ and $M_6X_8Y_6^{2-*}/$ $M_6X_8Y_6^{3-}$ conversions, respectively. The above calculations are predicated on adiabatic electron transfer. The calculated values of 0.15

Figure 13. Plot of $k_B T \ln k_q$ vs. $\Delta G°$ in CH_3CN at 23°C (numbering as in Tables 7 and 8) for (a) $Mo_6Cl_{14}^{2-*}$ quenched by organic acceptors; (b) $Mo_6Cl_{14}^{2-*}$ quenched by organic donors.

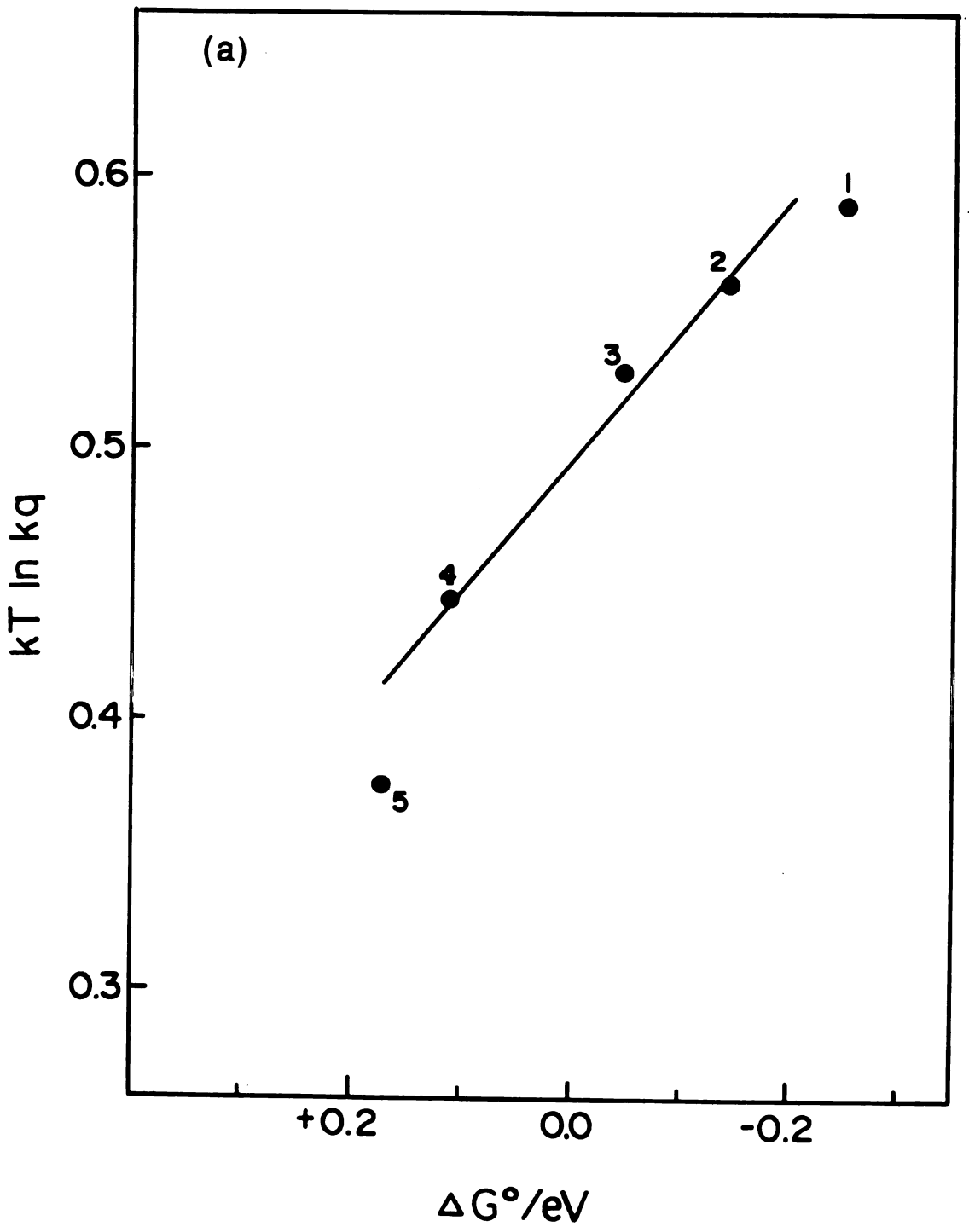

Figure 13

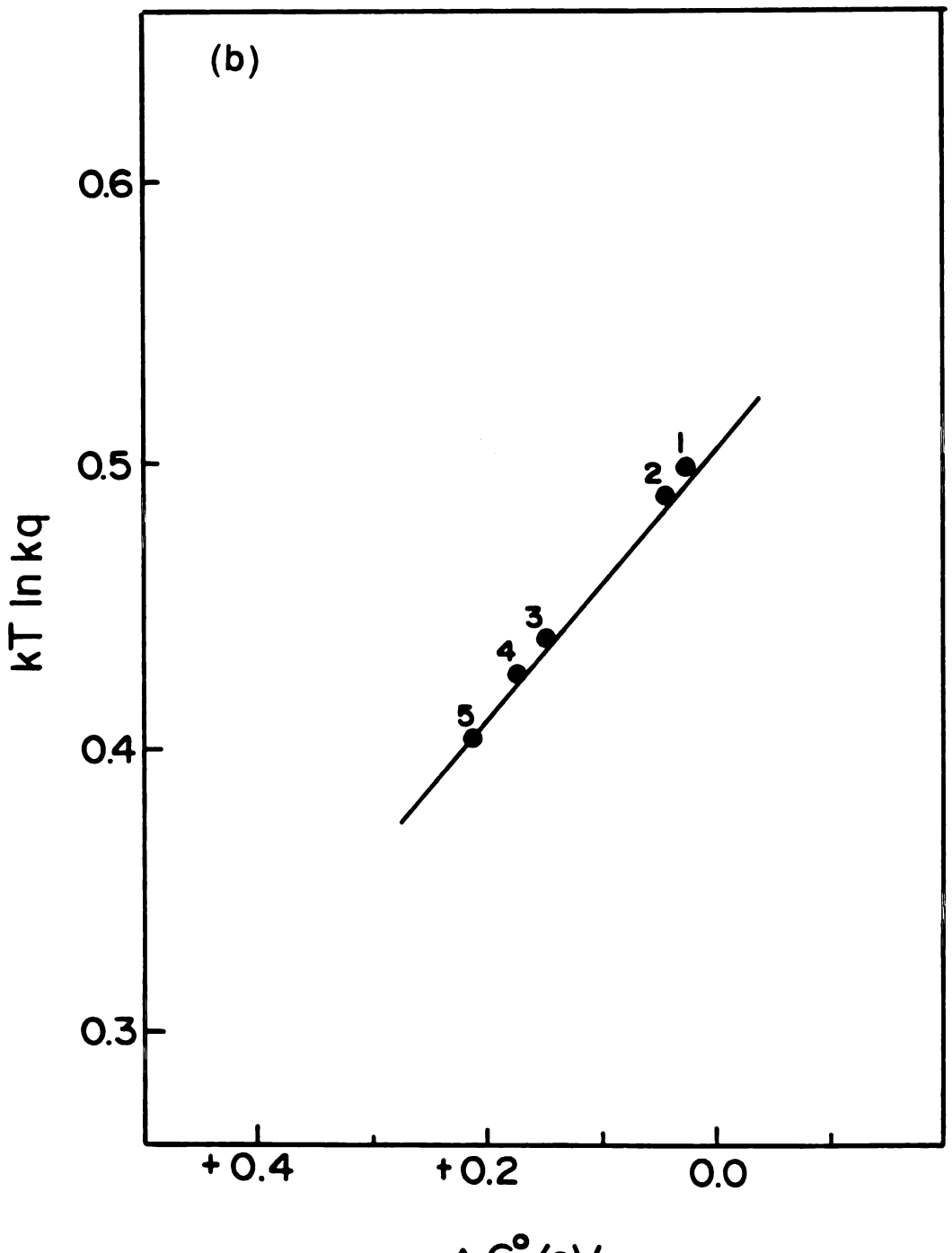

Figure 13

Table 9

Electron-Transfer Parameters Used in Calculating λ_i Values for Quenching Reactions

Electron Transfer Parameter	$M_6X_8Y_6^{2-*}/A$	$M_6X_8Y_6^{2-*}/D$
r/A[a]	9.5	9.5
w_r/eV[b]	0.00	0.00
w_p/eV[b]	+0.04	-0.11
λ_o/eV[c]	0.86	0.86
H_{AB}/eV[d]	0.022	0.022
Int/eV[e]	-0.49	-0.51
λ_i/eV	0.25	0.15

[a] r is the separation between reactants during electron transfer assumed to be the sum of the reactants' radii.

[b] w_r and w_p calculated from equations 5 and 6.

[c] λ_o calculated from equation 3.

[d] Typical value of H_{AB} for an adiabatic reaction.

[e] Intercept obtained from Figures 13a and 13b.

eV and 0.25 eV represent upper limits of λ_i, which decreases with increasing nonadiabaticity. Thus the observation of small and equal λ_i's ($0 < \lambda_i < 0.20$ eV) for reactions 28a and 28b is preserved even if the original assumption of adiabatic electron transfer is inaccurate. These small inner-sphere reorganizational energies most probably result from the fact the a_{2g} and e_g orbitals are delocalized over the metal core and any reorganization is dissociated over the 6 metal atoms of the octahedron.

Energy partitioning studies unequivocally demonstrate that electrochemical excitation energy in the $M_6X_8Y_6^-$ /$M_6X_8Y_6^{3-}$ annihilation reaction is channelled to either reactant with equal probability. Electronic structural similarities of the HOMO and LUMO orbitals are manifested in similar electronic coupling and inner-sphere reorganizational energies for the two excited state production pathways; and hence similar electron transfer rates. With the demonstrated ability to produce $M_6X_8Y_6^{2-*}$ from either $M_6X_8Y_6^-$ or $M_6X_8Y_6^{3-}$ coupled with the evaluation of the important electron transfer parameters such as electronic coupling and reorganizational energies of the $M_6X_8Y_6^-/M_6X_8Y_6^{2-*}$ and $M_6X_8Y_6^{3-}/M_6X_8Y_6^{2-*}$ conversions, the ecl reactions of the $M_6X_8Y_6^-$ and $M_6X_8Y_6^{3-}$ ions can now be independently investigated. An issue of particular importance is the dependence of production of $M_6X_8Y_6^{2-*}$ from $M_6X_8Y_6^-$ or $M_6X_8Y_6^{3-}$ on the free energy of the electron-transfer reaction.

CHAPTER IV

IV. THE EFFECTS OF DRIVING FORCE AND LONG-DISTANCE ELECTRON TRANSFER ON CHEMILUMINESCENCE EFFICIENCIES

A. Background

One of the principal themes that has emerged from mechanistic considerations of ecl and cl reactions is that the efficiency of excited-state production is related intimately to the energetics of electron transfer. Extensive investigations of ecl and cl reactivity have established two pathways for excited-state production.[83-89] The first pathway is shown in Scheme 5 where the driving force for the electron transfer reaction between A^- and D^+

$$A^- + D^+ \longrightarrow A^* + D$$

Scheme 5

is larger than the energy required to populate the emitting excited state of A or D. This process of directly forming the emitting excited state upon electron transfer is called an energy-sufficient route or S-route mechanism. Alternatively, as shown in Scheme 6 the driving force of the electron-transfer reaction is not sufficient to populate the emitting excited state. The production of the emitting excited state involves population of a nonluminescent

$$A^- + D^+ \longrightarrow {}^3A^* + D$$

$${}^3A^* + {}^3A^* \longrightarrow {}^1A^*$$

Scheme 6

intermediate triplet excited state and consequent annihilation of two of these lower energy excited states to produce one emitting state. This two step energy deficient mechanism is widely referred to as the T-route.

For typical organic ecl or cl systems, the high energy of the luminescent excited state (usually a singlet) precludes S-route reactivity and electron transfer produces a non-emissive triplet intermediate which undergoes annihilation to yield the emitting singlet state. Because triplet-triplet annihilation processes are inherently inefficient,[7b] the excited-state production yields of organic systems are generally limited to a few percent.[88a,90-92] In contrast, luminescence from transition metal complexes usually originates from the lowest energy electronic excited state and therefore S-route reactivity for inorganic species is governed by modest energies. In recent years, ecl and cl from a variety of inorganic compounds including $M(bpy)_3^{2+}$ (M = Ru, Os, Cr; bpy = 2,2'-bipyridine)[93,95] and related species,[96-98] Re(I) diimine complexes,[99] binuclear complexes possessing metal-metal bonds,[100,101] phthalocyanines,[102] square planar complexes of Pd(II)[103] and Pt(II)[81], and Ir(III)(2-phenylpyridine)$_3$, Tb(III) thenoyltriflouroacetonate, Pt(II)(8-quinolinolate)$_2$, [Cu(I)pyridine(I)]$_4$ complexes[104] have been reported. For all of these systems, the energy released from the electron-transfer reaction between oxidized and reduced forms of the parent molecule (i.e., commonly called the annihilation

reaction) is sufficiently energetic to directly populate the luminescent excited state. Nevertheless, despite this predicted and in some cases experimentally verified S-route behavior,[105,106] measured efficiencies for excited-state production are well below unity.[75] The reasons for the low yields of some of these systems are known. For example, an ecl yield of $<10^{-5}$ for the $Pt_2(H_2P_2O_5)_4^{4-}$ ion[107] can most certainly be attributed to the relatively short lifetime of $Pt_2(H_2P_2O_5)_5^{5-}$ in aqueous solution.[108] And low excited-state yields of RuL_3^{2+*} (L = polypyridyl) produced in the reaction of RuL_3^{3+} with CoL_3^{+} have been shown to result from an electron-transfer pathway competitive to cl in which a non-luminescent excited state of CoL_3^{2+} is populated.[109] For the most part, however, a general understanding of the low ecl and cl yields of inorganic systems has not been achieved.

The energetics of the $Mo_6Cl_{14}^{2-}$ ecl permit the energy dependence of ecl chemistry to be defined. The magnitudes of the $Mo_6Cl_{14}^{-/2-}$ and $Mo_6Cl_{14}^{2-/3-}$ reduction couples [$E_{1/2}(Mo_6Cl_{14}^{-/2-})$ = +1.53 V vs. sce, $E_{1/2}(Mo_6Cl_{14}^{2-/3-})$ = -1.56 V vs. sce in CH_3CN] and the relatively low energy of the $Mo_6Cl_{14}^{2-}$ excited state [$E_{em}(Mo_6Cl_{14}^{2-*})$ = 1.9 V] have allowed us to observe ecl from the annihilation of $Mo_6Cl_{14}^{-}$ and $Mo_6Cl_{14}^{3-}$ with a variety of electroactive donors (e.g., nitroaromatic radical anions) and acceptors (e.g., aromatic amine radical cations), respectively. By varying the reduction potential of the electroactive donor or acceptor,

the ecl dynamics of $Mo_6Cl_{14}^{2-}$ ion can systematically be investigated over a wide potential energy range.

This chapter describes our efforts to elucidate the factors which control the efficiency of $M_6X_8Y_6^{2-}$ ecl system. The results of the dependence of ecl quantum yields on the exergonicity of the electron-transfer reactions of $Mo_6Cl_{14}^{-}$ with a series of nitroaromatic radical anions (NA^-), pyridinium radicals (P), and bipyridinium cations (BP^+) and the reaction of $Mo_6Cl_{14}^{3-}$ with aromatic amine cations (A^+) in acetonitrile and dichloromethane are presented. Analysis of these yields in the context of current electron transfer theories is discussed. This analysis suggests that efficient ecl is circumvented by long-distance electron-transfer which can explain the low excited state yields for chemiluminescent reactions of other inorganic complexes.

B. Results

Electrochemical and quenching data in CH_3CN and CH_2Cl_2 are displayed in Tables 10 and 11 for aromatic amines, in Tables 12 and 13 for the nitroaromatics[110], in Tables 14 and 15 for pyridinium ions, and in Table 16 for bipyridinium ions employed as electroactive reagents in ecl studies. These acceptors and donors meet two important criteria for ecl free energy dependence studies in that their reduction potentials, determined by cyclic voltammetry, span a wide potential energy range and all compounds exhibit reversible one-electron processes in CH_3CN and CH_2Cl_2. Values of the

Table 10

Reduction Potentials, Quenching Rate Constants[a], and Ecl Quantum Yield Data[b] for Aromatic Amines Used in Ecl Studies[c]

Acceptors (A)	$E_{1/2}$,[d] V	$\Delta G_{gs}°$,[e] V	k_q[f] $M^{-1}\ s^{-1}$	ϕ_{ecl}[g]
1. phenothiazine	+0.52	-2.05	1.0×10^8	$< 10^{-6}$ [h]
2. dimethoxydiphenylamine	+0.51	-2.04	1.1×10^8	$< 10^{-6}$ [h]
3. 10-methylphenothiazine	+0.63	-2.16	2.3×10^7	6.0×10^{-4}
4. N,N-dimethyl-p-toluidine	+0.65	-2.18	2.0×10^7	6.6×10^{-4}
5. tris(p-tolyl)amine	+0.69	-2.22	8.0×10^6	3.1×10^{-3}
6. tris(4-bromophenyl)amine	+1.01	-2.54	5.8×10^5	2.5×10^{-2}

[a] Luminescence quenching of $Mo_6Cl_{14}^{2-}$ by neutral aromatic amines (A). [b] Ecl quantum yields for the reaction of $Mo_6Cl_{14}^{3-}$ with the aromatic amine cation radical (A^+). [c] All measurements were made in acetonitrile containing 0.1 M tetrabutylammonium perchlorate at 23 ± 2°C. [d] As reduction potentials for the $A^+/^0$ couple vs. sce. [e] Standard free energy change for the reaction of $Mo_6Cl_{14}^{3-}$ with A^+; $\Delta G_{gs}° = -[E_{1/2}(A^+/^0) - E_{1/2}(Mo_6Cl_{14}^{2-/3-})]$. [f] Quenching rate constants determined from steady-state emission measurements. [g] Number of moles of photons produced per number of equivalents of $Mo_6Cl_{14}^{3-}$ or A^+. [h] Detection limit of the ecl quantum yield is 10^{-6}. Error limits are +8%.

Table 11

Reduction Potentials, Quenching Rate Constants[a], and Ecl Quantum Yield Data[b] for Aromatic Amines Used in Ecl Studies[c]

Acceptors (A)	$E_{1/2}$,[d] V	$\Delta G_{gs}°$,[e] V	k_q,[f] $M^{-1}\ s^{-1}$	ϕ_{ecl}[g]
1. Dimethoxydiphenylamine	+0.43	-2.13	1.7×10^7	-
2. Phenothiazine	+0.45	-2.15	1.1×10^7	-
3. N,N-dimethyl-p-toluidine	+0.51	-2.21	1.9×10^6	2.7×10^{-3}
4. 10-Methylphenothiazine	+0.58	-2.28	2.9×10^6	6.7×10^{-3}
5. Tris(p-tolyl)amine	+0.67	-2.37	1.4×10^6	2.6×10^{-2}
6. Tris(4-bromophenyl)amine	+1.04	-2.74	6.9×10^4	5.1×10^{-2}

[a] Luminescence quenching of $Mo_6Cl_{14}^{2-}$ by neutral aromatic amines (A). [b] Ecl quantum yields for the reaction of $Mo_6Cl_{14}^{3-}$ with the aromatic amine cation radical (A^+). [c] All measurements were made in dichloromethane containing 0.1 M tetrabutylammonium perchlorate at 23 ± 2°C. [d] As reduction potentials for the $A^+/^0$ couple vs. sce. [e] Standard free energy change for the reaction of $Mo_6Cl_{14}^{3-}$ with A^+; $\Delta G_{gs}° = -[E_{1/2}(A^{+/0}) - E_{1/2}(Mo_6Cl_{14}^{2-/3-})]$. [f] Quenching rate constants determined from steady-state emission measurements. [g] Number of moles of photons produced per number of equivalents of $Mo_6Cl_{14}^{3-}$ or A^+. [h] Detection limit of the ecl quantum yield is 10^{-6}. Error limits are ±8%.

Table 12

Reduction Potentials, Quenching Rate Constants[a], and Ecl Quantum Yield Data[b] for Nitroaromatics and Aromatic Quinones Used in Ecl Studies

Donors (NA)	$E_{1/2}$,[d] V	$\Delta G_{gs}°$,[e] V	k_q[f] $M^{-1}\ s^{-1}$	ϕ_{ecl}[g]
1. p-benzoquinone	-0.55	-2.11	2.3×10^6	$<10^{-6}$ [h]
2. 2,6-dimethyl-p-benzoquinone	-0.72	-2.28	4.5×10^5	4.1×10^{-5}
3. p-dinitrobenzene	-0.75	-2.31	1.1×10^5	3.5×10^{-4}
4. o-dinitrobenzene	-0.91	-2.47	3.9×10^3	1.1×10^{-3}
5. p-nitrobenzaldehyde	-0.92	-2.48	5.8×10^4	1.4×10^{-3}
6. m-nitrobenzaldehyde	-1.09	-2.65	5.6×10^4	2.4×10^{-3}
7. 1-chloro-4-nitrobenzene	-1.13	-2.69	3.7×10^3	1.5×10^{-3}
8. 5-nitro-m-xylene	-1.26	-2.82	1.9×10^3	9.5×10^{-4}
9. 3-nitro-o-xylene	-1.39	-2.95	1.2×10^3	6.8×10^{-4}

[a] Luminescence quenching of $Mo_6Cl_{14}^{2-}$ by neutral donors (NA). [b] Ecl quantum yields for the reaction of $Mo_6Cl_{14}^-$ with reduced donors (NA^-). [c] All measurements were made in acetonitrile containing 0.1 M tetrabutylammonium perchlorate at 23 ± 2°C. [d] As reduction potentials for the $NA^{0/-}$ couple vs. sce. [e] Standard free energy change for the reaction of $Mo_6Cl_{14}^-$ with NA^-; $\Delta G_{gs}° = -[E_{1/2}(Mo_6Cl_{14}^{-/2-}) - E_{1/2}(NA^{0/-})]$. [f] Quenching rate constants determined from steady-state emission measurements. [g] Number of moles of photons produced per number of equivalents of $Mo_6Cl_{14}^-$ or NA^-. Error limits are + 10%. [h] Detection limit of the ecl quantum yield is 10^{-6}.

Table 13

Reduction Potentials, Quenching Rate Constants[a], and Ecl Quantum Yield Data[b] for Nitroaromatics and Aromatic Quinones Used in Ecl Studies

	Donors (NA)	$E_{1/2}$,[d] V	$\Delta G_{gs}°$,[e] V	k_q[f] $M^{-1}\ s^{-1}$	ϕ_{ecl}[g]
1.	2,6-dimethyl-p-benzoquinone	-0.85	-2.21	1.4×10^5	-
2.	p-Dinitrobenzene	-0.86	-2.22	1.1×10^6	-
3.	o-Dinitrobenzene	-0.97	-2.33	8.0×10^3	9×10^{-4}
4.	p-Nitrobenzaldehyde	-1.03	-2.39	1.6×10^4	2×10^{-3}
5.	m-Nitrobenzaldehyde	-1.17	-2.53	$<10^3$	4.6×10^{-3}
6.	1-Chloro-4-nitrobenzene	-1.23	-2.59	8.1×10^3	3.2×10^{-3}
7.	5-Nitro-m-xylene	-1.30	-2.66	1.7×10^3	5.7×10^{-3}
8.	3-nitro-oxylene	-1.51	-2.87	3.0×10^4	4.0×10^{-3}
9.	2-nitro-m-xylene	-1.65	-3.01	2.1×10^4	4.5×10^{-3}

[a]Luminescence quenching of $Mo_6Cl_{14}^{2-}$ by neutral donors (NA). [b] Ecl quantum yeilds for the reaction of $Mo_6Cl_{14}^-$ with reduced donors (NA^-). [c] All measurements were made in dichloromethane containing 0.1 M tetrabutylammonium perchlorate at 23 ± 2°C. [d] As reduction potentials for the $NA^{0/-}$ couple vs. sce. [e] Standard free energy change for the reaction of $Mo_6Cl_{14}^-$ with NA^-; $\Delta G_{gs}° = -]E_{1/2}(Mo_6Cl_{14}^{-/2-}) - E_{1/2}(NA^{0/-})]$. [f] Quenching rate constants determined from steady-state emission measurements. [g] Number of moles of photons produced per number of equivalents of $Mo_6Cl_{14}^-$ or NA^-. Error limits are ±10%. [h] Detection limit of the ecl quantum yield is 10^{-6}.

Table 14

Reduction Potentials, Quenching Rate Constants,[a] and Ecl Quantum Yield Data[b] for Pyridinium Salts Used in Ecl Studies.[c]

	Donors (P^+)[d]	$E_{1/2}$,[e] V	$\Delta G_{gs}°$,[f] V	k_q,[g] $M^{-1}\ s^{-1}$	ϕ_{ecl} [h]
1.	4-cyano-N-benzylpyridinium	-0.69	-2.25	2.2×10^7	2.4×10^{-3}
2.	4-cyano-N-methylpyridinium	-0.74	-2.30	4.4×10^5	6.1×10^{-3}
3.	4-carboethoxy-N-benzylpyridinium	-0.84	-2.40	4.9×10^4	1.2×10^{-2}
4.	4-carboethoxy-N-methylpyridinium	-0.88	-2.44	2.6×10^4	1.2×10^{-2}
5.	4-amido-N-benzylpyridinium	-0.96	-2.52	1.8×10^4	1.3×10^{-2}
6.	4-amido-N-methylpyridinium	-1.02	-2.58	1.2×10^4	1.5×10^{-2}

[a] Luminescence quenching of $Mo_6Cl_{14}^{2-}$ by pyridinium ions (P^+). [b] Ecl quantum yields for the reaction of $Mo_6Cl_{14}^-$ with one-electron reduced pyridinium ion (P). [c] All measurements were made in acetonitrile containing 0.1 M tetrabutylammonium perchlorate at 23 ± 2°C. [d] Hexafluorophosphate salts. [e] As reduction potentials for the $P^{+/0}$ couple vs. sce. [f] Standard free energy change for the reaction of $Mo_6Cl_{14}^-$ with P; $\Delta G_{gs}° = -[E_{1/2}(Mo_6Cl_{14}^{-/2-}) - E_{1/2}(P^{+/0})]$. [g] Quenching rate constants determined from steady-state emission measurements. [h] Number of moles of photons produced per number of equivalents of $Mo_6Cl_{14}^-$ or P. Error limits are ± 12%.

Table 15

Reduction Potentials, Quenching Rate Constants,[a] and Ecl Quantum Yield Data[b] for Pyridinium Salts Used in Ecl Studies[c]

Donors (P)[d]	$E_{1/2}$[e] V	$\Delta G_{gs}°$ [f] V	k_q[g] $M^{-1}\ s^{-1}$	ϕ_{ecl}[h]
1. 4-cyano-N-benzylpyridinium	-0.69	-2.22	5×10^7	-
2. 4-cyano-N-methylpyridinium	-0.74	-2.27	2×10^7	-
3. 4-carboethoxy-N-benzylpyridinium	-0.83	-2.36	5×10^5	0.036
4. 4-carboethoxy-N-methylpyridinium	-0.87	-2.40	2×10^5	0.034

[a] Luminescence quenching of $Mo_6Cl_{14}^{2-}$ by pyridinium ions (P^+). [b] Ecl quantum yields for the reaction of $Mo_6Cl_{14}^-$ with one-electron reduced pyridinium ion (P). [c] All measurements were made in acetonitrile containing 0.1 M tetrabutylammonium perchlorate at 23 ± 2°C. [d] Hexafluorophosphate salts. [e] As reduction potentials for the $P^{+/0}$ couple vs. sce. [f] Standard free energy change for the reaction of $Mo_6Cl_{14}^-$ with P; $\Delta G_{gs}° = -[E_{1/2}(Mo_6Cl_{14}^{-/2-}) - E_{1/2}(P^{+/0})]$. [g] Quenching rate constants determined from steady-state emission measurements. [h] Number of moles of photons produced per number of equivalents of $Mo_6Cl_{14}^-$ or P. Error limits are ±12%.

Table 16

Reduction Potentials and Ecl Quantum Yield Data[a] for Bipyridinium Salts Used in Ecl Studies[b]

Donors (BP^{2+})[c]	$E_{1/2}$[d] V	$\Delta G_{gs}°$[e] V	ϕ_{ecl}[f]
1. 4,4'-methyl-N,N'-ethylene-2,2'-bipyridinium	-0.60	-2.125	5.35×10^{-4}
2. 4,4'-methyl-N,N'-propyl-2,2'-bipyridinium	-0.77	-2.30	9.5×10^{-3}
3. 4,4'-methyl-N,N'-butyl-2,2'-bipyridinium	-0.89	-2.42	1.1×10^{-2}
4. N,N-methyl-2,4-bipyridinium	-1.17	-2.70	5.3×10^{-3}

[a] Ecl quantum yields for the reaction of $Mo_6Cl_{14}^-$ with one-electron reduced bipyridinium ion (BP^+). [b] All measurements were made in acetonitrile containing 0.1 M tetrabutylammonium hexafluorophosphate at 23 ± 2°C. [c] Hexafluorophosphate salts. [d] As reduction potentials for the $BP^{2+/+}$ couple vs. sce. [e] Standard free energy change for the reaction of $Mo_6Cl_{14}^-$ with BP^+; $\Delta G_{gs}° = [E_{1/2}(Mo_6Cl_{14}^{-/2-}) - E_{1/2}(D^{+/0})]$. [f] Number of moles of photons produced per number of equivalents of $Mo_6Cl_{14}^-$ or BP^+. Error limits are ± 15%.

ratio of anodic and cathodic current maxima i_c/i_a varied from 0.95 to 1.05 and plots of anodic and cathodic peak currents vs. (scan rate)$^{1/2}$ were linear with a zero intercept. Anodic to cathodic peak separations (ΔE_p) were almost identical to ferrocene in both solvents, thereby establishing that any deviations of ΔE_p from the theoretical value of 59 mV are due primarily to uncompensated cell resistance. Rate constants for the quenching of $Mo_6Cl_{14}^{2-}$ luminescence in CH_3CN and CH_2Cl_2 (μ = 0.1 M NBu_4ClO_4 or NBu_4PF_6 at 23 °C) were deduced from classical Stern-Volmer analysis of the emission intensity. All Stern-Volmer plots were linear over a quencher concentration range of 1-100 mM and k_q's were calculated from Stern-Volmer constants with τ_o ($Mo_6Cl_{14}^{2-*}$) = 180 μs in CH_3CN and τ_o($Mo_6Cl_{14}^{2-*}$) = 160 μs in CH_2Cl_2 (μ = 0.1 M NBu_4ClO_4 or NBu_4PF_6 at 23 °C).

Because $BP^{2+/+}$, $P^{+/0}$ and $NA^{0/-}$ reduction potentials are positive of the $Mo_6Cl_{14}^{2-/3-}$ couple and $A^{+/0}$ reduction potentials are positive of the $Mo_6Cl_{14}^{-/2-}$ couple, the electron-transfer reactions in equations 30 and 31 can be clearly established by standard electrochemical techniques.[111] Chemiluminescence from the $Mo_6Cl_{14}^{2-}$/donor

$$Mo_6Cl_{14}^{-} + \begin{pmatrix} NA^{-} \\ P^{0} \\ BP^{+} \end{pmatrix} \longrightarrow Mo_6Cl_{14}^{2-*} + \begin{pmatrix} NA \\ P^{+} \\ BP^{2+} \end{pmatrix} \quad (30a)$$

$$Mo_6Cl_{14}^{-} + \begin{pmatrix} NA^{-} \\ P^{0} \\ BP^{+} \end{pmatrix} \longrightarrow Mo_6Cl_{14}^{2-} + \begin{pmatrix} NA \\ P^{+} \\ BP^{2+} \end{pmatrix} \quad (30b)$$

$$Mo_6Cl_{14}^{3-} + A^{+} \longrightarrow Mo_6Cl_{14}^{2-*} + A \quad (31a)$$

$$Mo_6Cl_{14}^{3-} + A^{+} \longrightarrow Mo_6Cl_{14}^{2-} + A \quad (31b)$$

and acceptor systems is observed only when the potential applied to the working Pt electrode is stepped into the oxidation-reduction waves of the electroactive species. Tables 10-16 list the free energy changes and the ecl quantum yields, ϕ_{ecl}, for reactions 30 and 31 in CH_3CN and CH_2Cl_2. Owing to the formation of $(BP)Mo_6Cl_{14}$ salts, bipyridinium systems were studied only in CH_3CN. Even in this relatively high dielectric solvent, ion pairing was observed and hence ecl measurements are suspect. For this reason the ensuing discussion does not include the $Mo_6Cl_{14}^{2-}/BP^{2+}$ systems. Ecl quantum efficiencies were determined by dividing the number of einsteins emanating from the electrode surface by the number of equivalents of electrons used to generate the oxidant or reductant (i.e. the integrated anodic or cathodic charge passed into solution). As evidenced by the relatively small quenching rate

constants listed in Tables 10-15, acceptors and donors are inefficient quenchers of $Mo_6Cl_{14}^{2-}$ luminescence and therefore the measured ecl intensities are not attenuated by the presence of acceptor or donor. Of course quenching of $Mo_6Cl_{14}^{2-}$ luminescence by the oxidized or reduced donors is downhill and should be extremely efficient. However, the concentration profiles of electrogenerated intermediates do not significantly overlap in an ecl step experiment and hence $Mo_6Cl_{14}^{2-*}$ should not be quenched by the electrogenerated cluster or electroactive organic reactants. Even when the production of the electroactive organic reactant was doubled, significant quenching of the ecl was not observed. For systems exhibiting ecl, the spectrum is identical with the emission spectrum of $Mo_6Cl_{14}^{2-}$ in CH_3CN or CH_2Cl_2. The absence of acceptor or donor luminescence is consistent with spectroscopic data, which reveals that population of the lowest energy electronic excited state of these compounds collected in Tables 10-15 is an energetically unfavorable process.[112]

As described in Chapter I, ϕ_{es} is the parameter which best describes the efficiency of the ecl reaction. Plots of the ϕ_{es} vs. the free energy driving force of the excited state reactions ($\Delta G^\circ_{es} = \Delta G^\circ_{gs} + 2.0$ V) for acceptors and donors listed in Tables 10-15 are shown in Figure 14 and 15. The standard free energy, ΔG_{es}, of the excited-state electron-transfer pathway (reactions 30a and 31a) was calculated from $\Delta G^\circ_{gs} = \Delta G^\circ_{es} - \Delta G_{ES}$ where ΔG_{ES} is the free

Figure 14. Plot of log ϕ_{es} vs. ΔG_{es} for the electron-transfer annihilation reactions of the $Mo_6Cl_{14}^{3-}/A^+$ (O), $Mo_6Cl_{14}^-/P$ (Δ), and $Mo_6Cl_{14}^-/NA^-$ (□) systems in acetonitrile. The numbering scheme is defined in Tables 10, 12 and 14. The standard free energy change for the excited-state reaction pathways was evaluated as described in the text.

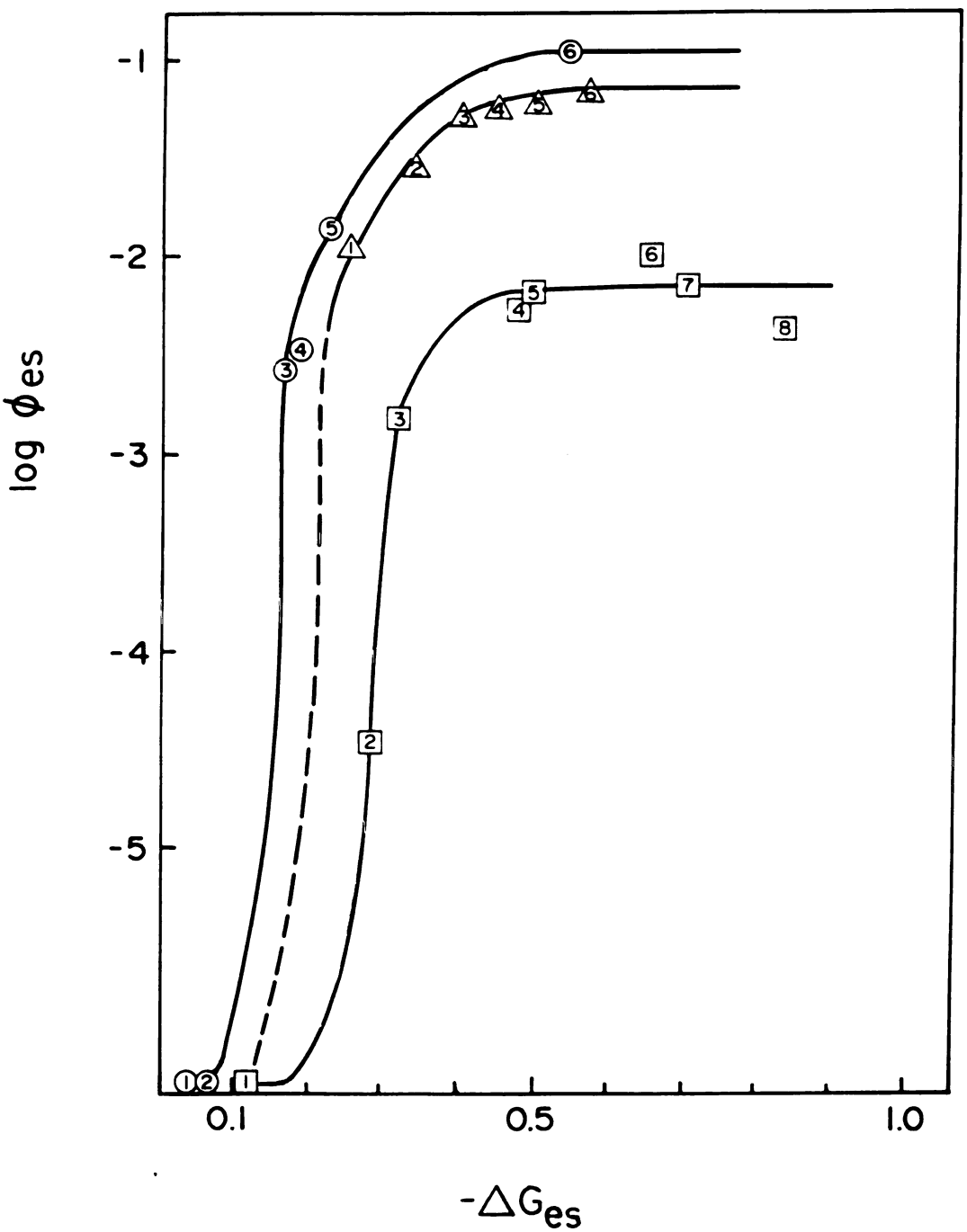

Figure 14

Figure 15. Plot of log ϕ_{es} vs. ΔG_{es} for the electron-transfer annihilation reaction of the $Mo_6Cl_{14}^{3-}/A^+$ (□), $Mo_6Cl_{14}^-/P$ (Δ), and $Mo_6Cl_{14}^-/NA^-$ (O) systems in dichloromethane. The numbering scheme is defined in Tables 11, 13, and 15. The standard free energy change for the excited-state reaction pathway was evaluated as described in the text.

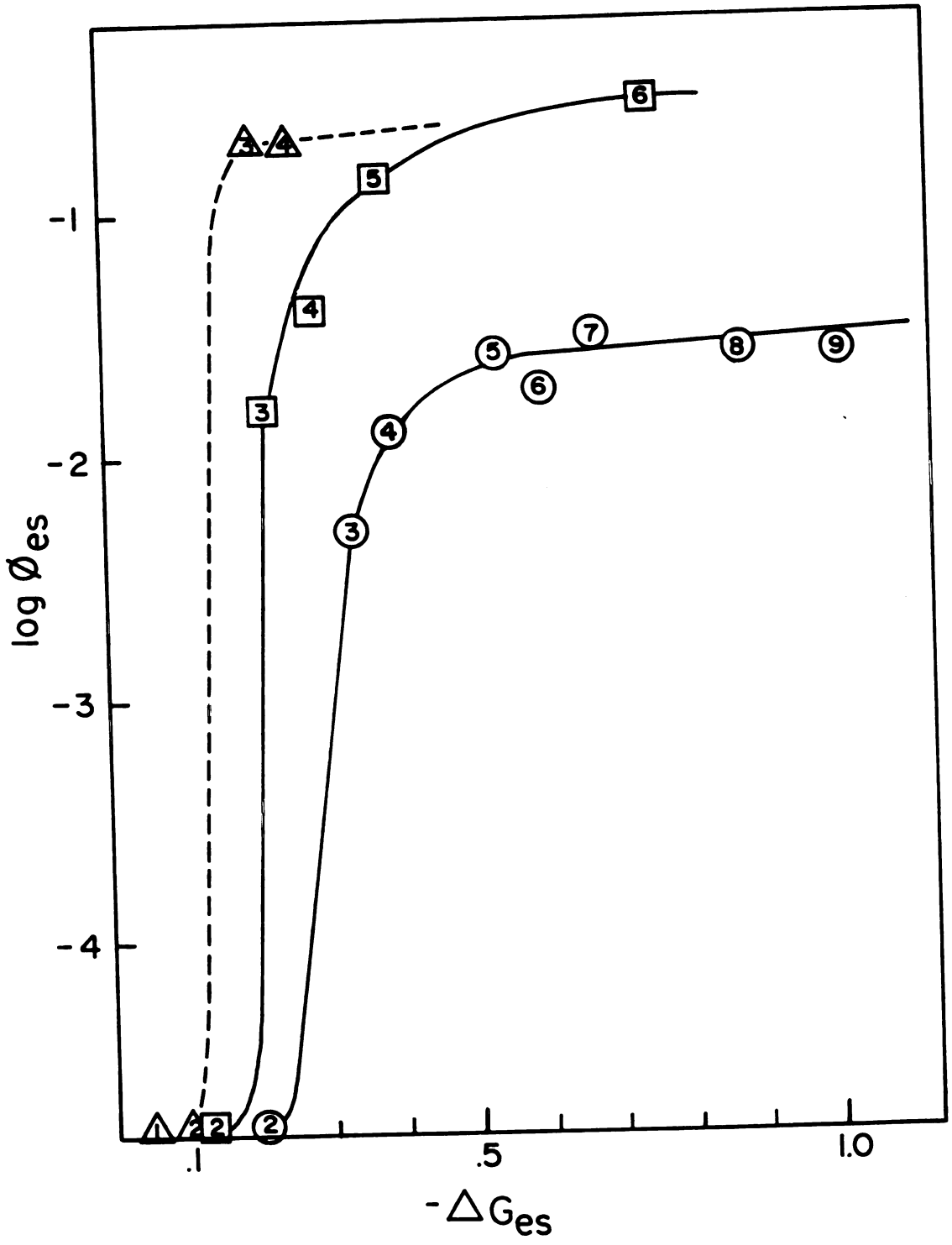

Figure 15

energy content of the $Mo_6Cl_{14}^{2-}$ excited state over the ground state and ΔG°_{gs} is the standard free-energy change of the ground-state reaction pathway. ΔG_{ES} can be estimated from the energy of 0-0 transition (E_{0-0} = 1.9 eV) with corrections for entropic contributions ($T\Delta S$ = 0.1 V).[113] The excited state yields were calculated with ϕ_e = 0.19 for $Mo_6Cl_{14}^{2-}$ in CH_3CN and ϕ_e = 0.18 for $Mo_6Cl_{14}^{2-}$ in CH_2Cl_2 at 23 °C.

C. DISCUSSION

Electronically excited $Mo_6Cl_{14}^{2-}$ ion is produced by the simple electron-transfer reactions of the electronically generated $Mo_6Cl_{14}^{-}$ and $Mo_6Cl_{14}^{3-}$ ions with electroactive donors and acceptors, respectively. This observation is consistent with energy partitioning studies of Chapter III which clearly demonstrated that the excited state can be produced by either oxidized or reduced cluster. As discussed in Chapter III the chemiluminescent reactivity of the oxidized and reduced forms of $Mo_6Cl_{14}^{2-}$ can be accomodated in terms of the hexanuclear clusters electronic structure. The ecl chemistry of the $Mo_6Cl_{14}^{-}$ and $Mo_6Cl_{14}^{3-}$ ions with donors and acceptors, respectively, can be described by the molecular oribtal representation depicted in Figure 16. For the $Mo_6Cl_{14}^{3-}/A^+$ series, the a_{2g} orbital is occupied prior to annihilation and therefore, transfer of an electron from the e_g orbital to the appropriate acceptor level will yield electronically excited cluster. Directly

Figure 16. Molecular orbital description for competitive electron transfer to give either ground- or excited-state $Mo_6Cl_{14}^{3-}$ by the reaction of (a) $Mo_6Cl_{14}^{2-}$ with oxidized aromatic amines (A^+) and (b) $Mo_6Cl_{14}^{-}$ with reduced nitroaromatics (NA^-) or pyridinium ions (P). Production of electronically-excited acceptors and donors is an energetically unfavorable proces.

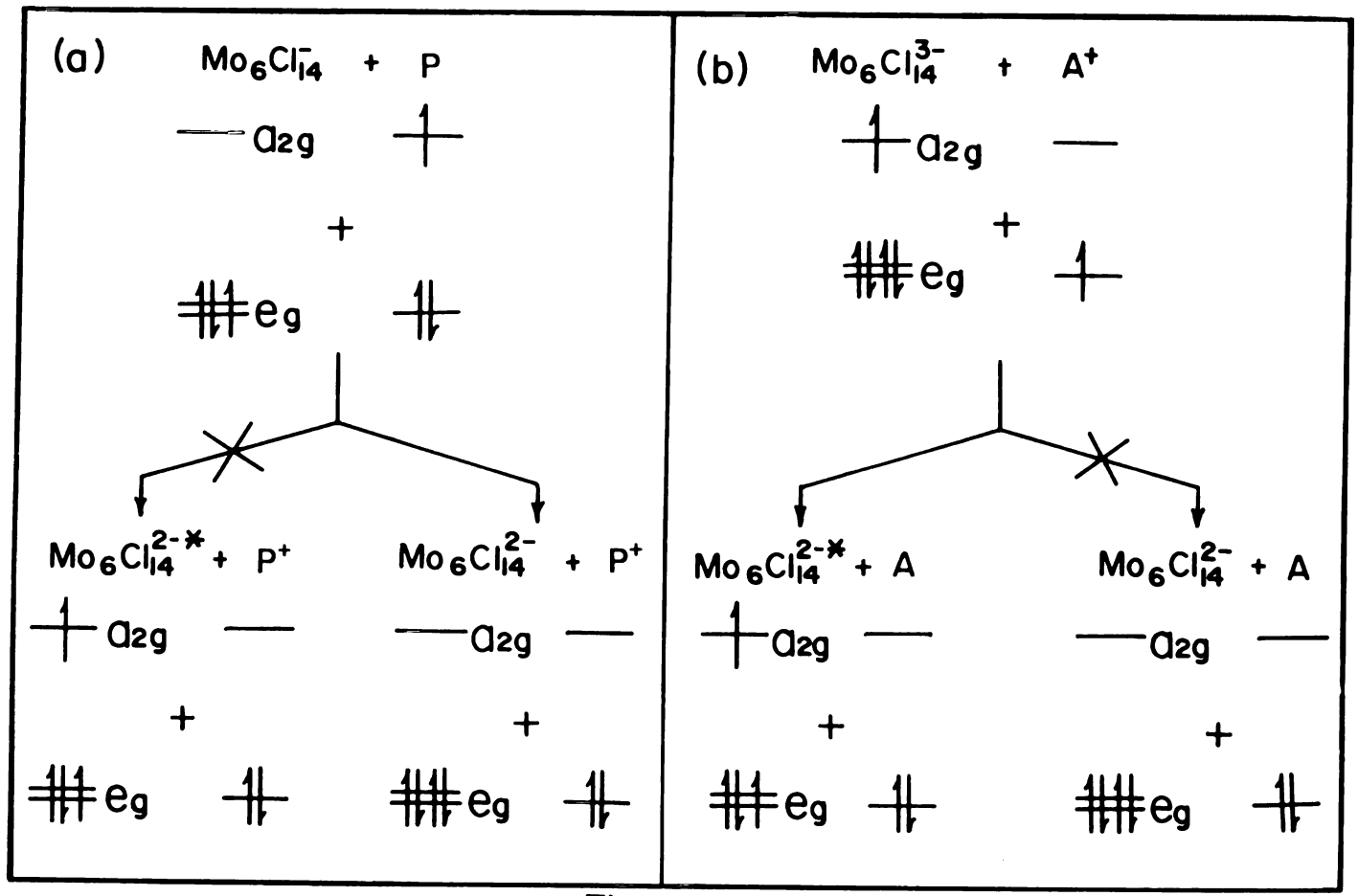
(a)
$Mo_6Cl_{14}^{-}$ + P
a_{2g}
+
e_g
$Mo_6Cl_{14}^{2-*}$ + P^+
a_{2g}
+
e_g
$Mo_6Cl_{14}^{2-}$ + P^+
a_{2g}
+
e_g
(b)
$Mo_6Cl_{14}^{3-}$ + A^+
a_{2g}
+
e_g
$Mo_6Cl_{14}^{2-*}$ + A
a_{2g}
+
e_g
$Mo_6Cl_{14}^{2-}$ + A
a_{2g}
+
e_g

Figure 16

opposing this excited-state pathway is removal of the electron from the a_{2g} orbital to afford ground-state cluster ion. In the case of the $Mo_6Cl_{14}^-/NA^-$ and P systems, transfer of an electron from the donor level to the cluster's a_{2g} orbital directly yields electronically excited ion whereas exchange to the e_g orbital brings the cluster ion to its ground state.

It is evident from Figure 16 that cl is directly competitive with the ground-state reaction. Specifically, the yield for excited-state production, given by eq 15 in Chapter I, is more conveniently expressed as,

$$\phi_{es} = \frac{k_{es}/k_{gs}}{(k_{es}/k_{gs}) + 1} \qquad (32)$$

where k_{es} and k_{gs} are the rate constants for electron transfer to produce excited-state and ground-state products, respectively. The functional dependence of ϕ_{es} on the driving force of the electron-transfer reaction is similar for the different donors and acceptors in CH_2Cl_2 and CH_3CN (See Figures 14 and 15). Namely, the $Mo_6Cl_{14}^{2-}$/acceptor and donor systems show no ecl at low driving forces. Ecl is observed at a threshold energy and at free energies negative of this threshold, ϕ_{es}, rapidly increases. Finally, with increasing exergonicity, the ϕ_{es} approaches a limiting value well below unity.

The energy dependence of ϕ_{es} for ecl measurements in CH_2Cl_2 and CH_3CN is almost equivalent. However, ensuing

electron transfer analysis will focus on CH_3CN because (i) more organic acceptors and donors are soluble in CH_3CN, (ii) the effects of work terms are minimized in CH_3CN, and (iii) electron transfer models are most accurate for reactions in high dielectric mediums.

Substitution of the asymptotically limiting values of the excited-state yields for the $Mo_6Cl_{14}^{3-}/A^+$, $Mo_6Cl_{14}^-/P$, and $Mo_6Cl_{14}^-/NA^-$ systems into eq 32 gives k_{es}/k_{gs} ratios of 0.15, 0.083, and 0.013, respectively. These values clearly establish that the excited-state reaction pathway is kinetically competitive with the ground-state reaction, even though the latter is favored thermodynamically by 2.0 V. This kinetic enhancement of the excited-state pathway may be understood within the context of an electron-transfer model for cl, first proposed by Marcus,[58] in which electron transfer to produce ground-state products is so exergonic that it lies in the inverted region and therefore is inhibited. In contrast, the modest exergonicity of the exchange reaction to produce excited-state products occurs in the normal region and consequently electron transfer proceeds at relatively rapid rates. More quantitatively, the ratio of the excited-state and ground-state rates is given by[12a]

$$2.3RT \log \frac{k_{es}}{k_{gs}} = \frac{1}{4}(\lambda_{gs}-\lambda_{es}) + \frac{1}{2}(\Delta G_{gs}^{\circ}-\Delta G_{es}^{\circ}) + \frac{1}{4}\left[\frac{(\Delta G_{gs}^{\circ})^2}{\lambda_{gs}} - \frac{(\Delta G_{es}^{\circ})^2}{\lambda_{es}}\right] \quad (33)$$

where λ_{es} and λ_{gs} are the reorganizational energies for excited-state and ground-state reactions. This rate expression assumes that electron transfer is adiabatic and occurs at a reaction distance of closest contact (i.e., $r_{ij} = a_i + a_j$ where a_i and a_j are the radii of the two reactants and r_{ij} is the distance between their centers).

The reorganizational energy for electron transfer comprises inner- and outer-sphere contributions ($\lambda = \lambda_i + \lambda_o$). The outer sphere reorganizational parameter is given by eq 3 in Chapter I. The structural similarities of the acceptors and donors listed in Tables 10-15 are manifested in a nearly constant value of $\lambda_o = 0.86 \pm 0.05$ eV for reactions 30 and 31. The values for a_i in eq 3 were calculated with radii equivalent to the sphere of equal volume, using the relation $a = 1/2(d_1d_2d_3)^{1/3}$ where d_i represents the van der Waals diameter along the three molecular axes. The inner-sphere reorganizational parameter depends on differences in equilibrium bond lengths and angles between reactants and products and thus is composed of the inner-sphere contributions of the acceptor or donor and cluster reactants. The contribution to the inner-sphere

reorganizational energy by acceptors and donors can be determined with measured self-exchange rate constants by using the Marcus self-exchange relation, $k = Z \exp(-\lambda/4RT)$ where $Z = 10^{11}\ s^{-1}$ and k is the measured self exchange rate constant. λ_i's associated with the electron-transfer reactions of these compounds are <0.05 eV.[114] For cluster reactants, the mixed cluster ecl and electron-transfer quenching studies described in Chapter III, establish the value of λ_i for the conversion of either $Mo_6Cl_{14}^-$ or $Mo_6Cl_{14}^{3-}$ to the excited state ion, $Mo_6Cl_{14}^{2-*}$ is 0.2 eV. These results suggest that the addition and removal of an electron from the a_{2g} orbital requires almost the same reorganization of the nuclei as the addition and removal of an electron from an e_g orbital. Therefore λ_i for reactions 30 and 31 is ~0.2 eV and values of λ ($=\lambda_i + \lambda_o$) for the excited-state pathway or ground-state pathway of the $Mo_6Cl_{14}^{3-}/A^+$, $Mo_6Cl_{14}^-/NA^-$ or $Mo_6Cl_{14}^-/P$ electron transfer reactions should be nearly equal and on the order of magnitude of 1.10 ± 0.10 eV at a reaction distance of closest contact.

With the appropriate values of λ_{es} and λ_{gs}, k_{es}/k_{gs} can now be evaluated for reactions 30 and 31. For purposes of comparison between the three series, we focus on the electron-transfer reactions of $Mo_6Cl_{14}^{3-}$/tris(4-bromophenyl)amine$^+$ (BPA; $\Delta G_{es}° = -0.54$ V, $\Delta G_{gs}° = -2.54$ V), $Mo_6Cl_{14}^-$/p-nitrobenzaldehyde$^-$ (NBA; $\Delta G_{es}° = -0.48$ V, $\Delta G_{gs}° = -2.48$ V), and $Mo_6Cl_{14}^-$/4-cyano-N-methylpyridinium (CMP;

ΔG_{es}° = -0.30 V, ΔG_{gs}° = -2.30 V) because these systems exhibit asymptotically limiting values of ϕ_{es} for their respective series. Using eq 33, we calculate values of k_{es}/k_{gs} = 5.6 x 10^6, 2.5 x10^3, and 8.3 x 10^5 for the $Mo_6Cl_{14}^{3-}/BPA^+$, $Mo_6Cl_{14}^{-}/CMP$ and $Mo_6Cl_{14}^{-}/NBA^-$ systems, respectively. These values are 10^5 - 10^8 greater than those determined from the measured excited-state yields listed in Tables 10, 12, 14 [$k_{es}/k_{gs}(Mo_6Cl_{14}^{3-}/BPA^+)$ = 0.15; $k_{es}/k_{gs}(Mo_6Cl_{14}^{-}/CMP)$ = 0.033; $k_{es}/k_{gs}(Mo_6Cl_{14}^{-}/NBA^-)$ = 0.0072]. This striking discrepancy between the theoretically predicted and experimentally measured rates of the ground- and excited-state electron transfer is not specific to $Mo_6Cl_{14}^{2-}$ ecl but, as mentioned above, is typical of many inorganic transition metal complexes displaying chemiluminescent reactivity[75]. Deviations from inverted-region behavior have been attributed to a variety of reasons including decomposition of the reactants before annihilation and to a failure of the Marcus model in the inverted region owing to the presence of competitive reaction pathways such as H-atom transfer or the formation of non-emissive excited-state products.[85a,88a] None of these reasons, however, satisfactorily explain the results of $Mo_6Cl_{14}^{2-}$ ecl. For example, invoking a competitive electron-transfer pathway to rationalize the low yields of systems in this study is not reasonable because acceptors and donors were judiciously chosen such that population of their excited states is an energetically unfavorable

process. In addition, we can explicitly rule out deviations from theoretical predictions resulting from the chemical instability of the reactants on the basis of the electrochemical reversibility of the cluster and electroactive organic reactants. Thus differences in calculated and observed rates of the $Mo_6Cl_{14}^{2-}$/acceptor and donor systems bear directly, by design, on the mechanistic features of electron transfer at high exergonicities.

A crucial mechanistic feature of reactions 30 and 31 not explicitly accounted for by the simple Marcus expressions used to derive eq 33 is that cl results from bimolecular electron transfer which can occur over a range of distances.[115] A more general expression is given by eqs 9-14. From these expressions, the distance dependence of the observed bimolecular rate constants of the excited-state and ground-state electron transfer annihilation reactions of the $Mo_6Cl_{14}^{2-}$/acceptor and donor systems, is explicity defined with a knowledge of λ_i $H_{AB}°$, and the driving force. The distance dependence of the excited-state and ground-state pathways is most easily illustrated by differentially solving the integrals in eqs 10 and 11 between r and r + dr for reaction separation distances from an arbitrarily large value of 22 Å to a closest contact distance of 9.5 Å. For this calculation the integrand in eq 11 can best be approximated by $k_{act} = (4\pi\ N/1000)g_e(r)\ k(r)\ r^2\delta r\ (^{-1}\ s^{-1})$ where δr = 0.8 Å.[116] We initially focus on the results of the $Mo_6Cl_{14}^{2-}$/pyridinium series because calculations for the

electron-transfer annihilation reactions of this system are simplified by the fact that $g_e(r) = 1$. Figure 17 shows a plot of the excited-state and ground-state differential rate constants ($k_{es,difn}$ and $k_{gs,difn}$, respectively) as a function of r for the electron-transfer reactions of $Mo_6Cl_{14}^-$ with CMP,

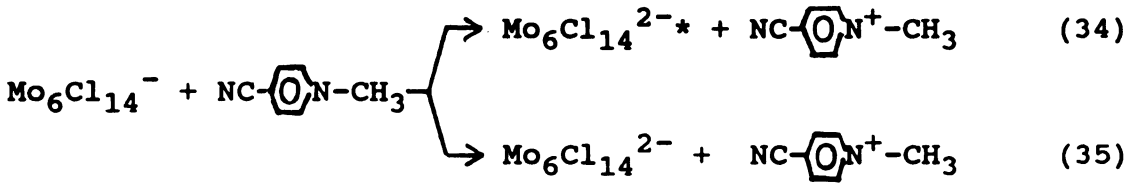

Equations 10 and 11 were evaluated by using an encounter distance, σ, of 9.5 Å, a diffusion coefficient of 5×10^{-6} cm^2 s^{-1}, H_{AB}° = 200 cal and β = 1.2 $Å^{-1}$ which are typical values for electronic coupling terms of transition metals in homogeneous solution.[18] The large value of $k_{es,difn}$ (= $k_{gs,difn} \times 10^5$) at $r = \sigma$ clearly establishes that formation of electronically excited $Mo_6Cl_{14}^{2-}$ is preferred for electron transfer occurring at a separation distance of closest approach. In this regard, the results of eq 10 and 11 at $r = \sigma$ are consistent with those obtained using eq 33. With increasing distance, however, $k_{es,difn}$ and $k_{gs,difn}$ exhibit striking differences in their functional dependences on r. This contrasting behavior of $k_{es,difn}$ and $k_{gs,difn}$ is derived from opposing contributions of λ_o to the electron-transfer rate in the normal and inverted region. As described in Chapter I, the electron-transfer rate is

Figure 17. Distance dependence of the differential bimolecular rate constant for the excited-state (es) and ground state (gs) electron-transfer channels for the reaction between $Mo_6Cl_{14}^-$ and one-electron reduced 4-cyano-N-methylpyridinium (CMP), calculated by solving eqs 3, 9-14 between r and r + αr using β = 1.2 A^{-1} and H_{AB}° = 200 cal.

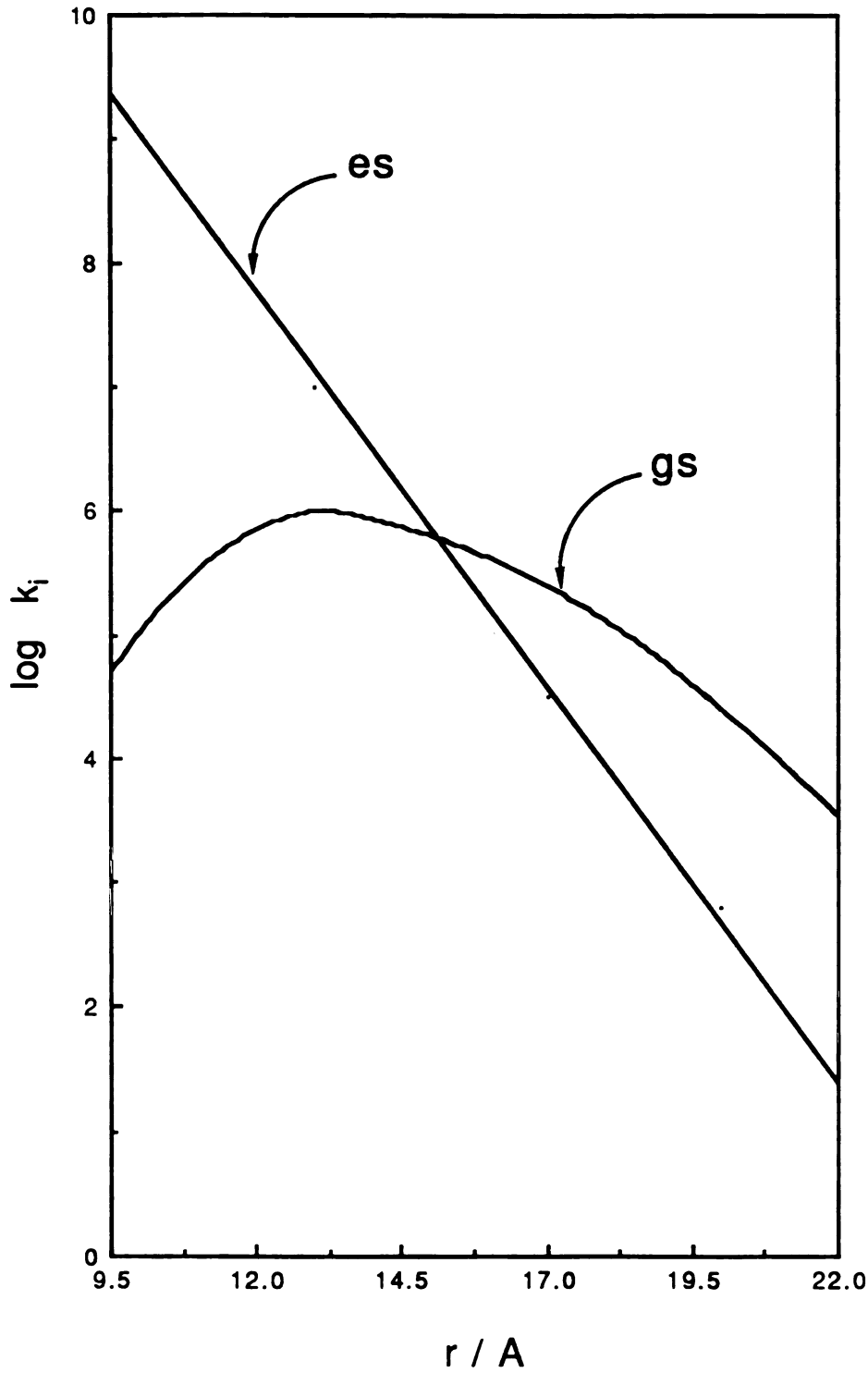

Figure 17

related to the separation distance via the electronic coupling element and outer-sphere reorganizational energy (λ_i is independent of r). From eqs 3 and 14, an increase in r causes λ_o to increase and H_{AB} to decrease in magnitude. For reactions in the normal region (i.e., $-\Delta G^\circ < \lambda$), as is reaction 34, an increase in λ_o raises the activation barrier to electron transfer and the rate becomes attenuated. Couple this effect with an abatement in rate due to decreasing H_{AB} and, as observed in Figure 17, an increase in r is accompanied by a steady diminution in $k_{es,difn}$. Conversely, although an exponential decrease of H_{AB} with r contributes to a decrease of the electron-transfer rate in the inverted region (i.e., $-\Delta G^\circ > \lambda$), it follows directly from eq 13 that the increase of λ_o causes an enhancement of the electron transfer rate in the inverted region. These opposing effects of H_{AB} and λ_o on the electron- transfer rate is reflected in a maximum of $k_{gs,difn}$ at r = 13 Å. The disparate behavior of differential excited-state and ground-state rates with separation distance has interesting implications for the chemiluminescent reactivity of the $Mo_6Cl_{14}^{2-}/CMP^+$ system. As Figure 17 clearly illustrates, the contribution of the ground-state pathway to the overall rate comes from $r > \sigma$, while most of the contribution for excited-state production comes from $r \sim \sigma$. Thus the appreciable values of $k_{gs,difn}$ at $r > \sigma$ suggests that electron transfer to yield ground state products is competitive with excited-state production.

The integral (or overall) excited-state (k_{es}) and ground-state (k_{gs}) rates are explicitly related to the experimentally measured chemiluminescence yields by eq 32. Accordingly, the reaction distance for electron transfer can be determined by integrating eqs. 10 and 11 from $r = \infty$ to a value of r that yields a k_{es}/k_{gs} ratio commensurate with that calculated from the observed chemiluminescence yields. For the $Mo_6Cl_{14}^-$/CMP annihilation reaction, an observed k_{es}/k_{gs} ratio of 0.033 yields an electron-transfer reaction distance of 18 Å. This result clearly implies that approach of the electrogenerated reactants to a distance of closest approach (σ = 9.5 Å) is impeded. Recent studies of outer sphere electron transfer reactions of inorganic metal complexes in nonaqueous solution have demonstrated that ion pairing decreases electron transfer rates by increasing the electron transfer distance (discussed in Chapter V). Considering the relatively high ionic strengths used in our ecl experiments, ion association between the supporting electrolyte and charged reactants is likely, and in this case, reaction at short distances will be inhibited. Indeed, we have observed a marked dependence of the ecl intensity on the concentration of supporting electrolyte (More detailed investigations aimed at assessing the influence of solvent and ion association on ecl will be reported in Chapter V). Thus our calculations indicate that electron transfer between $Mo_6Cl_{14}^-$ and CMP occurs at

reasonably rapid rates over large separation distances to produce $Mo_6Cl_{14}^{2-}$ ion.

The above analysis not only accounts for ϕ_{es} values of less than unity, but it also qualitatively explains the general dependence of ϕ_{es} on $\Delta G°$ for the acceptor and donor systems depicted in Figure 14. Differential ground- and excited-state rates obtained by numerically solving eqs. 10 and 11 for the remaining pyridinium systems are summarized in Figure 18. We have also included in Figure 18 calculations performed for hypothetical pyridinium systems with exergonicities below and near the ecl threshold free energy; these results are indicated by dashed lines. (Electron-transfer annihilation reactions between $Mo_6Cl_{14}^-$ and pyridinium radicals with driving forces less than the ecl threshold free energy, inferred from extrapolation of the data shown in Figure 14, were not investigated owing to our inability to find pyridinium reagents meeting the necessary criteria required of electroactive reagents for ecl studies.) Annihilation reactions possessing driving forces below the ecl threshold energy exhibit comparable excited- and ground-state differential rate constants at distances near close contact. Consequently, the ground-state electron transfer pathway is dominant over all r and, therefore, $k_{gs} >> k_{es}$ and $\phi_{es} << 1$. As the driving force of the annihilation reaction increases, electron transfer to yield excited-state products becomes competitive with the ground-state reaction pathway as evidenced by the

Figure 18. Distance dependence of the differential bimolecular rate constant for the excited-state (es) and ground-state (gs) electron transfer channels for the reaction of $Mo_6Cl_{14}^-$ with: (a) a hypothetical one-electron reduced pyridinium species with ΔG_{gs}° = -2.05 V, ΔG_{es}° = -0.05 eV; (b) a hypothetical one-electron reduced pyridinium species with ΔG_{gs}° = -2.15 V; ΔG_{es}° = -0.15 V; 4-cyano-N-benzylpyridinium; (d) 4-cyano-N-methylpyridinium; (e) 4-carboethoxy-N-benzylpyridinium; and (f) 4-carboethoxy-N-methylpyridinium. The standard fee energy driving forces for (c)-(f) are given in Table 14.

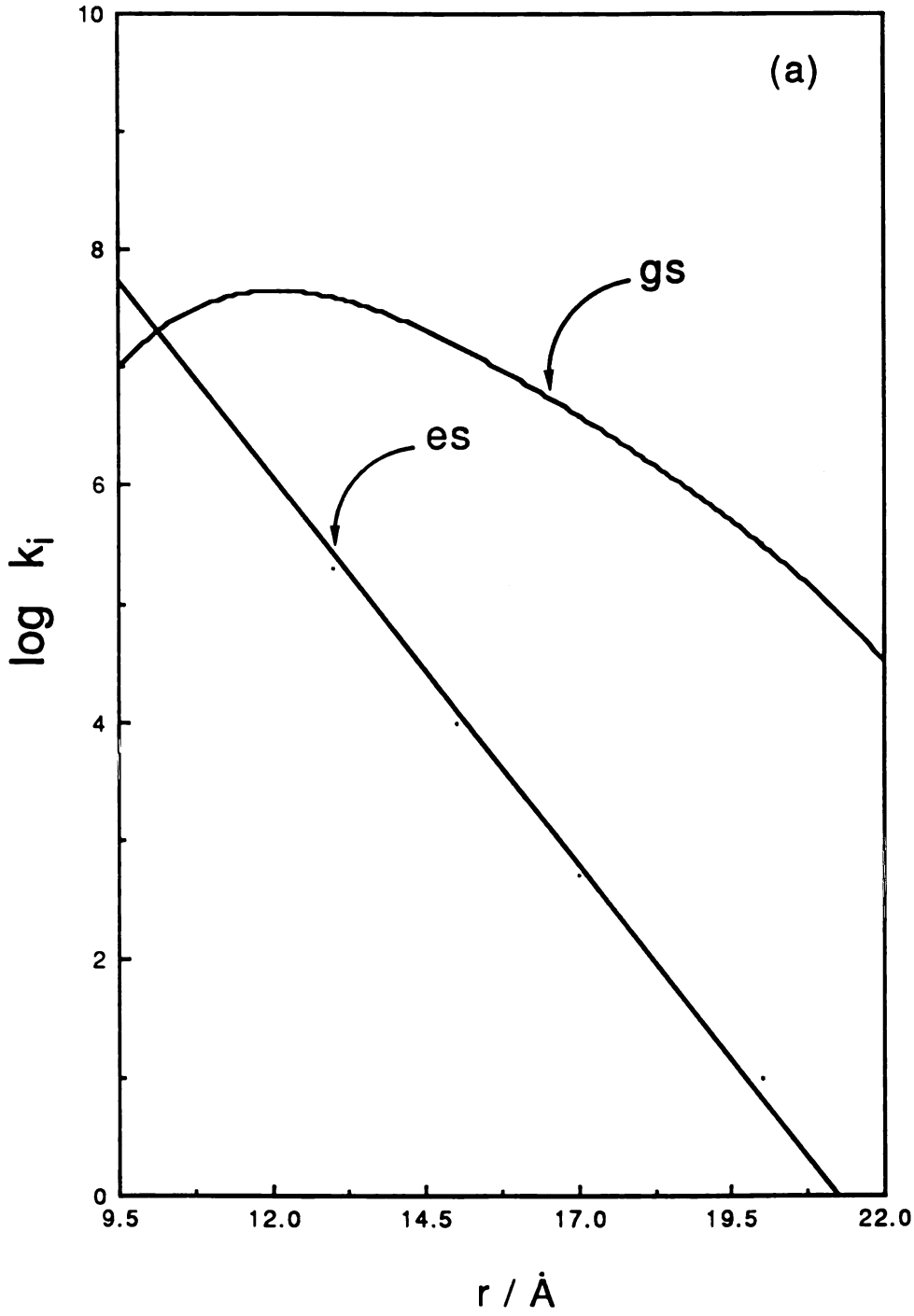

Figure 18

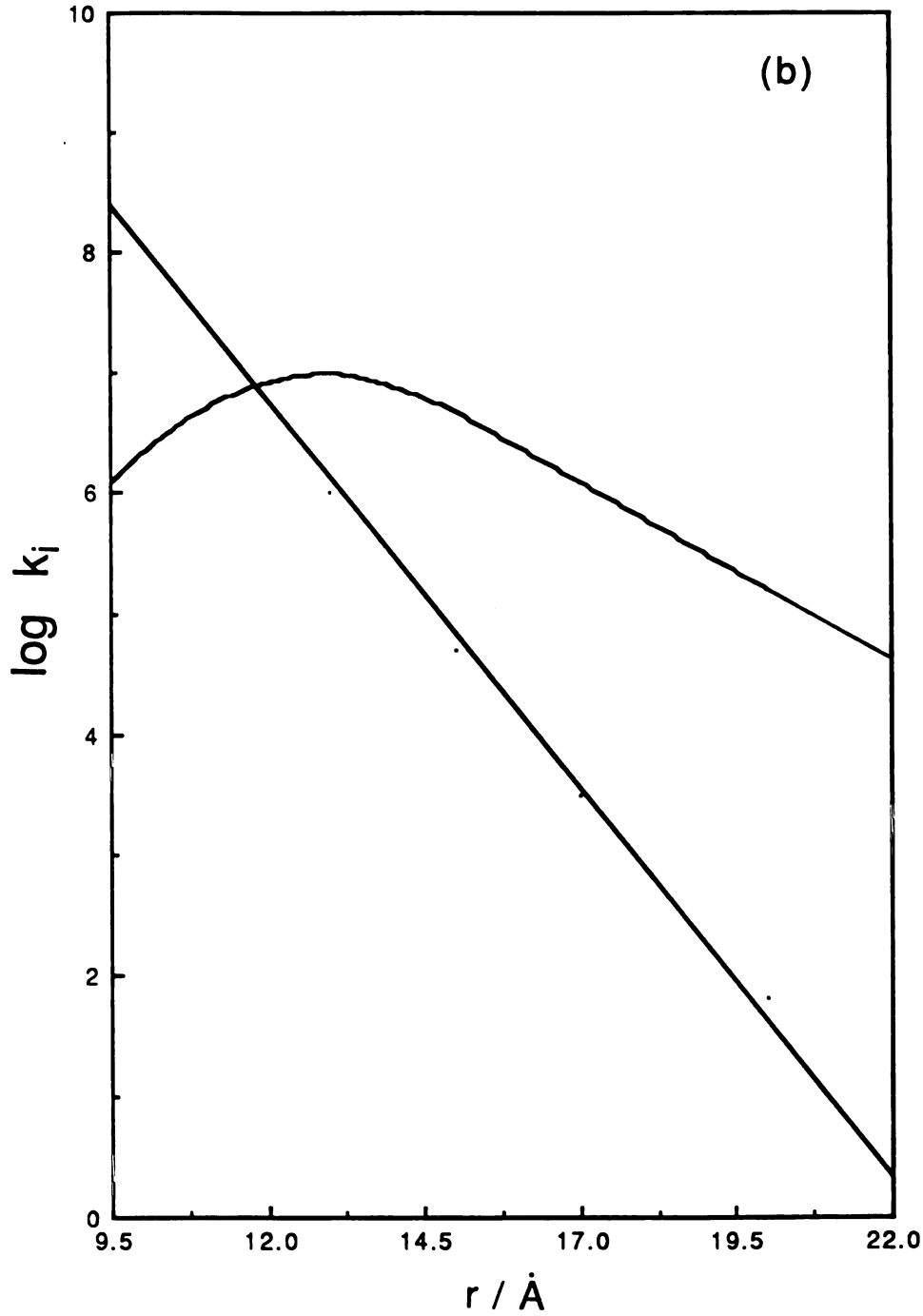

Figure 18

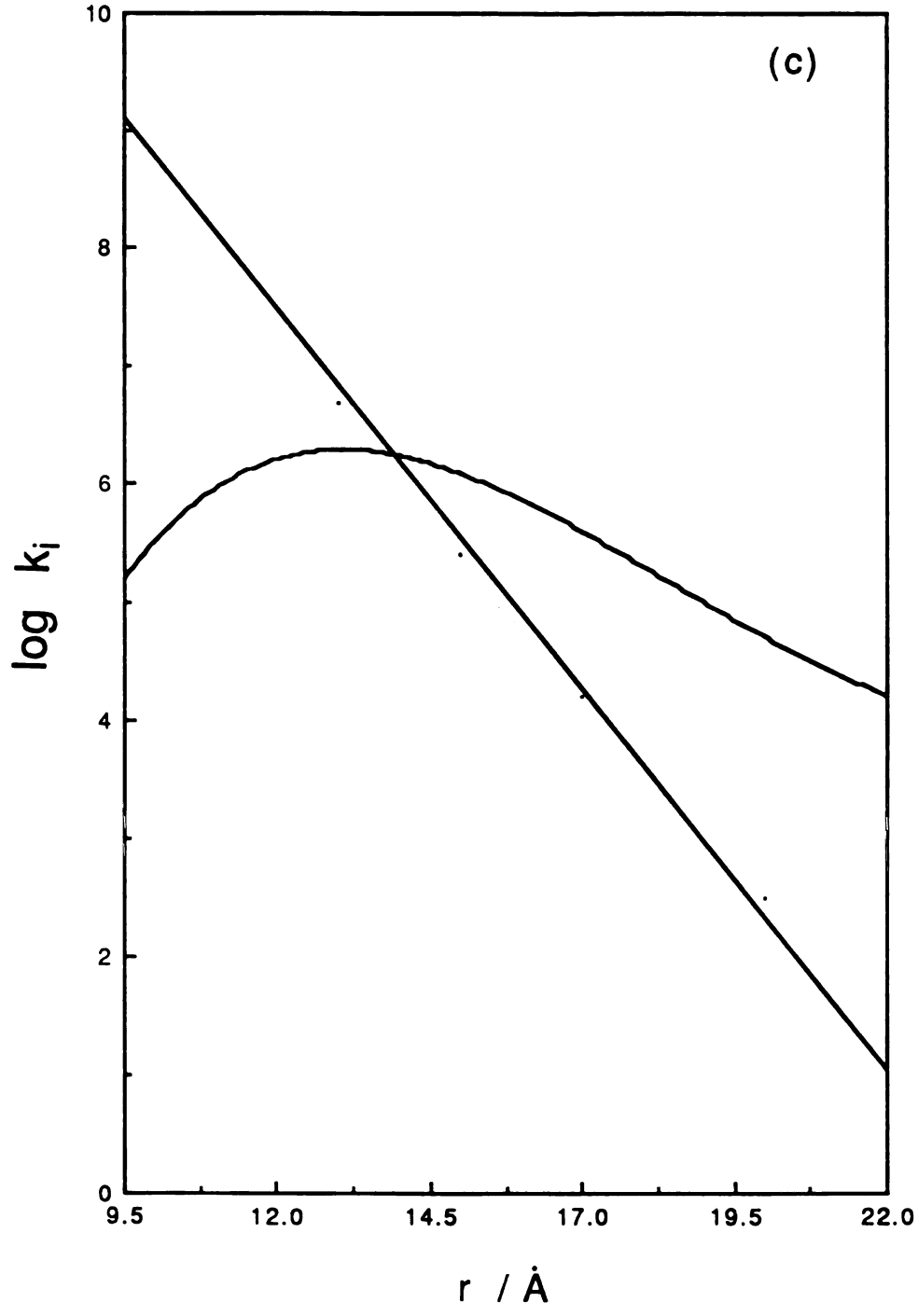

Figure 18

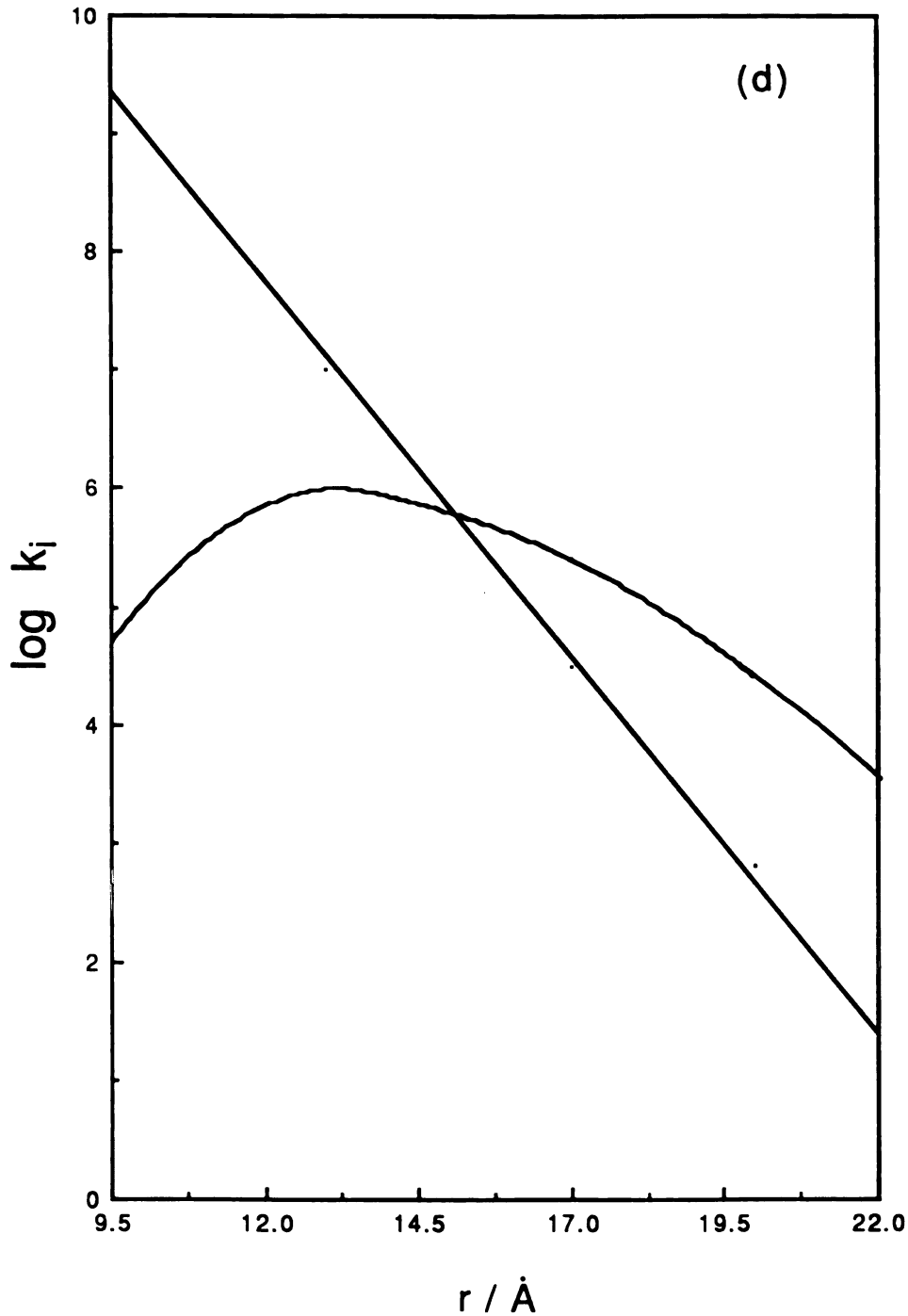

Figure 18

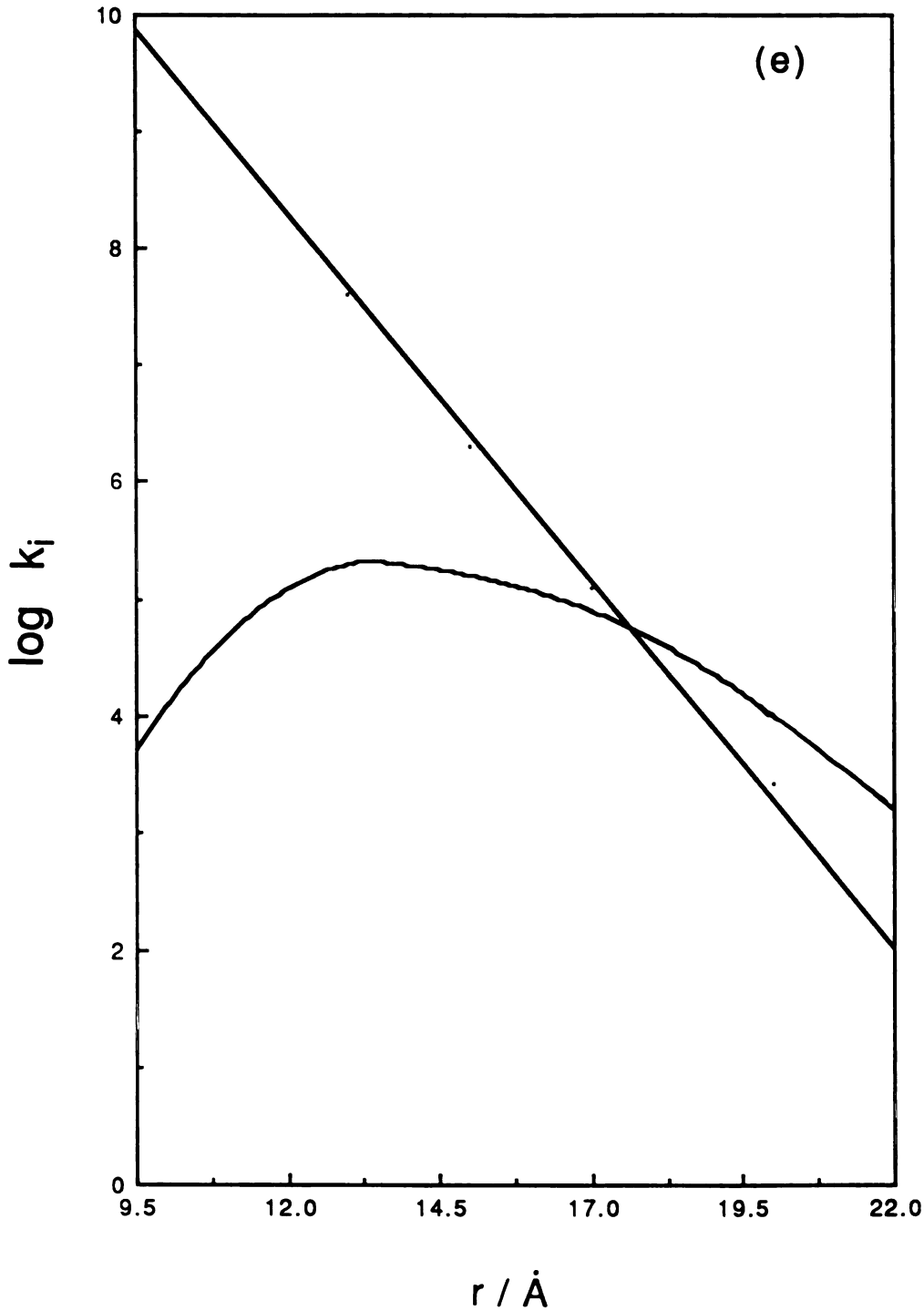

Figure 18

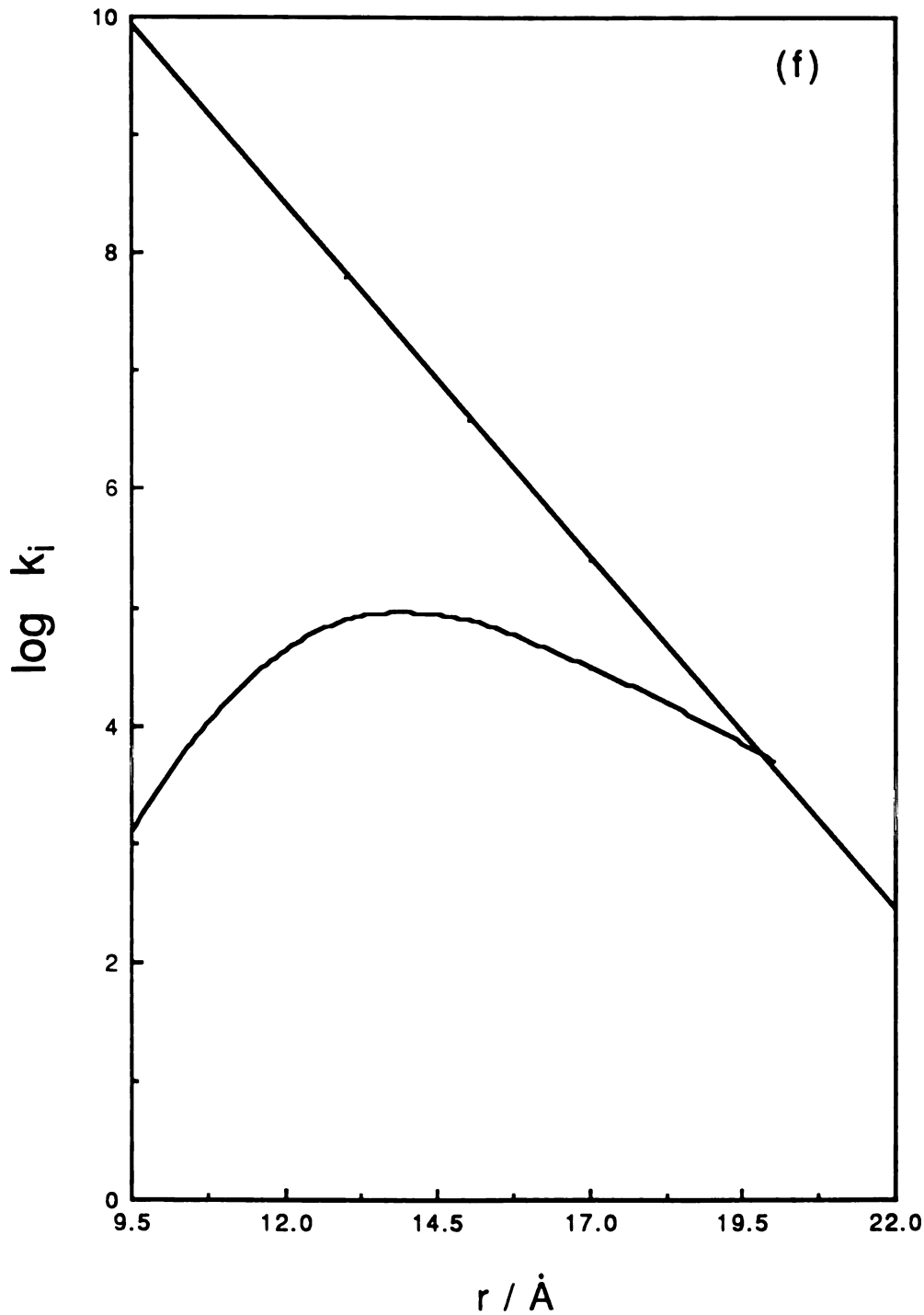

Figure 18

attenuation of $k_{gs,difn}$ and concomitant increase in $k_{es,difn}$ over all r. At large exergonicities, electron exchange to produce electronically excited cluster ion will predominate and ϕ_{es} should be unity. That ϕ_{es} appears to approach an asymptotically limiting value of less than unity (Figure 14) suggests that the ground-state reaction rate is not attenuated to the extent predicted by eq 13. We believe part of this anomalous behavior is nested in the fact that eq 13 is a classical expression and does not include nuclear tunneling effects which can significantly enhance the rate of electron transfer for reactions with large exergonicities[117].

The effects of nuclear tunneling can be evaluated with a semi-classical treatment of electron transfer. The nuclear tunneling factor is defined as[118]

$$\Gamma_n = \frac{\kappa_A}{(\kappa_B)_\infty} \tag{36}$$

κ_A is the nuclear transmission coefficient given by

$$\kappa_A = \exp\left\{-\frac{\Delta G^\circ}{2k_BT} - \frac{\lambda}{h\nu}\left[\coth\left(\frac{h\nu}{2k_BT}\right) - \left\{\frac{(\Delta G^\circ)^2}{\lambda^2} + \operatorname{csch}^2\left(\frac{h\nu}{2_BT}\right)\right\}^{1/2}\right.\right.$$

$$\left.\left. + \left(\frac{\Delta G^\circ}{\lambda}\right) \sinh^{-1}\left(\left(\frac{\Delta G^\circ}{\lambda}\right) \sinh\left(\frac{h\nu}{2k_BT}\right)\right)\right]\right\} \tag{37}$$

In the classical limit (i.e. $h\nu << k_BT$), eq 37 reduces to, eq 38,

$$(\kappa_A)^\infty = \exp\left[-\frac{(\lambda+\Delta G^\circ)^2}{4\lambda k_BT}\right] \tag{38}$$

where $h\nu$ is the intramolecular tunneling frequency. By assuming that the symmetrical metal-metal vibration, ν_{a2g} (Mo_6) = 120 cm^{-1}, is the important vibrational frequency, a nuclear tunneling factor of 1.4×10^2 is calculated for a ground state reaction with a driving force of -3.0 V. This is manifested in a direct enhancement of the ground state rate by two orders of magnitude while the excited state rate remains unaffected. However, this nuclear factor drops off to 3.0 at a driving force of -2.2 V. These results show that although nuclear tunneling does contribute to an increased contribution of the ground state pathway to annihilation at large driving forces, it is not large enough to fully account for a leveling of the excited state quantum yields at high driving forces. Parallel to this semi-classical approach, a complete quantum mechanic treatment of the ground state electron transfer reaction also increases electron transfer rates in the inverted region, however, this increase is relatively small owing to the low energy vibrations of cluster ions. Therefore, not even a quantum mechanical treatment can fully explain the leveling of ϕ_{es} at large driving forces.

Calculations of the integral rates k_{es} and k_{gs} for the $Mo_6Cl_{14}^{2-}/A$ and NA systems are similar to those of the $Mo_6Cl_{14}^{2-}/P^+$ system, however, the equilibrium pair distribution function must be evaluated for the former series. Parallel to the results described above, although formation of excited-state $Mo_6Cl_{14}^{2-}$ is favored for electron exchange between proximate reactants, the long-distance electron transfer channel yielding ground-state products contributes significantly to $Mo_6Cl_{14}^{3-}/A^+$ and $Mo_6Cl_{14}^{-}/NA^-$ annihilation. Solving eqs 10 and 11 with the experimentally measured yields of the $Mo_6Cl_{14}^{3-}/A^+$ and $Mo_6Cl_{14}^{-}/NA^-$ systems listed in Tables 10 and 12 gives reaction separation distances ranging from 18 Å to 20 Å.

Evaluation of eqs 10 and 11 for the $Mo_6Cl_{14}^{2-}$/acceptor and donor systems necessarily relies on estimates of H_{AB}° and β. It is satisfying that the general conclusions derived from Figures 17 and 18 do not significantly depend on these estimates. Specifically, the relative dependence of the ground- and excited-state rates vary only marginally over the rather large interval $0.8\ \text{Å}^{-1} < \beta < 1.8\ \text{Å}^{-1}$ which includes any reasonable value of β for the reactions of the type described in our ecl studies. Furthermore, H_{AB}° is a constant and therefore the excited- and ground-state electron-transfer pathways exhibit a parallel dependence on the electronic coupling element. This result is predicated on our tacit assumption that H_{AB}° is similar for the ground- and excited-state pathways. As discussed in Chapter III the

annihilation involves electrons residing in the metal-based e_g and a_{2g} orbitals of the cluster core. Owing to the similar radial distributions of these metal based orbitals, the electronic factors of the excited- and ground-state electron transfer pathways are more closely related than those of any cl or ecl system studied to date. Nevertheless, our assumption of similar values of $H_{AB}^{\bullet}$ for the two reaction pathways, at best, is tenuous.

The electron-transfer chemistry of $Mo_6Cl_{14}^-$ and $Mo_6Cl_{14}^{3-}$ ions can be described in terms of two competing reaction channels: a highly exergonic electron-transfer pathway yields ground-state products and less exergonic exchange leads to the formation of electronically excited $Mo_6Cl_{14}^{2-}$ ion. The ratio of the electron-transfer rates for these two channels, deduced from measurements of ecl yields, is a powerful experimental quantity which has provided us with the opportunity to address fundamental aspects of electron transfer in highly exergonic regions. Specifically, the observation of ecl from $Mo_6Cl_{14}^{2-}$/acceptor and donor systems is evidence of the Marcus inverted region. Moreover, the cl electron transfer chemistry, interpreted within the context of the theoretical prediction of Marcus and Siders[19,53] and of Brunschwig, Ehrenson, and Sutin[115] that the electron transfer rate in the inverted region will accelerate with increasing distance owing to an increase in the solvent reorganizational parameter, suggests that

excited state production yields of less than unity result from facile electron transfer over long distances.

CHAPTER V

V. ENVIRONMENTAL EFFECTS ON $M_6X_8Y_6^{2-}$ CHEMILUMINESCENCE EFFICIENCIES

A. Background

The electron transfer formalism developed in Chapter IV provides a framework in which to elucidate intrinsic mechanistic details of cl or ecl reactions. The role of distance of the electron-transfer annihilation reaction bears directly on partitioning between the normal and inverted regions and hence the ecl efficiency. Therefore the influence of solvent and supporting electrolyte in mediating distance will be important to the development of efficient cl or ecl systems. For the case of $M_6X_8Y_6^{2-}$ ecl, these influences will be augmented by the fact that the electrogenerated reactants carry second coordination spheres composed of supporting electrolyte and a tight solvent shell owing to the high charges of the reactants.

The role of solvent in electron-transfer reactions has recently come into question because of the inability of current electron-transfer theories to rationalize the absence of the inverted region and other anomalous behavior of bimolecular electron-transfer events.[118-122] Breakdown of a dielectric continuum treatment of the solvent during electron transfer has come under intense scrutiny. Experimentally, this issue has been addressed by considering the role of solvent and ionic strength for the following reaction[123]

$$Fe(Cp)_2 + Co(dmg)_3(BF)_2^+ \longrightarrow Fe(Cp)_2^+ + Co(dmg)_3(BF)_2 \quad (39)$$

(dmg = dimethylglyoxine, Cp = cyclopentadiene)

An observed decrease in rate of the electron transfer with increasing ionic strength was attributed to increased ion-pairing of the charged reactant. Moreover, for a given ionic strength, plots of the log of the rate vs. $(1/D_{op}-1/D_s)$, which is directly proportional to the outer-sphere reorganizational energy, showed no obvious correlation. These results suggested that the solvent and ionic strength might affect the transition state structure (localized structure about reactants different than the bulk solution) or increase the distance of electron transfer.

The idea of a discrete solvent structure (i.e., nondielectric continuum model) about the transition state during electron transfer has been treated by Ulstrup and co-workers by using a nonlocal electrostatic theory.[124] In this approach, a nonlocal dielectric constant, which arises from solvent not being subjected to full dielectric polarization by an ionic field at molecular distances, is used instead of the bulk dielectric constant of the solvent. The nonlocal dielectric constant emphasizes the contribution of electrostatic potentials in determining reaction distances, and is calculated from eq 40 where

$$D_{eff}(r) = D_s / \left[1 + \left(\left(D_s/D_i\right) - 1\right) \quad \exp\left(-r/\Lambda\right)\right] \qquad (40)$$

D_i is a "short-range" dielectric constant corresponding to electronic and molecular polarization and Λ is a

"correlation length". The dependence of the electron-transfer rate of cobalt polypyridyl complexes in different solvent mediums of varying ionic strength has been shown to correlate, not with a continuum dielectric constant, but with the effective dielectric constant described by eq 40.

A more radical deviation from conventional dielectric solvent models has been proposed by Truong who considers every reactant to possess a specific interaction with its solvent shell.[125] At equilibrium conditions, the solvent shell is treated as a charge transfer ligand which acquires the partial charge of the reactant. Electron exchange to or from the reactant must occur through the solvent shell, which is now formulated as a hard sphere imbedded in a dielectric continuum. Effectively, inclusion of the immediate solvent shell as part of the overall charge-transfer complex increases the reaction distance by at least the diameter of two solvent molecules, and its redistribution upon electron transfer contributes significantly to the inner-sphere reorganizational energy. A striking prediction of the theory is that λ_i is a linear function of ΔG° ($=E_{1/2}{}^{ox} - E_{1/2}{}^{red}$). The variation of electron-transfer rate is predominated by λ_i and, therefore log k_{obs} will vary linearly over all driving forces at a given pH and ionic strength. Although these predictions are substantiated by data for several electron-transfer studies, the theory is still under examination, and has yet gained wide acceptance. Nevertheless, this work clearly

demonstrates that specific solvent and supporting electrolyte structures about the transition state will mediate simple electron exchange predictions.

Experimental parameters other than solvent or solute interactions may also bear directly on ecl efficiencies. Variations in the nature of the face-bridging and axial ligands may alter electronic coupling and hence from eq 13 the partitioning between normal and ground-state electron transfer pathways.[24,126] Temperature can play an important role in electron-transfer reactions[127] and hence, ecl chemistry by changing the population distribution between the transition state of the normal and inverted regions. Alternatively, the effects of ligand substitution and temperature may not be so subtle. The stability of the electrogenerated reactants in $M_6X_8Y_6^{2-}$ ecl may be enhanced at low temperatures or preferred for clusters with specific ligand coordination spheres. In these cases, ecl efficiency will simply be related to temperature and ligand substitution inasmuch as they affect the stability of the electrogenerated reactant. This chapter describes efforts to define the effect of solvent, solute, ligation sphere, temperature and other experimental variables such as the ecl potential pulse sequence on the efficiency of $M_6X_8Y_6^{2-}$ ecl.

B. Solvent

The excellent solubility of $(NBu_4)_2M_6X_8Y_6$ clusters in many different solvents permits the investigation of

$M_6X_8Y_6^{2-}$ ecl under a variety of solvent conditions. The electrochemical properties of the $Mo_6Cl_{14}^{2-}$ ion in several nonaqueous solvents is shown in Table 17. The reversibility of the $Mo_6Cl_{14}^{-/2-}$ redox couple is maintained throughout the solvent series. However, as the coordinating ability of the solvent decreases the $Mo_6Cl_{14}^{2-/3-}$ couple becomes quasi-reversible as evidenced by the anodic and cathodic waves becoming broader and more separated. The wide range of dielectric constants of the solvents, shown in Table 18 allows the dependence of the ecl efficiency on solvent to be ascertained by analysis of the solvent reorganizational energy. These solvents, which possess longitudinal relaxation-times too fast for dynamical electron transfer effects, have been shown to behave ideally in electron-transfer studies.[128-135]

The excited state production quantum yields of the annihilation reaction between $Mo_6Cl_{14}^{-}$ with $Mo_6Cl_{14}^{3-}$ or neutral pyridinium radicals (reactions 17 and 30) in different nonaqueous solvents are summarized in Table 19. From straightforward electron-transfer analysis, a decrease in λ will be accompanied by a decreased activation barrier in the normal region and increased barrier in the inverted region. Consequently from eq 15, the ecl yield should increase with decreasing λ and hence $(1/D_{op} - 1/D_s)$. Although the production yields depend significantly on solvent, a plot of ϕ_{es} vs. $(1/D_{op} - 1/D_s)$, which is directly proportional to the outer sphere reorganizational energy,

Table 17

Electrochemical Properties of $Mo_6Cl_{14}^{2-}$ in Various Nonaqueous Solvents

	Solvent	$E_{1/2}(-/2-)$[a] vs SCE V	$E_{1/2}(2-/3-)$[b] vs SCE V
1.	Acetonitrile	+1.53	-1.56
2.	Propionitrile	+1.49	-1.60
3.	Butrylonitrile	+1.45	-1.64[c]
4.	Acetone	+1.46	-1.73
5.	Benzonitrile	+1.48	-1.61
6.	Dichloromethane	+1.38	-1.70[c]
7.	1,2-dichloroethane	+1.36	-1.73[c]

[a] As reduction potential for the $Mo_6Cl_{14}^{-/2-}$ couple vs SCE at 23°C.

[b] As reduction potential for the $Mo_6Cl_{14}^{2-/3-}$ couple vs SCE at 23°C.

[c] Reduction couples are quasi-reversible.

Table 18

Physical Properties of Solvents Used in Ecl Studies

	D_{op}	D_s	τ_D/sec[a]	τ_L/sec[b]	Dipole Moment x 10^{18}/esu·cm
1. Acetonitrile	1.80	37.5	3.3×10^{-12}	0.2×10^{-12}	3.92
2. Propionitrile	1.87	27.2	6.5×10^{-12}	0.5×10^{-12}	3.56
3. Butrylonitrile	1.92	20.3	-	-	4.07
4. Acetone	1.84	20.7	3.3×10^{-12}	0.3×10^{-12}	3.88
5. Benzonitrile	2.38	25.2	3.8×10^{-12}	5.8×10^{-12}	4.18
6. Dichloromethane	2.03	9.08	1.5×10^{-12}	0.4×10^{-12}	1.20
7. 1,2-dichloroethane	2.08	10.8	6.9×10^{-12}	1.6×10^{-12}	1.60

[a] Debye relaxation times from ref. 128a and 128d.

[b] Longitudinal solvent relaxation time determined from corresponding values of τ_D, D_s and D_{op} by $\tau_L = (D_{op}/D_s)\ \tau_D$.

Table 19

Excited State Production Efficiencies for Ecl Reactions in Several Nonaqueous Solvents

		ϕ_{es_3}[a]	ϕ_{es_4}[b]	$(1/D_{op}-1/D_s)$[c]
1.	Acetonitrile	0.065	0.075	0.53
2.	Propionitrile	0.065	0.16	0.49
3.	Butrylonitrile	0.040	0.092	0.47
4.	Acetone	0.014	0.051	0.49
5.	Benzonitrile	0.10	0.12	0.38
6.	Dichloromethane	0.50	0.50	0.38
7.	1,2-dichloroethane	0.50	0.50	0.39

[a] Excited state quantum yield of $Mo_6Cl_{14}^{2-}$ in the electron transfer reaction between $Mo_6Cl_{14}^{-}/Mo_6Cl_{14}^{3-}$ at 23°C, μ = 0.1 NBu_4PF_6.

[b] Excited state quantum yield of $Mo_6Cl_{14}^{2-}$ in the electron transfer reaction between $Mo_6Cl_{14}^{-}$/4-cyano-N-methylpyridinium at 23°C, μ = 0.1 NBu_4PF_6.

[c] Dielectric term in the outer sphere reorganizational energy from eq 3.

shows no obvious relation between dielectric and ecl efficiency (Figure 19). The similarity of the plots for reactions 17 and 30 demonstrates that a correlation between ϕ_{es} and $(1/D_{op} - 1/D_s)$ is not obscured by work term contributions. These observations are consistent with similar plots of several other inorganic bimolecular electron transfer reactions in nonaqueous solutions.[123]

The data in Figure 19 clearly establish that electron transfer is not occurring between reactants at a distance of closest contact in a dielectric continuum. Alternatively, the data suggests that the solvent is directly mediating the electron-transfer distance. Inspection of Table 19 reveals that efficiency of the ecl reaction is loosely correlated with the solvents' dipole moment (Table 18). A tight second solvent shell coordination sphere will inhibit the reactants from approaching closest contact distance. As discussed in Chapter IV, distances greater than closest contact cause the contribution of the ground state electron-transfer pathway to become more competitive with, and in some cases surpass that of, the excited state pathway. Electron transfer distances for the electron-transfer reaction in these solvent systems can be ascertained from ϕ_{es} by the analysis described in Chapter IV. As previously discussed, calculations of the reaction distance are facilitated by the absence of work terms. The parameters of the integrand in eqs 10 and 11 and the reaction distances for the $Mo_6Cl_{14}^-$/4-cyano-N-methylpyridinium in various solvents are shown in

Figure 19. Plot of log ϕ_{es} vs. $(1/D_{op} - 1/D_s)$ for: (a) $Mo_6Cl_{14}^-/Mo_6Cl_{14}^{3-}$; and (b) $Mo_6Cl_{14}^-/P$ in various nonaqueous solvents, numbering as in Table 19.

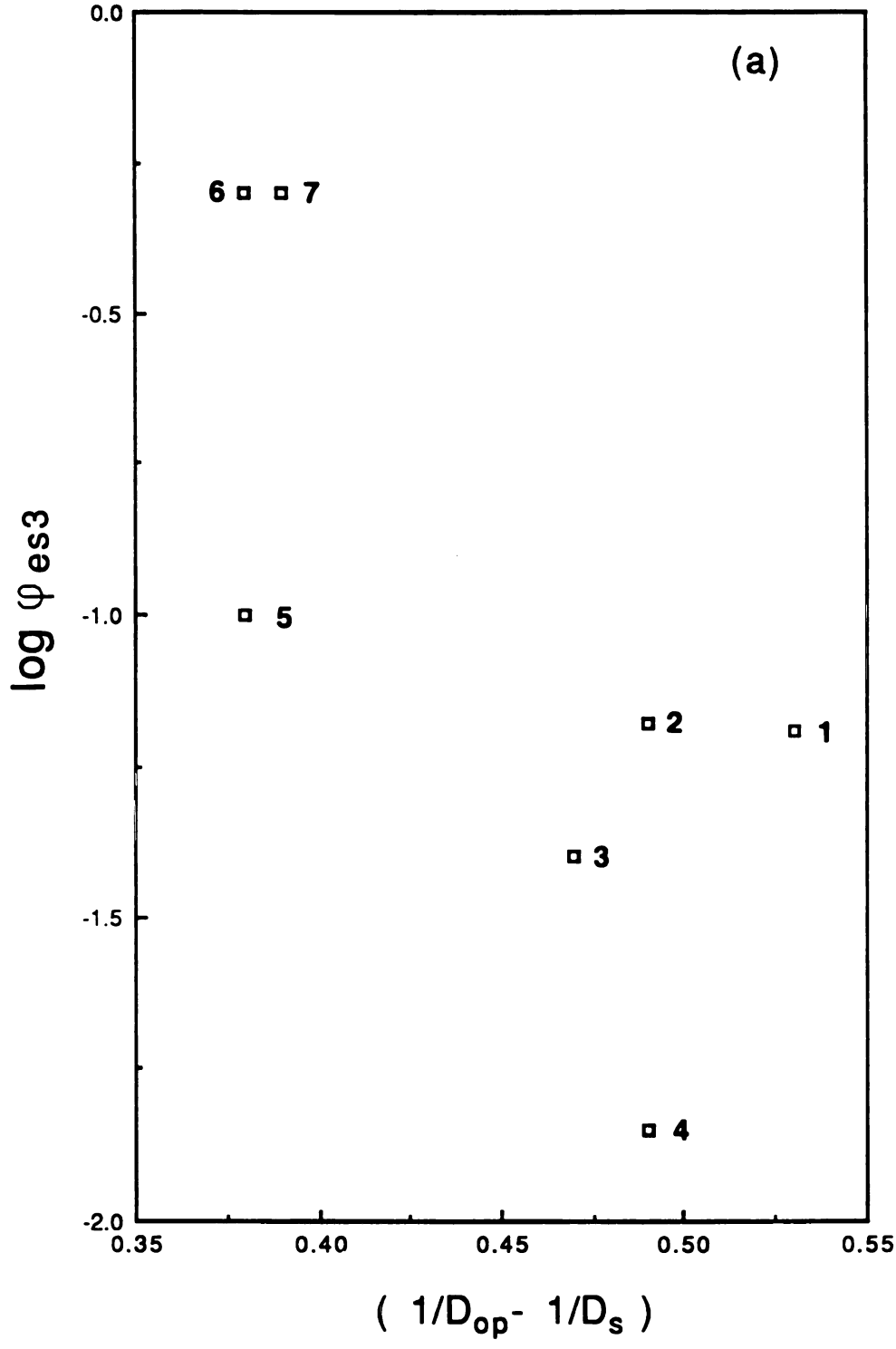

Figure 19

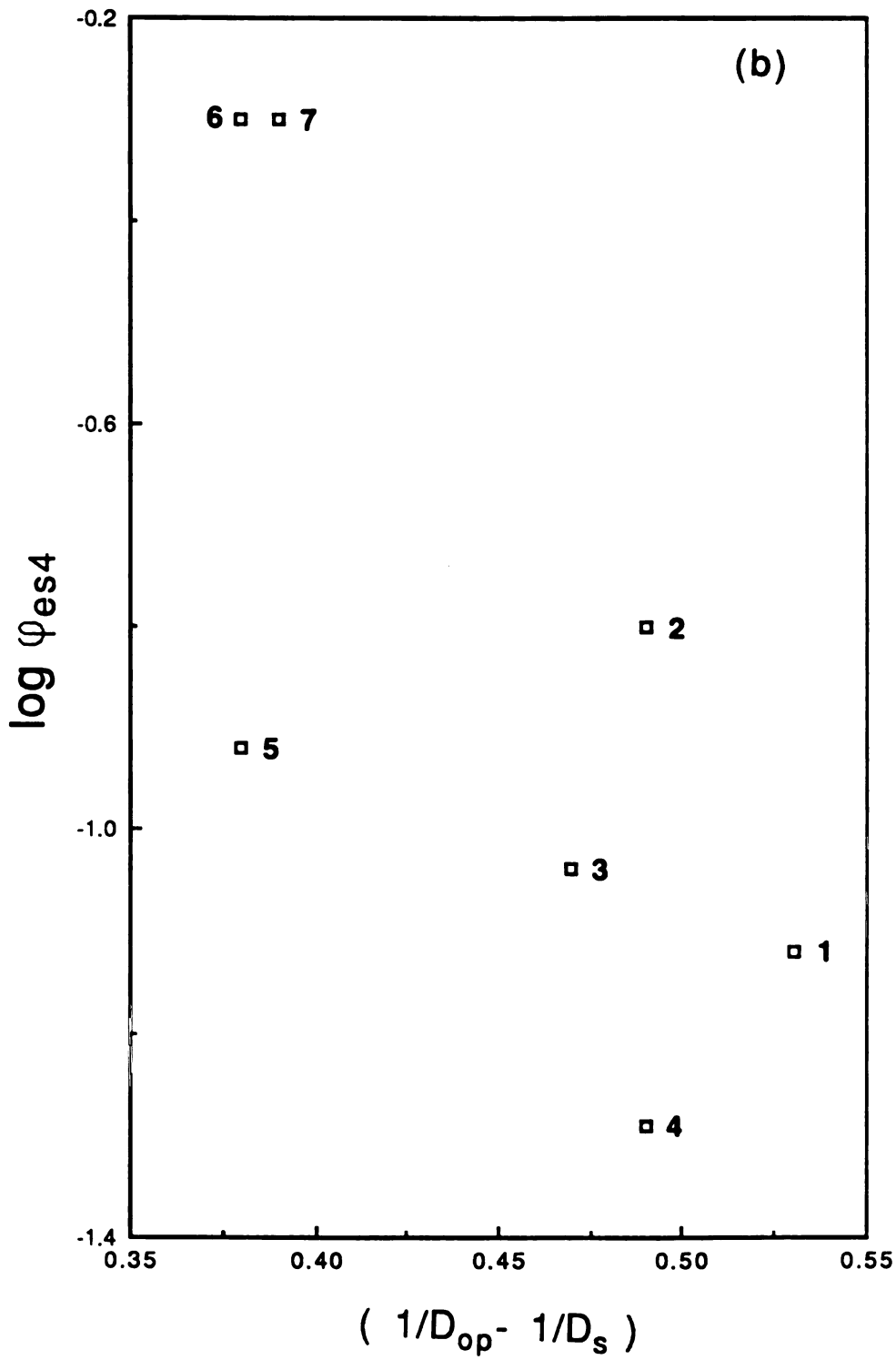

Figure 19

Table 20. In each solvent the calculated r value is much larger than the closest contact of 9.5 Å. That the difference between the observed reaction distance and distance of closest contact, (Δr) listed in Table 21, in each solvent varies despite the same supporting electrolyte, implies that the observed reaction distance is directly related to the solvent. We see, with inspection of the kinetic diameters of each solvent (Table 21), that Δr is approximately equal to the diameter of two solvent molecules. Thus, these data suggest that electron transfer occurs between reactants separated by two solvent molecules.

Our prediction that two solvent molecules mediate the electron transfer distance of $M_6X_8Y_6^{2-}$ ecl is supported by a qualitative comparison of the ecl quantum yields of reactions 17 and 30 in various solvents. Substitution of the neutral pyridinium for $Mo_6Cl_{14}^{3-}$ is accompanied by an increase in the ecl efficiency in all coordinating solvents. The more highly charged trianion should possess a much larger solvation shell than the neutral pyridinium donor and hence electron transfer of the former system should occur over longer distances.

The solvation studies show that solvent plays a critical role in $M_6X_8Y_6^{2-}$ ecl. The origins of solvent effects are not directly related to the solvents dielectric but from the more subtle contributions of the solvent in mediating the electron transfer distance. For the case of $M_6X_8Y_6^{2-}$/4-cyano-N-methylpyridinium ecl chemistry, the

Table 20

Electron Transfer Parameters and Reaction Distances for the Ecl Reaction of $Mo_6Cl_{14}^-$/4-cyano-N-methylpyridinium

	$H_{AB}°$ [a]	w_r/eV [b]	w_p/eV [b]	λ/eV [c]	ΔG_{es}/eV [d]	r/A [e]
Acetonitrile	0.0087	0.0	0.076	1.06	0.30 eV	17 A
Propionitrile	0.0087	0.0	0.10	0.90	0.27 eV	18.5 A
Butyronitrile	0.0087	0.0	0.14	0.74	0.24 eV	22 A
Acetone	0.0087	0.0	0.13	0.99	0.26 eV	21 A
Benzonitrile	0.0087	0.0	0.11	0.90	0.19 eV	-

[a] Electronic coupling element estimated from typical transition metal electron transfer reactions.

[b] Work terms calculated from eqs 5 and 6, μ = 0.1 M NBu_4PF_6 at 23°C.

[c] Total reorganizational energy determined from eq 3 with a inner sphere contribution equal to 0.2 eV.

[d] Driving force to produce the excited state of $Mo_6Cl_{14}^{2-}$.

[e] Electron transfer distance calculated with the method used in Chapter IV.

Table 21

Solvent Diameters and Δr Values for $Mo_6Cl_{14}^-$/ 4-cyano-N-methylpyridinium Ecl Reactions

	Δr/A[a]	k_d/A[b]
Acetonitrile	7.5	4.0
Propionitrile	9	4.7
Butyronitrile	12.5	5.7
Acetone	11.5	5.5
Benzonitrile	-	8.0

[a] Is the difference between the observed reaction distance and closest contact.

[b] Kinetic diameter of the solvent calculated from a sphere of equal volume using the relation $k_d = (d_1 d_2 d_3)^{1/3}$ where d_i is the diameter along the three molecular axes.

proposed model consisting of two reactants separated by a distance of approximately two solvent molecules, is concordant with Truong's approach in which the reactants solvent shell is preserved in the transition state. A localized solvent microstructure, which is typically not addressed in electron transfer studies, most likely is important not only in ecl reactions, but bimolecular electron transfer reactions in general.

C. Ionic Strength Effects

Supporting electrolyte can play a role in determining ecl efficiencies. For the $Mo_6Cl_{14}^-/Mo_6Cl_{14}^{3-}$ ecl reaction, in CH_2Cl_2 the concentration of supporting electrolyte dramatically alters ϕ_{es}, (Figure 20). The effect of supporting electrolyte concentration on ecl efficiency is attenuated in CH_3CN. This trend is consistent with a decrease in work terms associated with $Mo_6Cl_{14}^-/Mo_6Cl_{14}^{3-}$ electron transfer as the medium's dielectric is increased. Similar arguments have been used to previously interpret ionic strength effects observed for other ecl systems in which both reactants are charged.[136,137]

From simple charge considerations the anion of the supporting electrolyte should not perturb the $Mo_6Cl_{14}^{2-}$ ecl efficiency. This expectation is confirmed by the data shown in Table 22, changing the anion from BF_4^-, ClO_4^-, AsF_6^-, PF_6^-, and $CF_3SO_3^-$, while keeping the cation constant (NBu_4^+), has little effect on the overall excited state

Figure 20. Plot of log ϕ_{es} vs ionic strength, μ, for the electron transfer of $Mo_6Cl_{14}^-/Mo_6Cl_{14}^{3-}$ in CH_2Cl_2 (□) and CH_3CN (■) at 23°C.

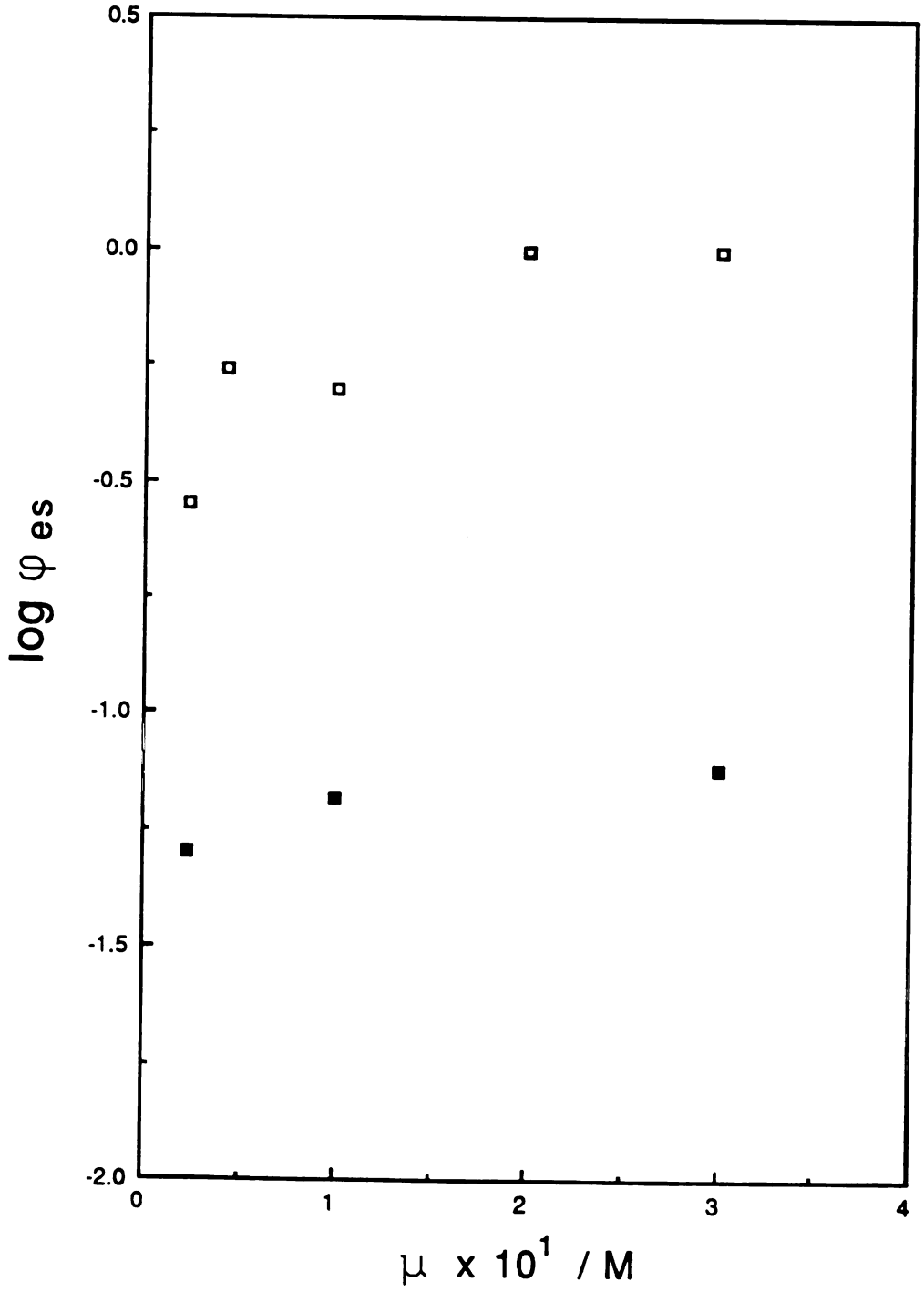

Figure 20

Table 22
Supporting Electrolyte Studies
for the $Mo_6Cl_{14}^{2-}$ Ecl Reaction

Supporting Electrolyte	conc./M	$\phi_{es}(CH_2Cl_2)$[a]	$\phi_{es}(CH_3CN)$[b]
NBu_4PF_6	0.10	0.50	0.065
NBu_4ClO_4	0.10	0.33	0.025
NBu_4BF_4	0.10	0.50	-
NBu_4AsF_6	0.10	0.33	-
$NBu_4CF_3SO_3$	0.10	0.47	-
NBu_4PF_6	0.30	1.00	0.074
NBu_4PF_6	0.02	0.55	0.060
NBu_4PF_6	0.04	0.28	-

[a] Excited state quantum yield for the annihilation reaction of $Mo_6Cl_{14}^-/Mo_6Cl_{14}^{3-}$ in CH_2Cl_2 at 23°C.
[b] Excited state quantum yield for the annihilation reaction of $Mo_6Cl_{14}^-/Mo_6Cl_{14}^{3-}$ in CH_3CN at 23°C.

yield. The decreased durability of $Mo_6Cl_{14}^{2-}$ ecl and varying day to day ecl yields were observed when ClO_4^- was the supporting electrolyte anion. These observations are explained by the more nucleophilic behavior of ClO_4^- and its tendency to promote interfering, but ill-defined side reactions.[137b,138]

Much larger perturbations of the ecl yield by the supporting electrolyte should be observed with changes of the cation. If ion-pairing is important in determining reaction distance, then variation of the cation's size should significantly affect the rate of excited state production.[123,126] A dramatic decrease in ϕ_{es} in CH_3CN is observed along the series $NBu_4^+ > NEt_4^+ \cong NMe_4^+$ (Table 23). These data conflict with ion-pairing considerations which predict an increase in ϕ_{es} with decreasing size of the cation. Indeed, the behavior of the ecl yield with the supporting electrolyte appears to be much simpler in origin. The decrease in ϕ_{es} is related to the decreased solubility of $Mo_6Cl_{14}^{2-}$ in CH_3CN containing NEt_4^+ and NMe_4^+. We expect the trianion to be even less soluble than the dianion. Indeed, after scanning the reduction wave of $Mo_6Cl_{14}^{2-}$ in CH_3CN solution containing NMe_4^+ or NEt_4^+ large anodic peaks due to cluster absorbed on the electrode are observed. Moreover, decreased ecl yields are not observed for annihilation reactions between $Mo_6Cl_{14}^-$ and reduced pyridinium (Table 23). These results clearly suggest that the decrease in ecl efficiencies is not due to larger

Table 23

Dependence of Ecl Efficiencies on Supporting Electrolyte Cation

Supporting Electrolyte	conc/M	ϕes_5[a]	ϕes_6[b]
NBu_4PF_6	0.10	0.065	0.10
NEt_4PF_6	0.10	0.006	0.16
NMe_4PF_6	0.10	0.008	0.22

[a] Excited state quantum yield for the annihilation reaction of $Mo_6Cl_{14}^-/Mo_6Cl_{14}^{3-}$ in CH_3CN at 23°C.

[b] Excited state quantum yield for the annihilation reaction of $Mo_6Cl_{14}^-$/4-amido-N-methylpyridinium in CH_3CN at 23°C.

reaction distances owing to ion-pairing, but to depleted concentration of the trianion resulting from the formation of insoluble NMe_4^+ and NEt_4^+ salts in the diffusion layer.

D. Ligand Coordination Sphere Effects

Study of the effect of various ligands on the production efficiency of the excited state in the $Mo_6X_8Y_6^-$ /$Mo_6X_8Y_6^{3-}$ annihilation reaction is facilitated by the ability to synthesize virtually any axially or face-bridging substituted cluster complex. The electrochemical properties of various $Mo_6X_8Y_6^{2-}$ clusters in CH_2Cl_2 was presented previously in Chapter III. The excited state production efficiency of the ecl reactions of these clusters is shown in Table 24. Inspection of Table 24 shows the ecl efficiency of these $Mo_6Cl_8Cl_nX_{6-n}$ (X = Br,I; n = 0-6) efficiency depends dramatically on the axial substitutent; ϕ_{es} is greatly diminished when bromide or iodide is substituted in the axial positions (Figure 21). For the $Mo_6Cl_{12}I_2^{2-}$ and $Mo_6Cl_8I_6^{2-}$ ions, the extremely low values of ϕ_{es} are most likely attributed to degradation of cluster oxidation as evidenced by the multiple oxidation waves in the cyclic voltammogram. However, this explanation is not valid for the bromide substituted $Mo_6Cl_{14}^{2-}$ ($Mo_6Cl_8Cl_nBr_{6-n}^{2-}$) cluster owing to its chemically and electrochemical reversibility. If the bromide-substituted trianion is removed from the annihilation reaction and

Table 24

Excited State Production Efficiencies for $Mo_6Cl_8Cl_nX_{6-n}$ in CH_2Cl_2

Cluster	ϕes_1[a]	ϕes_2[b]
$Mo_6Cl_{14}^{2-}$	0.50	0.50
$Mo_6Cl_{13}Br^{2-}$	0.005	-
$Mo_6Cl_{12}Br_2^{2-}$	0.003	0.18
$Mo_6Cl_{11}Br_3^{2-}$	0.002	-
$Mo_6Cl_8Br_6^{2-}$	0.001	0.027
$Mo_6Cl_{12}I_2^{2-}$	-	-
$Mo_6Cl_8I_6^{2-}$	-	-

[a] Excited state quantum yield for the annihilation reaction of $Mo_6Cl_8Cl_nX_{6-n}^{-}/Mo_6Cl_8Cl_nX_{6-n}^{3-}$ in CH_2Cl_2 at 23°C.

[b] Excited state quantum yield for the annihilation reaction of $Mo_6Cl_8Cl_nX_{6-n}$/4-carboethoxy-N-methylpyridinium in CH_2Cl_2 at 23°C.

Figure 21. Plot of log ϕ_{es} vs. no. of bromides substituted in the axial position for the $Mo_6Cl_8Cl_nBr_{6-n}^{2-}$ ecl reaction in CH_2Cl_2 at 23°C (μ = 0.10 M NBu_4PF_6).

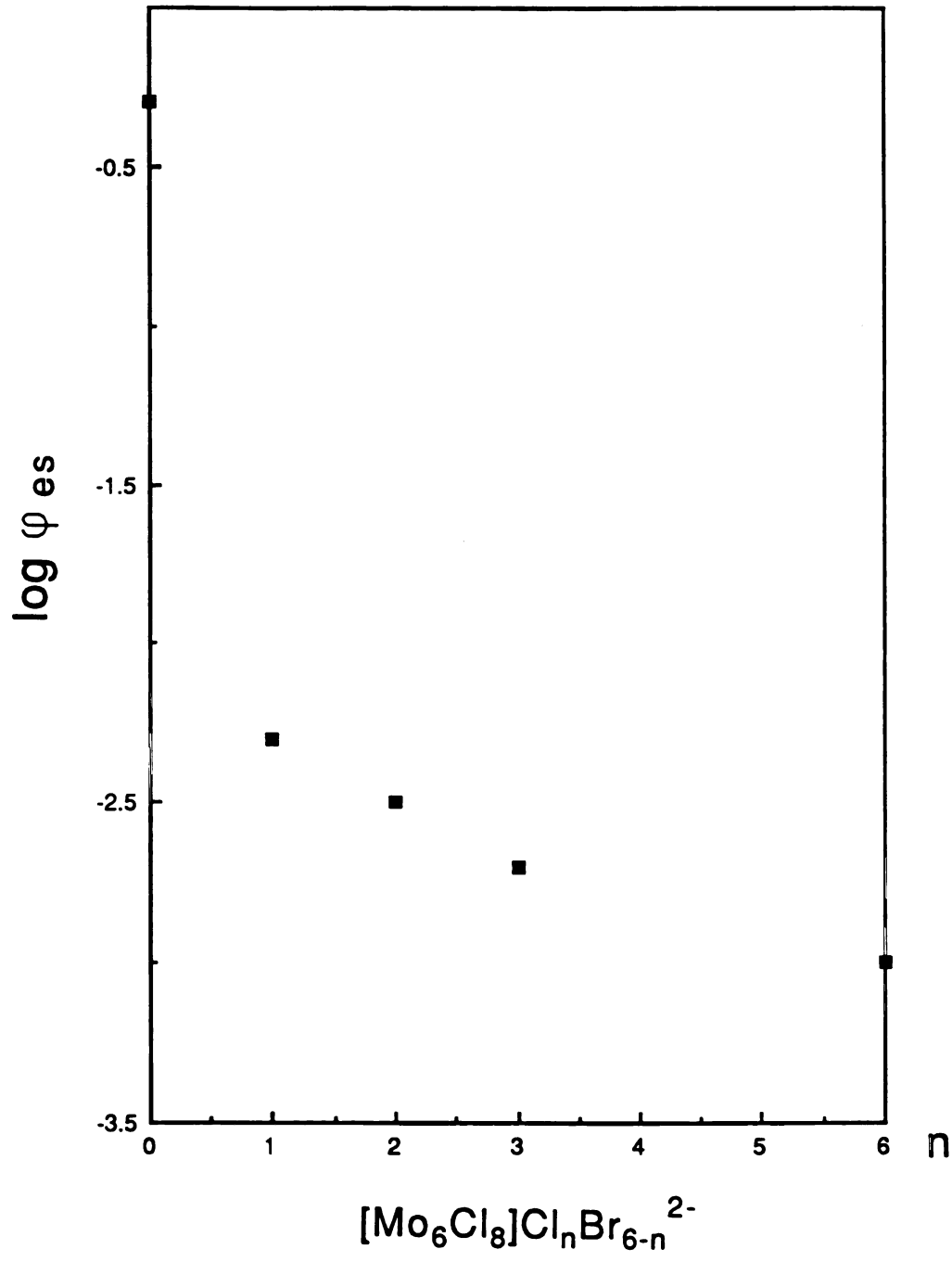

Figure 21

replaced by a neutral pyridinium radical (reaction 41) the ecl efficiency increases

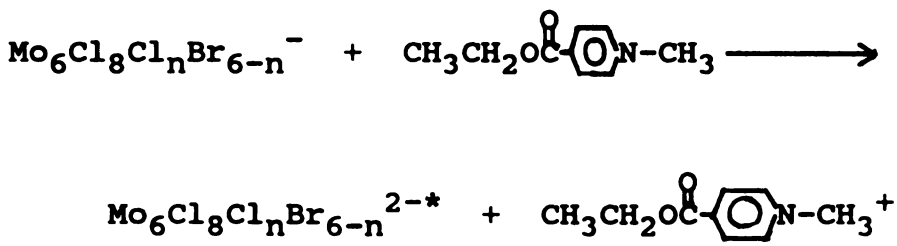

substantially (Table 24). These data clearly show that the diminished ecl yield is associated with the $Mo_6Cl_8Cl_nBr_{6-n}^{3-}$ ion. Addition of bromide to the solutions of $Mo_6Cl_8Cl_nBr_{6-n}^{2-}$ significantly improved the reversibility of the $Mo_6Cl_8Cl_nBr_{6-n}^{2-/3-}$ couple (Figure 22). These results strongly suggest that the low ϕ_{es} yields of $Mo_6Cl_8Cl_nBr_{6-n}^{2-}$ ecl chemistry is due to bromide dissociation from the cluster core upon its one-electron reduction. The decrease cannot be ascribed to low ecl yields of a coordinatively unsaturated intermediate because the $Mo_6Cl_{13}^-$ was prepared and the efficiency for production of the excited state in the ecl reaction (eq 42) is almost equal to that of $Mo_6Cl_{14}^{2-}$ ($\phi_{es}(Mo_6Cl_{13}^-) = 0.40$).

$$Mo_6Cl_{13}^{2-} + Mo_6Cl_{13} \longrightarrow Mo_6Cl_{13}^{-*} + Mo_6Cl_{13}^- \qquad (44)$$

This result demonstrates that the Br^- directly interferes with the cluster's ecl chemistry. A mechanism consistent with these observations is shown in Figure 23. Reduction of

Figure 22. Cyclic voltammogram (CH_2Cl_2 solution at 23°C, 0.1 M NBu_4PF_6) for $Mo_6Cl_8Br_6^{2-}$ (3 mM) ----; $Mo_6Cl_8Br_6^{2-}$ (3 mM) and NBu_4Br (1 mM) ——.

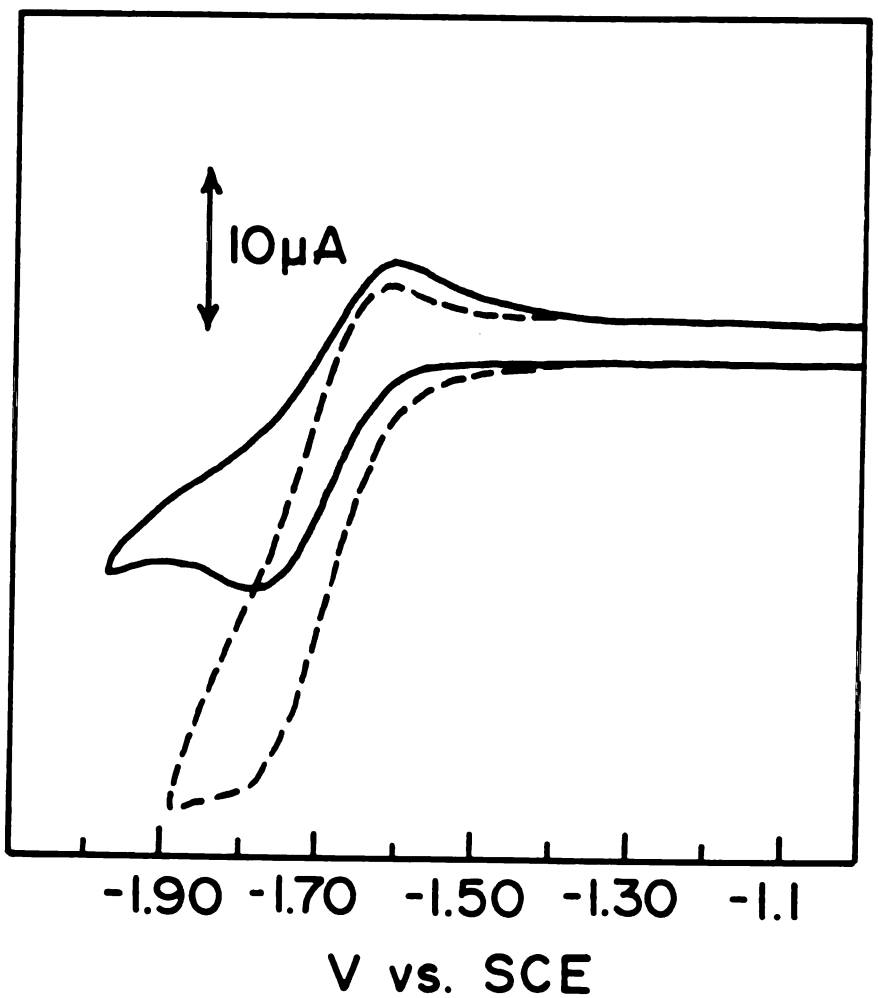

Figure 22

Figure 23. Mechanism for Br^- interference of $Mo_6Cl_8Cl_nBr_{6-n}^-/Mo_6Cl_8Cl_nBr_{6-n}^{3-}$ annihilation reaction.

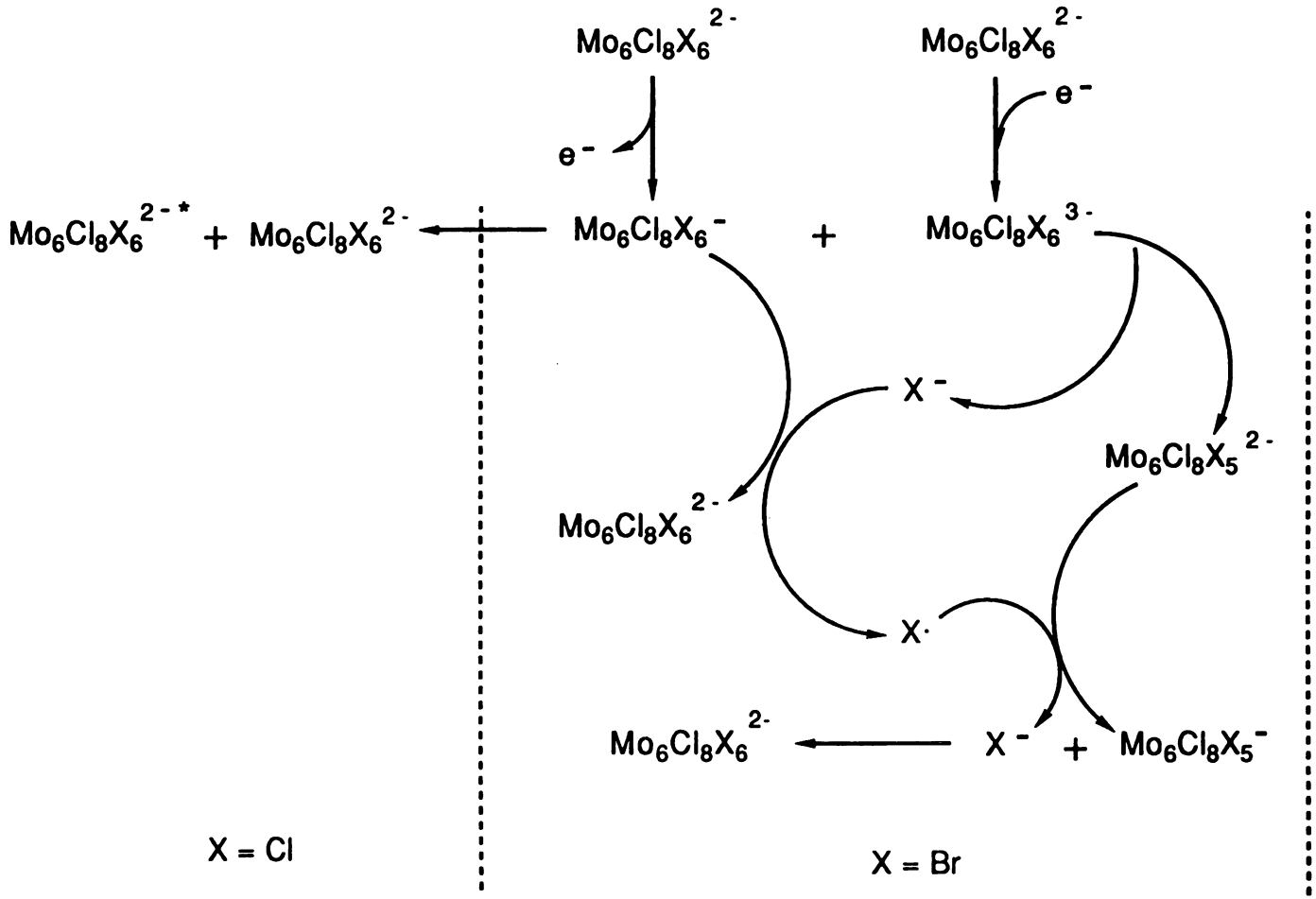
$Mo_6Cl_8X_6^{2-}$
$Mo_6Cl_8X_6^{2-}$
e^-
e^-
$Mo_6Cl_8X_6^{2-*}$ + $Mo_6Cl_8X_6^{2-}$
$Mo_6Cl_8X_6^{-}$ + $Mo_6Cl_8X_6^{3-}$
X^-
$Mo_6Cl_8X_5^{2-}$
$Mo_6Cl_8X_6^{2-}$
$X^{\cdot}$
$Mo_6Cl_8X_6^{2-}$
X^- + $Mo_6Cl_8X_5^{-}$
X = Cl
X = Br

Figure 23

$Mo_6Cl_8Cl_nBr_{6-n}^{2-}$ causes prompt dissociation of bromide from the cluster core to produce unsaturated reduced cluster, $Mo_6Cl_8Cl_mBr_{5-m}^{2-}$ (m = 0-5) and free bromide. Ensuing oxidation of the bromide by $Mo_6Cl_8Cl_nBr_{6-n}^{-}$ yields the dianion and radical halide, which in turn can react with the unsaturated reduced cluster to produce Br^- and $Mo_6Cl_8Cl_mBr_{5-m}^{-}$. Subsequent addition of Br^- to the coordinative unsaturated cluster yields starting dianion. Thus, the ecl mechanism (i.e. $Mo_6Cl_8Cl_nBr_{6-n}^{-}$ /$Mo_6Cl_8Cl_nBr_{6-n}^{3-}$ annihilation) is efficiently circumvented. The crucial step of this mechanism, namely oxidation of bromide by the one-electron oxidized cluster has been independently verified. Figure 24 shows the decrease of the $Mo_6Cl_8Cl_nBr_{6-n}^{2-}$ luminescence during bulk electrolysis to produce $Mo_6Cl_8Cl_nBr_{6-n}^{-}$. Addition of Br^- to freshly oxidized solutions leads to virtually complete recovery of the luminescence intensity. This mechanism does not appear to be important for all chloride clusters because the ϕ_{es} values of $Mo_6Cl_{14}^{-}/Mo_6Cl_{14}^{3-}$ and $Mo_6Cl_{14}^{-}$/P annihilation reactions of equal driving forces are nearly identical.

E. Temperature Effects

The effect of temperature on $Mo_6Cl_{14}^{2-}$ ecl in dichloromethane and acetone is shown in Figure 25. The ecl efficiency increases substantially as the temperature is lowered. Similar observations of other ecl systems have been attributed to increased stability of the

Figure 24. Decrease in $Mo_6Cl_8Br_6^{2-}$ luminescence during bulk electrolysis (——); Increase in luminescence after adding Br^- (----).

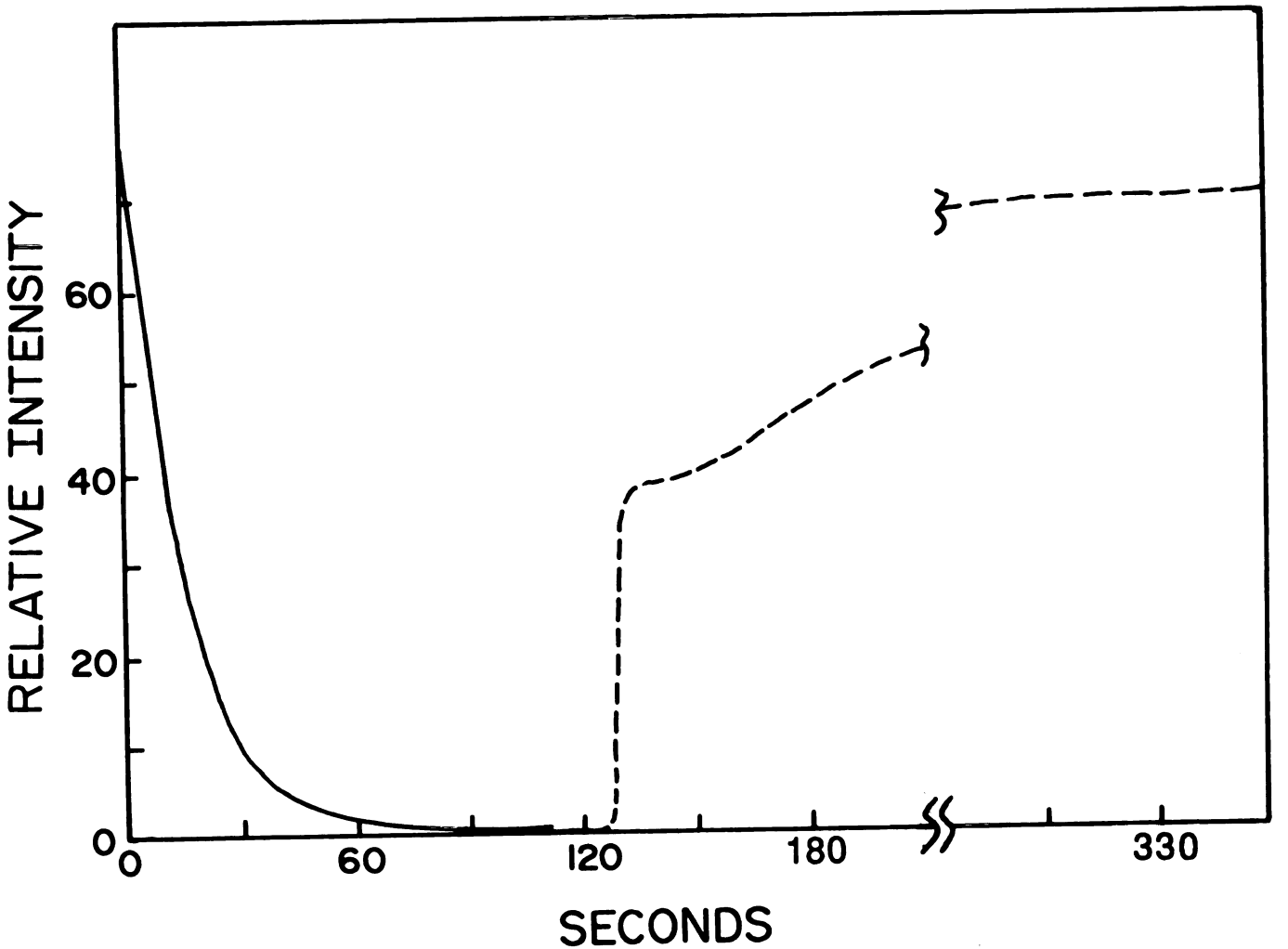

Figure 24

Figure 25. Plot of log ϕ_{es} vs. temperature for the annihilation of $Mo_6Cl_{14}^-/Mo_6Cl_{14}^{3-}$ in dichloromethane (——); $Mo_6Cl_{14}^-$/4-carboethoxy-N-methylpyridinium in dichloromethane (····); $Mo_6Cl_{14}^-/Mo_6Cl_{14}^{3-}$ (----) in acetone at μ = 0.10 NBu_4PF_6.

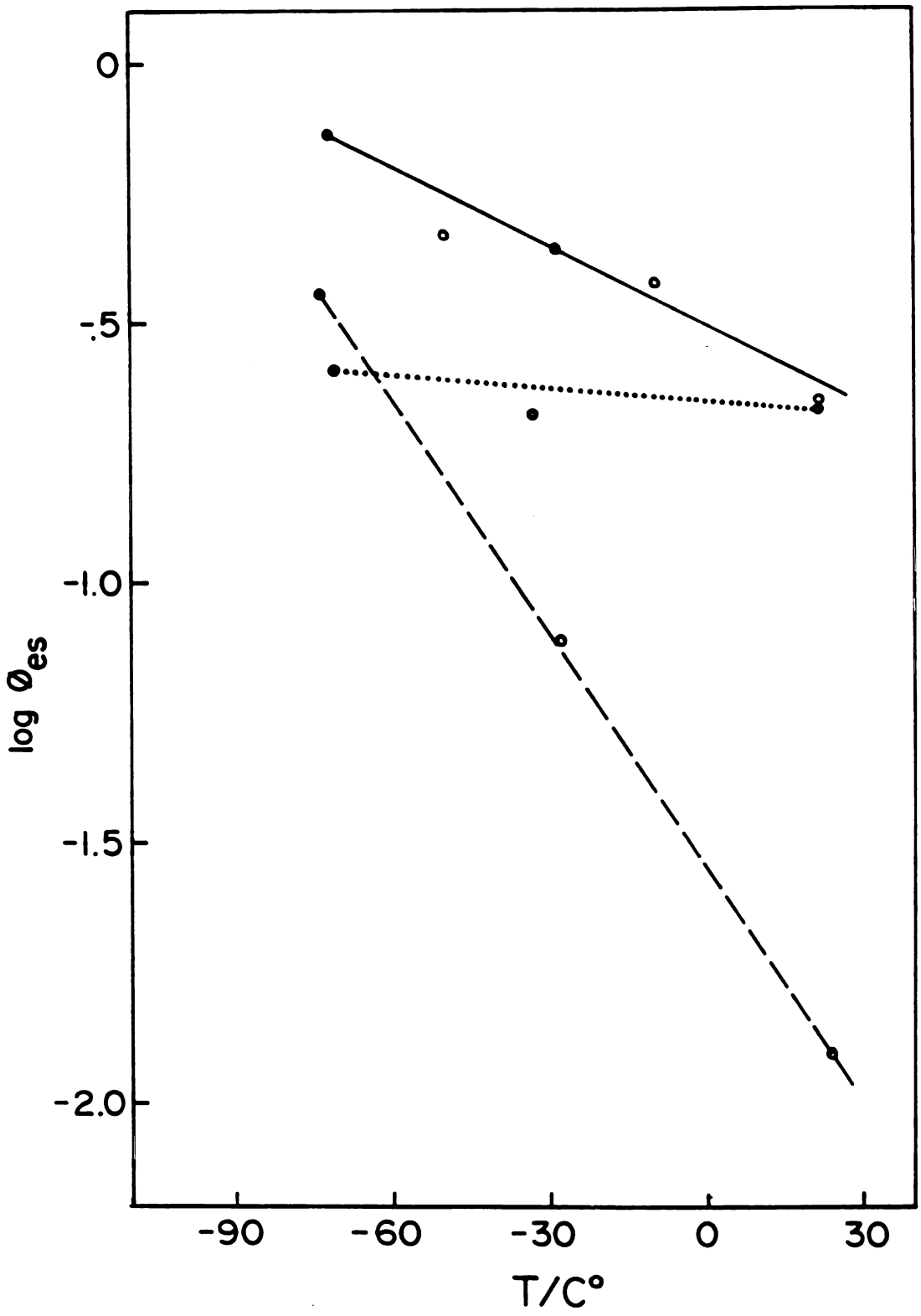

Figure 25

electrogenerated reactants at low temperatures.[75,139] This may be the case here, but our experience is that with the appropriately chosen pulse sequence (vida infra) the electrogenerated reactants are stable on the time scale of the ecl experiment.

A more intriguing explanation for the temperature dependence lies in the analysis of the ecl energetics. The driving force for the excited state pathway (ΔG_{es} = 1.1 eV) is equal in magnitude to the total reorganizational energy of the electron transfer reaction. From eq 2, the excited state pathway is activationless (ignoring work terms) and therefore the population of the activated complex should be temperature independent. However, this is not the case for the inverted pathway. Reaction to ground state must surmount a non-zero activation barrier and hence the rate will diminish with decreasing temperature. Thus, the chemiluminescence electron-transfer pathway will increasingly dominate as the temperature is lowered. Further support of this hypothesis comes from the attenuated temperature dependencies of $Mo_6Cl_{14}^{2-}/A$ and $Mo_6Cl_{14}^{2-}/P^+$ ecl. For these reactions, the activation barrier to excited states is non-zero. The temperature dependence of normal and inverted pathways in these systems will be more similar and therefore the ecl efficiency will, as observed, exhibit a smaller temperature effect. This work provides support of Faulkner and Kim's earlier contention that temperature effects in ecl could be explained by differences in

activation barriers between normal and inverted region pathways.[137a]

F. Potential Step Program Effects

The ecl efficiency of the $Mo_6Cl_{14}^-/Mo_6Cl_{14}^{3-}$ system depends on the potential step sequence. An anodic to cathodic potential pulse sequence (initial production of $Mo_6Cl_{14}^-$) produces ecl 6 times the intensity of a cathodic to anodic pulse program (initial production of $Mo_6Cl_{14}^{3-}$). This observation supports the fact that $Mo_6Cl_{14}^{3-}$ is chemically unstable over long periods of time. For the latter pulse sequence $Mo_6Cl_{14}^{3-}$ is diffusing away from the electrode during the cathodic pulse and then diffuses back to the electrode during the anodic pulse. The longest residency time of the $Mo_6Cl_{14}^{3-}$ generated for a 100 msec pulse sequence in the diffusion layer is approximately 200 msec. On the other hand, the residency time of $Mo_6Cl_{14}^{3-}$ during the former pulse sequence is less than 10 msec (diffusion away from the electrode). That the ecl yields of experiments possessing pulse sequences, which result in long $Mo_6Cl_{14}^{3-}$ residency times, are low clearly demonstrates that the trianion undergoes decomposition reactions. We approximate the decay reaction to occur with a half life on the order of 100 ms.

Two empirical observations relating ecl efficiencies with potential step sequences are shown in Figures 26 and 27. A plot of pulse frequency vs. log ϕ_{es} (Figure 26) shows

Figure 26. Plot of log ϕ_{es} vs. pulse frequency in CH_3CN for the $Mo_6Cl_{14}^-/Mo_6Cl_{14}^{3-}$ (□) and $Mo_6Cl_{14}^-$/4-amido-N-methylpyridinium (■) at 23°C (μ = 0.1 M NBu_4PF_6).

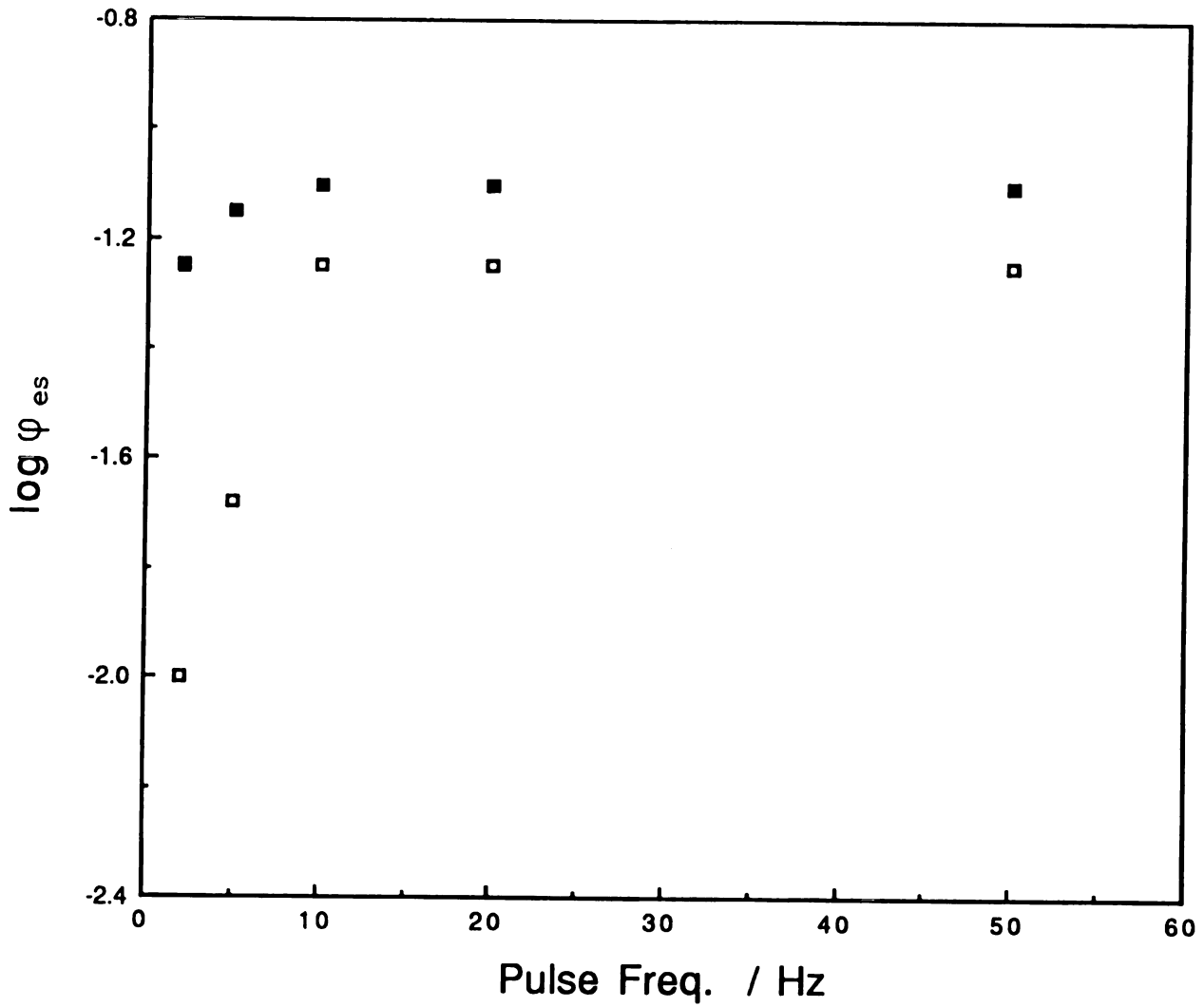

Figure 26

Figure 27. Plot of the log ϕ_{es} vs. no. of pulses in CH_3CN for $Mo_6Cl_{14}^-/Mo_6Cl_{14}^{3-}$ (●) and $Mo_6Cl_{14}^-$/4-amido-N-methyl pyridinium (O) at 23°C (μ = 0.1 NBu_4PF_6).

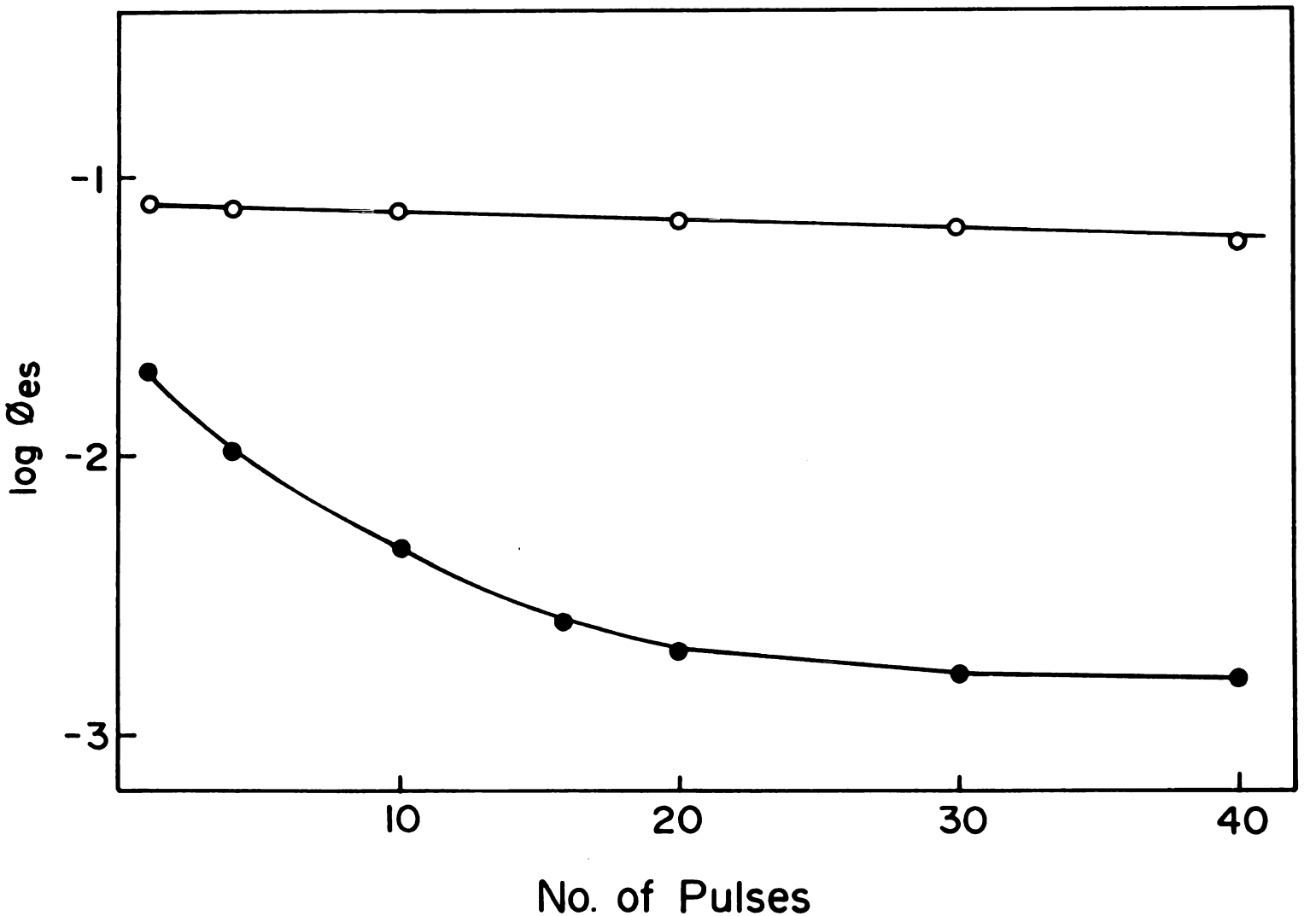

Figure 27

that ecl efficiency is fairly constant at long pulse frequencies, but as the pulse frequency decreases the ecl efficiency diminishes. This effect is attenuated for the $Mo_6Cl_{14}^{2-}$/pyridinium ecl reaction. Figure 27 shows the dependence of the ecl efficiency on the number of consecutive pulses. For $Mo_6Cl_{14}^{-}/Mo_6Cl_{14}^{3-}$ ecl, the efficiency steadily diminishes as the number of pulses increases to a value ten times less than the maximum. Once again, the effect is attenuated for the $Mo_6Cl_{14}^{2-}$/pyridinium ecl system. Both studies suggest side decomposition reactions of $Mo_6Cl_{14}^{3-}$ over long times. Substitution of the reduced pyridinium for $Mo_6Cl_{14}^{3-}$ eliminates this problem, and the ecl efficiency is restored.

CHAPTER VI

VI. FINAL REMARKS

Most electron-transfer reactions only allow the study of rates in either the normal or inverted region. Chemiluminescence is unique because normal and inverted region electron-transfer pathways are competitive and changes in reaction conditions are directly reflected in differences in ground and excited-state rates. The $M_6X_8Y_6^{2-}$ systems have provided insight into the parameters which control ground (inverted region) and excited state (normal region) reaction pathways and hence, the efficiency of the ecl process. An important result of the work described herein is that the efficiency of ecl is circumvented by long-distance electron transfer. This observation implies that the most efficient cl or ecl systems will be those possessing annihilation reactions between redox centers chemically linked over short separation distances. An obvious avenue of future exploration is to construct electrode microstructures in which the cluster and its redox partner are covalently or electrostatically bound at fixed distances. The versatile substitution chemistry of $M_6X_8Y_6^{2-}$ clusters permits straightforward covalent attachment of a variety of redox active groups (e.g. pyridinium) in the cluster's axial positions. In these systems, ecl can be established between the reduced substituent in the axial position and the oxidized metal core. Of course, the success of this electron-transfer chemistry assumes that the hole and electron are localized on the respective cluster core and axial substituent (i.e. weakly coupled system).

Spectroscopic properties of $Mo_6X_8Y_5L$ clusters indicate that the excited state and oxidation-reduction properties are not strongly coupled with ligands in axial positions. Thus the assumption of localized state appears to be valid and ecl experiments between an axial substituent and cluster core appear to be feasible. Alternatively, bridging ligands such as pyrazine can be used to form dicluster units immobilized to metalloxide or activated graphite electrode surfaces by using well established methods.[140] Because the cluster is charged, the ions can be incorporated into polyelectrolyte electrode films by simple ion-exchange methods.[140,142,143] For instance, $M_6X_8Y_6^{2-}$ clusters bound in bipyridium and pyridinium films have recently been prepared. The observation of an oxidation wave of the cluster and reduction wave of the polymer has resulted in the observation of weak chemiluminescence from annihilation reactions analogous to those found in homogeneous solution. This inherently low ecl efficiency is caused by negligible exergonic excited state driving forces, and thus different polymer environments providing driving forces well above the ecl threshold are currently being sought. The results from these linked ecl systems will allow the electron-transfer distances in ecl reactions to be precisely defined and mediating factors such as solvent and solute interactions to be quantitatively investigated.

The criteria of high electrical efficiencies over long lifetimes has deterred successful development of ecl

systems.[59-63] A renewed interest in developing practical applications of ecl systems, has been rekindled with many of the discoveries presented in this thesis. Not only will the construction of electrode microstructures improve efficiencies by maximizing the fundamental factors crucial to efficient excited state production, but attachment of the cluster ions to the electrode surface should improve luminosity and durability of cluster based ecl devices while structures will also minimize the adverse solvent and solute effects. In this regard, these systems potentially constitute the fundamental building blocks of solid state electroluminescent devices.

The research described herein establishes the utility, at a quantitative level, of chemiluminescence in determining electron transfer mechanism. The importance of electron transfer distance and factors mediating this distance (e.g. solvent, solute) in governing the electron-transfer pathway are results which are not only prerequisite for chemiluminescence reactions but pertain to all bimolecular electron-transfer reactions as well. The existence of numerous redox active, luminescent molecules coupled with the dynamic interplay between electron-transfer theory and experiment ensures that chemiluminescence will continue to provide valuable insight into the mechanism of electron transfer reactions.

VII. REFERENCES

REFERENCES

1. Kalyanasundaram, K.; Gratzel, M.; Pelizzetti, E. Coord. Chem. Rev. **1986**, 69, 57-125.
2. Gratzel, M. (Ed.), "Energy Resources Through Photochemistry and Catalysis", Academic Press: New York, 1983.
3. Fendler, J.H. J. Phys. Chem. **1985**, 89, 2730-2740.
4. Masters, C., "Homogeneous Transition-Metal Catalysis", Chapman and Hall: New York, 1981.
5. Sutterfield, G.N. "Heterogeneous Catalysis in Practice", McGraw-Hill: New York, 1980.
6. Addision, A.W.; Cullen, W.R.; Dalphin, D.; James, B.R. (Eds.), "Biological Aspects of Inorganic Chemistry", Wiley-Interscience: New York, 1977.
7. Govidjee (Eds.), "Photosynthesis: Energy Conversion by Plants and Bacteria", Academic Press: New York, 1982, Vol. 1.
8. Isied, S.S. Prog. Inorg. Chem. **1984**, 32, 443-517.
9. (a) Marcus, R.A.; Sutin, N. Biochimica et Biophysica Acta **1985**, 811, 265-322. (b) Newton, M.D.; Sutin, N. Ann. Rev. Phys. Chem. **1984**, 35, 437- 480.
10. McLendon, G., Guarr, T.; McGuire, M.; Simola, K.; Strauch, S.; Taylor, K. Coord. Chem. Rev. **1985**, 64, 113-124.

11. Meyer, T.J. Prog. Inorg. Chem. **1983**, 30, 389-440.

12. (a) Marcus, R.A. Ann. Rev. Phys. Chem. **1964**, 15, 155-196. (b) Marcus, R.A. J. Chem. Phys. **1956**, 24, 966-978.

13. Hush, N.S. Trans. Faraday Soc. **1961**, 57, 557-580. Hush, N.S. Prog. Inorg. Chem. **1967**, 8, 391-444.

14. Hopfield, J. J. Proc. Nat'l. Acad. Sci. **1974**, 71, 3640-3644.

15. Chance, B.; DeVault, D.C.; Frauenfelder, H.; Schrieffer, J.R.; Sutin, N., Eds., "Tunneling in Biological Systems", Academic Press: New York, 1979.

16. Marcus, R.A. in "Third International Symposium on Oxidases", King, T.E.; Mason, H.S.; Morrison, M., Eds., July 1-4, 1979.

17. Brunschwig, B. S.; Logan, J.; Newton, M. D.; Sutin, N. J. Am. Chem. Soc. **1980**, 102, 5798-5809.

18. Sutin, N. Acc. Chem. Res. **1982**, 15, 275-282.

19. Siders, P.; Marcus, R. A. J. Am. Chem. Soc. **1981**, 103, 741-747.

20. DeVault, D. "Quantum-Mechanical Tunneling in Biological Systems", Cambridge University:New York, 1984.

21. Brunschwig, B.S.; Sutin, N. Comments Inorg. Chem. **1987**, 6, 209-235.

22. Endicott, J.F.; Ramassami, T. J. Phys. Chem. **1986**, 90, 3740-3747.

23. Balzani, V.; Scandola, F.; Orlandi, G.; Sabbatini, M.; Indelli, M.T. J. Am. Chem. Soc. **1981**, 102, 3370-3378.

24. Nielson, R.M.; Golovin, M.N.; McManis, G.E.; Weaver, M.J. J. Am. Chem. Soc., **1988**, 110, 1745-1749.

25. (a) Mayo, S.L.; Ellis, W.R.; Coutchley, R.J.; Gray, H.B. Science **1986**, 233, 948-952. (b) Axup, A.W.; Albin, M.; Mayo, S.L.; Crutchley, R.J.; Gray, H.B. J. Am. Chem. Soc. **1988**, 110, 435-439.

26. McLendeon, G. Acc. Chem. Res. **1988**, 21, 160-167.

27. Elias, H.; Chou, M.H.; Winkler, J.R. J. Am. Chem. Soc. **1988**, 110, 429-434.

28. (a) Miller, J. R.; Calcaterra, L. T.; Closs, G. L. J. Am. Chem. Soc. **1984**, 106, 3047-3049. (b) Miller, J. R.; Beitz, J. V.; Huddleston, R. K. J. Am. Chem. Soc. **1984**, 106, 5057-5068. (c) Closs, G. L.; Calceterra, L. T.; Green, N. J.; Penfield, K. W.; Miller, J. R. J. Phys. Chem. **1986**, 90, 3673-3683. (d) Closs, G.L.; Miller, J.R. Science **1988**, 240, 440-447.

29. Wasielewski, M. P.; Niemczyk, M. P.; Svec, W. A.; Pewitt, E. B. J. Am. Chem. Soc. **1985**, 107, 1080-1082.

30. Heitele, H.; Michel-Beyerle, M.E. J. Am. Chem. Soc. **1985**, 107, 8286-8288.

31. Harrison, R.J.; Pearce, B.; Beddard, G.S.; Cowan, J.A.; Sanders, J.K.M. Chem. Phys. **1987**, 116, 429-448.

32. Guerr, T.; McGuire, M.E.; McLendon, G. J. Am. Chem. Soc. **1985**, 107, 5104-5111.

33. Oevering, H.; Padden-Row, N.M.; Heppener, M.; Oliver, A.M.; Cotsaris, E.; Verhoeven, J.W.; Hush, N.S. J. Am. Chem. Soc., **1987**, 109, 3258-3269.

34. Rehm, D.; Weller, A. Isr. J. Chem. **1970**, 8, 259-271.

35. (a) Creutz, C.; Sutin, N. J. Am. Chem. Soc. **1977**, 99, 241-243. (b) Lin, C.-T.; Bottcher, W.; Chou, M.; Creutz, C.; Sutin, N. J. Am. Chem. Soc. **1976**, 98, 6536-6544.

36. (a) Ballardini, R.; Varani, G.; Indelli, M. T.; Scandola, F.; Balzani, V. J. Am. Chem. Soc. **1978**, 100, 7219-7223. (b) Scandola, F.; Balzani, V.; Schuster, G. B. J. Am. Chem. Soc. **1981**, 103, 2519-2523. (c) Indelli, M. T.; Ballardini, R.; Scandola, F. J. Phys. Chem. **1984**, 88, 2547-2551.

37. Nagle, J. K.; Dressick, W. J.; Meyer, T. J. J. Am. Chem. Soc. **1979**, 101, 3993-3995.

38. (a) Nocera, D. G.; Gray, H. B. J. Am. Chem. Soc. **1981**, 103, 7349-7350. (b) Marshall, J. L. ; Stobart, S. R.; Gray, H. B. J. Am. Chem. Soc. **1984**, 106, 3027-3029.

39. Heuer, W. B.; Totten, M. D.; Rodman, G. S.; Hebert, E. J.; Tracy, H. J.; Nagle, J. K. J. Am. Chem. Soc. **1984**, 106, 1163-1164.

40. Kavarnos, G. J.; Turro, N. J. Chem. Rev. **1986**, 86, 401-449.

41. Evidence for the inverted region has been observed in geminate radical pairs: (a) Ohno, T. J. Phys. Chem. **1985**, 89, 5709-5713. (b) Ohno, T. Yoshimura, A.; Mataga, N. J. Phys. Chem. **1986**, 90, 3295-3297. (c) Ohno, T.; Yoshimura, A.; Shioyama, H.; Mataga, N. J. Phys. Chem. **1987**, 91, 4365-4370.

42. Rehm, D.; and Weller, A. Ber. Bunsgenges. Phys. Chem. **1969**, 73, 834-839.

43. (a) Agmon, N.; Levine, R.D. Chem. Phys. Lett. **1977**, 52, 197-201. (b) Agmon, N. J. Chem. Soc. Faraday Trans. II **1978**, 74, 388-404.

44. Scandola, F.; Balzani, V. J. Am. Chem. Soc. **1979**, 101, 6140-6142.

45. (a) Van Duyne, R. P.; Fischer, S. F. Chem. Phys. **1974**, 5, 183-197. (b) Fischer, S. F.; Van Duyne, R. P. Chem. Phys. **1977**, 26, 9-16.

46. Kestner, N. R.; Logan, J.; Jortner, J. J. Phys. Chem. **1974**, 78, 2148-2165.

47. (a) Ulstrup, J.; Jortner, J. J. Chem. Phys. **1975**, 63, 4358-4368. (b) Jortner, J.; Ulstrup, J. J. Am. Chem. Soc. **1979**, 101, 3744-3754.

48. Newton, M. D. Int. J. Quantum Chem. **1980**, 14, 364-391.

49. Webman, I.; Kestner, N. R. J. Chem. Phys. **1982**, 77, 2387-2398.

50. Beitz, J.V.; Miller, J.R. J. Chem. Phys. **1979**, 71, 4579-4595.

51. Marcus, R.A. Int. J. Chem. Kinet. **1981**, 13, 865.

52. (a) Weller, A.; Zachariasse, K. Chem. Phys. Lett. **1971**, 10, 590-594. (b) Joussot-Dubian, J.; Albrecht, A.C.; Garischer, H.; Knox, R.S.; Marcus, R.A.; Schott, M.; Weller, A.; Willig, F. Life Sci. Res. Rep. **1979**, 12, 129.

53. Marcus, R.A.; Siders, P. J. Phys. Chem. **1982**, 86, 622-630.

54. Marcus, R. A. Discus. Faraday Soc. **1960**, 29, 129-131.

55. Noyes, R. M. Prog. React. Kinet. **1961**, 1, 129-160.

56. Debye, P. Trans. Electrochem. Soc. **1942**, 82, 265-272.

57. McLendon, G.; Guarr, T. Coord. Chem. Rev. **1985**, 68, 1-52.

58. Marcus, R.A. J. Chem. Phys. **1965**, 43, 2654-2657.

59. (a) Schaper, H.; Schnedler, E. J. Phys. Chem. **1982**, 86, 4380-4385. (b) Schaper, H.; Kostlin, H.; Schnedler, E. Philips Tech. Rev. **1982**, 40, 69-80.

60. Laser, D.; Bard, A.J. J. Electrochem. Soc. **1975**, 122, 632-640.

61. Brilmeyer, G.H.; Bard, A.J. J. Electrochem. Soc. **1980**, 127, 104-110.

62. Heller, C.A.; Jernigan, J.L. Appl. Optics **1977**, 16, 61-66.

63. (a) Measures, R.M. Appl. Optics **1975**, 14, 909-916. (b) Measures, R.M. Appl. Optics, **1974**, 13, 1121-1133.

64. Maverick, A. W.; Najdzionek, J. S.; MacKenzie, D.; Nocera, D. G.; Gray, H. B. J. Am. Chem. Soc. **1983**, 105, 1878-1882. (b) Zietlow, T.C.; Gray, H.B. Inorg. Chem. **1986**, 25, 631-634.

65. Nocera, D.G.; Gray, H.B. J. Am. Chem. Soc. **1984**, 106, 824-825.

66. Sheldon, J.C. J. Chem. Soc. **1960**, 1007-1014.

67. Sheldon, J.C. J. Chem. Soc. **1962**, 410-415.

68. Dorman, W.C.; McCarley, R.E. Inorg. Chem. **1974**, 13, 491-493.

69. Hogue, R.D.; McCarley, R.E. Inorg. Chem. **1970**, 9, 1354-1359.

70. Walter, R.I. J. Am. Chem. Soc. **1955**, 77, 5999-6002.

71. Mussell, R.D.; Kassel, D.; Allison, J.; Nocera, D.G., manuscript in preparation.

72. Gagne, R.R.; Koval, C.A.; Lisensky, G.C. Inorg. Chem. **1980**, 19, 2854-2855.

73. Newsham, M.D., Ph.D. Dissertation, Michigan State University, 1988.

74. Keszthelyi, C.P.; Tokel-Takvoryan, N.E.; Bard, A.J. Anal. Chem. **1975**, 47, 249-255.

75. (a) Wallace, W.L.; Bard, A.J. J. Phys. Chem. **1979**, 83, 1350-1357. (b) Itoh, K.; Honda, K. Chem. Lett. **1979**, 99-102.

76. Bolleta, F.; Bonafede, S. Pure & Appl. Chem. **1986**, 58, 1229-1232.

77. (a) Dye, J.L.; Nicely, V.A. J. Chem. Ed. **1971**, 48, 443-448. (b) Turro, N.J. "Modern Molecular Photochemistry", Benjamin/Cummings:Menlo Park, CA, 1978; Chapter 9.

78. Hughbanks, T.; Hoffman, R. J. Am. Chem. Soc. **1983**, 105, 1150-1162.

79. (a) Seifert, G.; Grossman, G.; Muller, H. J. Mol. Struct. **1980**, 64, 93-102. (b) Tyler, D. R., University of Oregon, personal communication, 1986.

80. Zietlow, T. C.; Nocera, D. G.; Gray, H. B. Inorg. Chem. **1986**, 25, 1351-1353.

81. (a) The effect of disparate values of the electronic coupling element on chemiluminescent reactivity has been addressed for annihilation reactions involving transition metal polypyridyl complexes.[81b] (b) Bonafede, S.; Ciano, M.; Bolletta, F.; Balzani, V.; Chassot, L.; Zelewsky, A. J. Phys. Chem. **1986**, 90, 3836-3841.

82. Scandola, F.; Balzani, V.; Schuster, G.B. J. Am. Chem. Soc. **1981**, 103, 2519-2523.

83. Faulkner, L. R.; Bard, A. J. J. Am. Chem. Soc. **1969**, 91, 209-210.

84. Bezman, R.; Faulkner, L. R. J. Am. Chem. Soc. **1972**, 94, 6317-6323.

85. (a) Hercules, D. M. Acc. Chem. Res. **1969**, 2, 301-306. (b) Hercules, D. M. "Physical Methods in Organic Chemistry" Weissberger, A.; Rossiter, B. Eds.; Academic: New York, 1971; Part II, Chapter 13.

86. Chandross, E. A. Trans. N.Y. Acad. Sci., Ser. 2 **1969**, 31, 571-583.

87. Weller, A.; Zachariasse, K. "Chemiluminescence and Bioluminescence" Cormier, M.; Hercules, D. M.; Lee, J., Eds.; Plenum: New York, 1973.

88. (a) Faulkner, L. R. Int. Rev. Sci. Phys. Chem. Ser. Two **1975**, 9, 213-263. (b) Faulkner, L. R. Meth. Enzymol. **1978**, 57, 494-526. (c) Faulkner, L. R.; Glass, R. S. "Chemical and Biological Generation of Excited States" Adam, W.; Gilento, G., Eds.; Academic: New York, 1982.

89. Park, S.-M.; Tryk, D. A. Rev. Chem. Intermediates **1981**, 4, 43-79

90. Pighin, A. Can. J. Chem. **1973**, 51, 3467-3472.

91. Bard, A. J.; Keszthelyi, C. P.; Tachikawa, H.; Tokel, N. E. "Chemiluminescence and Bioluminescence" Cormier, M., Hercules, D. M.; Lee, J., Eds.; Plenum: New York, 1973.

92. (a) Itoh, K.; Honda, K.; Sukigara, M. Electrochim. Acta **1979**, 24, 1195-1198. (b) Itoh, K.; Honda, K.; Sukigara, M. J. Electroanal. Chem. **1980**, 110, 277-284.

93. Tokel, N. E.; Bard, A. J. J. Am. Chem. Soc. **1972**, 94, 2862-2863.

94. Abruna, H. D. J. Electroanal. Chem. **1984**, 175, 321-326.

95. Kane-Maguire, N.A.P.; Guckart, J.A.; O'Neil, P.J. Inorg. Chem. **1987**, 26, 2340-2342.

96. Tokel-Takvoryan, N. E.; Bard, A. J. J. Am. Chem. Soc. **1973**, 95, 6582-6589.

97. Abruna, H. D. J. Electrochem. Soc. **1985**, 132, 842-849.

98. (a)Gonzales-Velasco, J.; Rubinstein, I.; Crutchley, R. J.; Lever, A. B. P.; Bard, A. J. Inorg. Chem. **1983**, 22, 822-825. (b) Lee, C.-W.; Ouyang, J.; Bard, A.J. J. Electroanal. Chem. **1988**, 244, 319-324.

99. Luong, J. C.; Nadjo, L.; Wrighton, M. S. J. Am. Chem. Soc. **1978**, 100, 5790-5795.

100. Vogler, A.; Kunkely, H. Angew. Chem. Int. Ed. Engl. **1984**, 23, 316-317.

101. Ouyang, J.; Zietlow, T. C.; Hopkins, M. D.; Fan, F.-R. F.; Gray, H. B.; Bard, A. J. J. Phys. Chem. **1986**, 90, 3841-3949.

102. Wheeler, B. L.; Nagasubramanian, G.; Bard, A. J.; Schechtman, L. A.; Dininny, D. R.; Kenney, M. E. J. Am. Chem. Soc. **1984**, 106, 7404-7410.

103. Tokel-Takvoryan, N. E.; Bard, A. J. Chem. Phys. Lett. **1974**, 25, 235-238.

104. Volger, A.; Kunkely, H. ACS Symp. Series **1987**, 333, 155-168.

105. Luttmer, J. D.; Bard, A. J. J. Phys. Chem. **1981**, 85, 1155-1159.

106. Glass R. S.; Faulkner, L. R. J. Phys. Chem. **1981**, 85, 1160-1165.

107. Kim, J.; Fan, F. F.; Bard, A. J.; Che, C.-M.; Gray, H. B. Chem. Phys. Lett. **1985**, 121, 543-546.

108. Che, C.-M.; Atherton, S. J.; Butler, L. G.; Gray, H. B. J. Am. Chem. Soc. **1984**, 106, 5143-5145.

109. Liu, D. K.; Brunschwig, B. S.; Creutz, C.; Sutin, N. J. Am. Chem. Soc. **1986**, 108, 1749-1755.

110. Owing to our inability to find nitroaromatics that are reduced at potentials less negative then p-dinitrobenzene, some aromatic quinones were employed for the reaction of $Mo_6Cl_{14}^-$ with negatively charged donors.

111. Faulkner, L. R.; Bard, A.J. J. Electroanal. Chem. **1977**, 10, 1-95.

112. The lowest excited-state energies for donors and acceptors used in ecl studies are: 2,6-dimethyl-p-benzoquinone, ET = 2.32 V (Trommsdorff, H. P. J. Chem. Phys. **1972**, 56, 5358-5372); p-dinitrobenzene, ET = 2.54 V (Brown, R. G.; Harriman, A.; Harris, L. J. Chem. Soc. Faraday Trans. 2, **1978**, 74, 1193-1199); o-dinitrobenzene, ET = 2.55 V, and phenothiazine, ET = 2.62 V (Alkaitis, S. A.; Gratzel, M.; Henglein, A. Berg. Bunsenges. Phys. Chem. **1975**, 79, 541-546); 10-methylphenothiazine, ET = 2.66 V (Rothenberger, G.; Infelta, P. P.; Gratzel, M. J. Phys. Chem. **1979**, 83, 1871-1876); tris(p-tolyl)amine, ET = 3.0 V (Zachariasse, K. A. Ph.D. Thesis, Free University Press: Amsterdam, 1972); tris(4-bromophenyl)amine, ET > 3.1 V (Terenen, A.; Ermolaev, V. Soviet Physics Doklady **1962**, 6, 600-602).

113. Faulkner, L. R.; Tachikawa, H.; Bard, A. J. J. Am. Chem. Soc. **1972**, 94, 691-699).

114. Kowert, B. A.; Marcoux, L.; Bard, A. J. J. Am. Chem. Soc. **1972**, 94, 5538-5550.

115. Brunschwig, B. S.; Ehrenson, S.; Sutin, N. J. Am. Chem. Soc. **1984**, 106, 6858-6859.

116. Sutin, N.; Brunschwig, B. S. ACS Symp. Ser. **1982**, 198, 105-125.

117. Sutin, N. Prog. Inorg. Chem. **1983**, 30, 441-498.

118. Kakitani, T.; Mataga, N. J. Phys. Chem. **1987**, 91, 6277-6285.

119. Hupp, J.T.; Weydert, J. Inorg. Chem. **1987**, 26, 2657-2660.

120. Ennix, K.S.; McMahon, P.T.; Rosa, R.; Curtis, J.C. Inorg. Chem. **1987**, 26, 2660-2666.

121. Kahlow, M.A.; Kana, T.J.; Barbara, P.F. J. Phys. Chem. **1987**, 91 6452-6455.

122. Boyd, D.C.; Rodman, G.S.; Mann, K.R. J. Am. Chem. Soc. **1986**, 108, 1779-1784.

123. (a) Borchardt, D.; Pool, K.; Wherland, S. Inorg. Chem. **1982**, 21, 93-97. (b) Nielson, R.M.; Wherland, S. Inorg. Chem. **1984**, 23, 1338-1344. (c) Borchardt, D.; Wherland, S. Inorg. Chem. **1984**, 23, 2537-2542. (d) Nielson, R.M.; Wherland, S. Inorg. Chem. **1986**, 25, 2437-2440. (e) Stebler, M.; Nielson, R.M.; Siems, W.F.; Hunt, J.P.; Dodgen, H.W.; Wherland, S. Inorg. Chem. **1988**, 27, 2893-2897.

124. (a) Kjaer, A.M.; Ulstrup, J. Inorg. Chem. **1986**, 25, 644-654/ (b) Kjaer, A.M.; Ulstrup, J. Inorg. Chem. **1987**, 26, 2052-2058.

125. (a) Truong, T.B. J. Phys. Chem. **1984**, 88, 3906-3913. (b) Truong, T.B. Pure & Appl. Chem. **1986**, 58, 1279-1284.

126. Rustman, P.; Brown, T.L. J. Am. Chem. Soc. **1987**, 109, 3632-3639.

127. Koller, K.B.; Hawkridge, F.M. J. Am. Chem. Soc. **1985**, 107, 7412-7417.

128. (a) Nielson, R.M.; McManis, G.E.; Golovin, M.N.; Weaver, M.J. J. Phys. Chem. **1988**, 92, 3441-3450. (b) Nielson, R.M.; Golovin, M.N.; McManis, G.E.; Weaver, M.J. J. Am. Chem. Soc. **1988**, 110, 1745-1749. (c) McManis, G.E.; Mishra, A.K.; Weaver, M.J. J. Phys. Chem. **1987**, 86 5550-5556. (d) McManis, G.E.; Golovin, M.N.; Weaver, M.J. J. Phys. Chem. **1986**, 90, 6563-6570.

129. (a) Nadler, W.; Marcus, R.A. J. Chem. Phys. **1987**, 86, 3906-3924. (b) Sumi, H.; Marcus, R.A. J. Electroanal. Chem. **1986**, 204, 59-67.

130. Calef, D.F.; Wolynes, P.G. J. Phys. Chem. **1983**, 87, 3387-3400.

131. Hynes, J.T. J. Phys. Chem. **1986**, 90, 3701-3706.

132. Simon, J.D. Acc. Chem. Res. **1988**, 21, 128-134.

133. Cukier, R.I. J. Chem. Phys. **1988**, 91, 3938.

134. (a) Rips, I.; Jortner, J. Chem. Phys. Lett. **1987**, 133, 411-414. (b) Rips, I.; Jortner, J. J. Chem. Phys. **1988**, 88, 818-822.

135. McGuire, M.; McLendon, G. J. Phys. Chem. **1986**, 90, 2549-2551.

136. Keszthelyi, C.P.; Tokel-Takveryan, N.E.; Tachikawa, H.; Bard, A.J. Chem. Phys. Lett. **1973**, 23, 219.

137. (a) Kim, J.; Faulkner, L.R. J. Am. Chem. Soc. **1988**, 110, 112-119. (b) Kim, J.; Faulkner, L.R. J. Electroanal. Chem. **1988**, 242, 107-121.

138. Zoski, C.G.; Sweigart, D.A.; Stone, N.J.; Rieger, P.H.; Mocellin, E.; Mann, T.F.; Mann, D.R.; Gosser, D.K.; Doeff, M.M.; Bond, A.M. J. Am. Chem. Soc. **1988**, 110, 2109-2116.

139. Gonzales-Velasco, J. J. Phys. Chem. **1988**, 92, 2202-2207.

140. Murray, R.W. "Electroanalytical Chemistry"; Bard, A.J., Ed.; Dekker:New York, 1983; Vol. 13, p. 191-368.

141. (a) Potts, K.T.; Usifer, D.A.; Guadalupe, A.; Abruna, H.D. J. Am. Chem. Soc. **1987**, 109, 3961-3967. (b) Guadalupe, A.; Usifer, D.A.; Potts, K.T.; Hurrell, H.C.; Mogstad, A.-E.; Abruna, H.D. J. Am. Chem. Soc. **1988**, 110, 3462-3466.

142. Sharp, M. J. Electroanal. Chem. **1987**, 230, 109-124.

143. Hupp, J.T.; Meyer, T.J. J. Electroanal. Chem. **1987**, 224, 59-65.

144. Bettelheim, A.; White, B.A.; Raybuck, S.A.; Murray, R.W. Inorg. Chem. **1987**, 26, 1009-1017.

145. Redepenning, J.; Anson, F.C. J. Phys. Chem. **1987**, 91, 4549-4553.